Modifications of the Target or Therapeutic for Improved Drug Delivery

by

Aaron Dolor

DISSERTATION

Submitted in partial satisfaction of the requirements for the degree of

DOCTOR OF PHILOSOPHY

in

Pharmaceutical Sciences and Pharmacogenomics

in the

GRADUATE DIVISION

of the

UNIVERSITY OF CALIFORNIA, SAN FRANCISCO

[redacted]

Acknowledgements

All the work described here could not be completed without the assistance of several people. I only hope to be able to repay the help they provided.

First, I want like to thank my mentor Frank Szoka for his guidance throughout my time. From the first day I rotated in the laboratory he provided the right balance of direction and space for my development. His wealth of knowledge constantly granted me an opportunity to learn. On top of my scientific development, I truly valued the opportunity to explore my other interests while working in the lab.

Second, I want like to thank all my previous and current mentors. Dr. Charles Drain for enabling my first exposure to laboratory science at Hunter College. Dr. Victoria Luine, Dr. Mathew Jurow, Dr. Chirs Farley, Dr. Amit Aggarwal, John Rose, and Dr. Marcia Cantarella for making my time successful at Hunter College, allowing me to attend UCSF. Dr. Aaron Fields for challenging me to learn at UCSF in a way that I have not been challenged in the past. He truly allowed me to grow and made me feel passionate about science even when things were not working out experimentally. Dr. Deanna Kroetz and Dr. Tejal Desai for guidance from my qualifying exam throughout my thesis. Dr. Steven Rosen for all his help with my qualifying exam.

Third, I would like to thank all the former members of the Szoka laboratory, Dr. Aditya Kohli, Dr. Dipali Ruhela, Dr. Mathew Tiffany, and Dr. Jonathan Sockolosky. In particular, Dr. Vincent Venditto for refining my ability to perform chemistry early-on and Dr. Simon Lee for being a lifeline and a constant voice of reason the last few years in the lab.

Fourth, I want to thank all those that helped me along the way. Dr. Zhipeng Dai, Dr. Charles Nobel, and Dr. Mark Hayes of ZoneOnePharma are the true experts in all things liposomes and HPLC. Without a question, they contributed to some portion of all my experiments directly or indirectly. I also want to thank all my classmates especially Katherina Chua, Ken Hallenbeck, and Peter Westcott for their help completing experiments throughout the years. On both a personal and academic level my classmates were invaluable. In addition, I am grateful for the administrative help from Steve Ha and Debbie Acoba. I want to also thank all my family and close friends for the continued support. Without all of you standing with me this work would not be possible.

Lastly, the work describe here would also not be completed without funding and support from the National Science Foundation Graduate Research Fellowship Program, NIH T32 GM007175, and Pharmaceutical Sciences and Pharmacogenomics program.

The text of this dissertation contains reprinted sections of the material as it appears in “Sulfated Quaternary Amine Lipids: A New Class of Inverse Charge Zwitterlipids” and “Digesting a Path Forward: The Utility of Collagenase Tumor Treatment for Improved Drug Delivery”. The co-author listed in the publication “Digesting a Path Forward: The Utility of Collagenase Tumor Treatment for Improved Drug Delivery” directed and supervised the research that forms the basis for the dissertation/thesis.

Chapter 2 includes data from “Sulfated Quaternary Amine Lipids: A New Class of Inverse Charge Zwitterlipids”. Aaron Dolor contributed to the synthesis and characterization of the molecules described.

Modifications of the Target or Therapeutic for Improved Drug Delivery

Aaron Dolor

Abstract

Liposomes featuring a lipid bilayer surrounding an aqueous core, have been utilized as carriers for drugs and macromolecules since the 1970s. Liposomal drug encapsulation improves the pharmacokinetics, biodistribution, and pharmacodynamics of drugs. This research has culminated in over ten approved liposomal therapies, including Doxil® for the treatment of Kaposi's sarcoma.

Despite the longevity, further clinical adoption of liposomes and nanomaterials has been limited due to a lack of effective targeting, undesired drug release kinetics, or inadequate drug penetration. In this dissertation, we present strategies to improve nanoparticle drug delivery through synthetic modifications of the particle or alterations of the target tissue. Our initial efforts centered on synthesizing novel lipids to focus the release of drugs or augment nanoparticle stability. Specifically, we detail the synthesis and characterization of sulfolipids with the potential for triggered-release of drug cargo in the tumor microenvironment through the use of sulfatases. These sulfolipids formed highly stable aggregates that were unable to form vesicles. Next, we describe the synthesis and biophysical characteristics of a modified polyethylene glycol (PEG), a key component for extending the circulation of nanomaterials. We anchored PEG to cholesterol to improve the interactions with neighboring lipids. These sterol-anchored

PEG molecules exhibited an array of canonical liposome behaviors including the formation of vesicles, encapsulation of drugs, and limited non-specific protein adhesion.

Subsequently, we turned our focus to approaches to make the target tissue more receptive to drug delivery. We communicate procedures to recombinantly purify matrix metalloproteinase-8 (MMP-8), a key enzyme for tissue remodeling. We demonstrate methods to utilize MMPs in drug delivery through the attachment to the surface of liposomes. These procedures enabled the use of MMP-8 to improve the permeability of cartilage endplate tissue through removal of inhibitory extracellular matrix components. Altogether, the work presented provides several strategies to enhance the utility of liposomes through improvements in the release of drug cargo, particle stability and tissue penetration.

Table of Contents

List of Figures

List of Tables

1 Chapter 1: Overview of approaches to improve drug delivery

1.1 Introduction

Ever year there are approximately 2 million newly diagnosed cases of cancer and 500,000 mortalities worldwide.[1] With these numbers only expected to increase, significant efforts have been made to broaden the repertoire of available cancer therapies beyond traditional small molecule drugs. As such, macromolecular medicines utilizing therapeutic nanoparticles have become more common in oncology.[2,3] The success of these therapies is dependent on large particles penetrating into tumors and delivering drug cargo. To achieve this desired pharmacokinetics, researchers opted to either modify the drug itself or to alter the tumor microenvironment for drug accessibility.

Modification of nanoparticles is the most common approach to improve drug delivery. Efforts have been focused on improving stability to ensure sufficient circulation to reach tumors, enhancing targeting to allow tumor accumulation while minimizing accumulation in other tissues, and maximizing the release of drug cargo at the target tissue. These promising approaches have expanded the effectiveness of nanoparticle therapies and as such, have been extensively reviewed elsewhere.[4–8] Conversely, the alternative approach of modifying the tumor microenvironment is less widely explored despite the requirement that all drugs, whether modified or not, must inevitably navigate the tumor microenvironment to attain efficacy.

One of the key elements within the tumor microenvironment that restricts drug penetration into tumor cells is the extracellular matrix (ECM). Several tumors, including breast, pancreatic, colorectal, ovarian, and lung exhibit a dense ECM where higher

collagen or hyaluronan content correlates with poor prognosis.[9,10] Cancer associated fibroblasts produce large amounts of ECM components which are associated with tumor promoting activities including angiogenesis,[11,12] cell proliferation,[13] and the creation of "highways" for extravasation of metastatic cells or intravasation of pro-tumor immune cells (Figure 1-1).[9,13] Tumor ECM, which is composed primarily of collagen and hyaluronic acid (HA), contributes to several aspects of the tumor microenvironment that obstructs drug delivery, including: the compression of blood vessels, decreasing blood perfusion, and restricting adequate vascular access to portions of the tumor;[14] the restriction of drug trafficking through the tumor matrix interstitium, preventing drugs from reaching their cellular targets;[15,16] and the maintenance of a high interstitial fluid pressure (IFP) generated by plasma leakage from blood, mechanical stress within the tumor, and a lack of proper lymphatic drainage (Figure 1-2).[17] The confined proliferation of tumor cells further contributes to the mechanical stress within the tumor microenvironment.[17] All of these restrict the movement of drugs from the blood into tumor cells.[14,16]

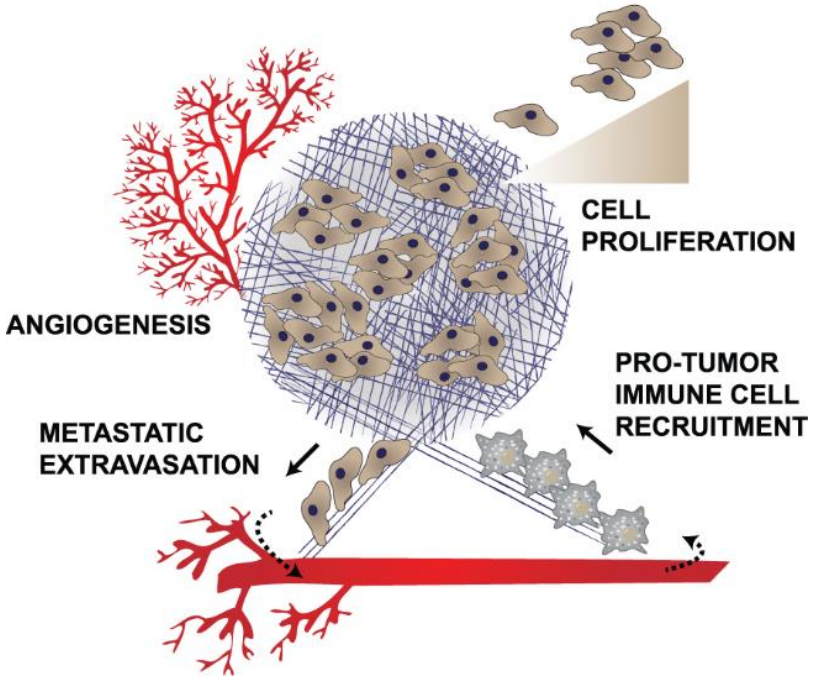

Figure 1-1: ECM components enable tumor promoting activities. ECM in tumors causes increased angiogenesis to supply nutrients for the growing tumor; growth factor signaling leading to cell proliferation; the recruitment of anti-inflammatory, protumor immune cells; and the creation of a path for metastatic cells to extravasate from the primary tumor.

In theory, approaches to decrease the tumor ECM should increase drug penetration and enable higher drug concentrations within tumor cells. There is a subtle aspect to this approach. Complete removal of all biopolymers in the tumor interstitial space may collapse the tumor and decrease drug penetration; as such, normalization of the ECM has been suggested as the primary goal of such therapies.[13,15–19] In this introduction, we highlight key approaches for ECM degradation but focus on the activity of collagenases since these enzymes are less widely used yet can be mechanistically distinguished from matrix degradation achieved through the reduction of HA.

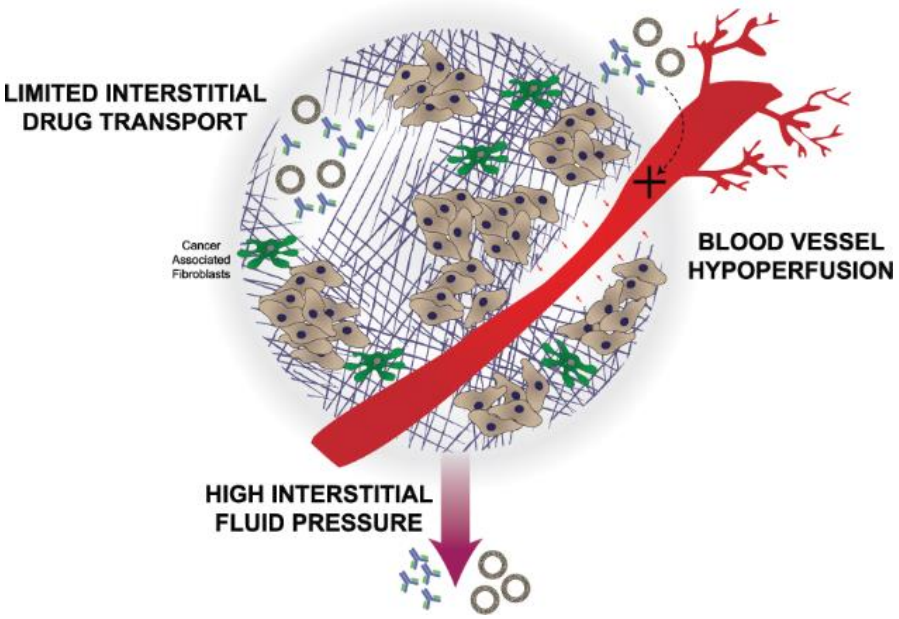

Figure 1-2: A dense tumor extracellular matrix limits adequate delivery of drugs. Blood vessels can become compressed preventing drugs from reaching the tumor. Those drugs that are able to enter the tumor microenvironment are faced with a high interstitial fluid pressure and limited interstitial drug transport.

1.2 Physical ECM Modification

Various external stimuli have been utilized to modify the tumor microenvironment. Thermal, magnetic, radiographic, and ultrasonic tools demonstrated increased vascular permeability, membrane fluidity and drug penetration in solid tumors.[20] Broadly, physical ECM modification causes perturbations in the tumor microenvironment allowing for improved diffusivity and biodistribution of therapeutics. Although physical modifications demonstrate promise clinically, they rely on well-defined tumor boundaries to enable proper targeting and to reduce off-site toxicity in addition to precise timing to apply the external stimuli once the therapy circulated to the tumor site. This added complexity may limit the clinical adoption of these approaches. Physical ECM modifications and their

associated complications, particularly for nanoparticle therapies, have been thoroughly reviewed previously.[21–23]

1.3 HA Modification

One of the earliest strategies to deplete the tumor ECM is to target HA either by preventing its production or by digesting what is present in the tumor ECM.[24] The utility of HA inhibition has been comprehensively reviewed elsewhere.[25,26] Notably, 4-methylumbelliferone (4-MU) has been utilized to prevent HA formation in a variety of tumors by depleting the substrate required for hyaluronan synthesis.[27–29] It also downregulates expression of hyaluronan synthase 2 and 3.[28] The use of 4-MU illustrates the potential dual effect achieved from inhibiting tumor ECM. It directly decreased tumor growth and metastasis in prostate, liver, breast and skin cancer due to a reduction in tumor HA.[25] In addition, treatment of tumored animals with 4-MU enhanced the extravasation of nanoparticles from the blood vessels into the tumor. For example, a combination therapy of a liposome-encapsulated 4-MU prodrug with liposomal doxorubicin decreased tumor volume and increased overall survival compared to liposomal doxorubicin alone in an orthotopic murine tumor.[30] The therapeutic enhancement was a result of the improved distribution of liposomal doxorubicin due to a reduction in tumor ECM.[30] Oral 4-MU (Cantabiline®), is approved in Europe and Asia as a dietary supplement to increase bile flow. It is a safe drug but has very low oral bioavailability (<3%),[26] and its efficacy in oncology remains an open question.

Alternatively, hyaluronidase has been extensively used to enzymatically digest HA.[31] Hyaluronidase efficiently degrades large HA polymers comprised of up to 25,000 monosaccharide units down to simple polysaccharides under 10 units.[32] Hyaluronidase

was explored in oncology clinical trials starting in the 1980s,[33] where pretreatment displayed improved outcomes in head and neck, brain, bladder, and gastrointestinal cancer clinical trials.[18] Notably, 1 in 3 patients developed immune reactions to the bovine hyaluronidase.[33] Detailed assessments of the utility of hyaluronidase for improving interstitial and tumor penetration were previously written. [18,19,34–37] A pegylated human hyaluronidase (PEGPH20) introduced by Halozyme Therapeutics has advanced to late stage clinical trials. This polymer-modified formulation of hyaluronidase reduces immune recognition and promotes extended circulation, giving the enzyme ample time to accumulate in the tumor ECM.[34] PEGPH20 in combination with gemcitabine and nab-paclitaxel (Abraxane®) in a phase II metastatic pancreatic cancer trial showed an increased overall survival in treated patients compared to the control group.[38] This is currently the most advanced ECM removal strategy. It will be interesting to learn if the beneficial effects are replicated in the phase III trial, or in an upcoming gastric cancer trial combining PEGPH20 with anti-PDL1 immunotherapy.[39]

1.4 Collagen Modification

Similar to efforts to remove HA from the tumor matrix, attempts have also been made to limit the synthesis or promote the breakdown of extracellular tumor collagen. Reducing collagen synthesis has been achieved most aggressively through TGF-β inhibition, altering its regulatory role in collagen synthesis.[40] The Jain group has spearheaded this effort through the use of losartan, an angiotensin II inhibitor, and the use of anti-TGF-β antibodies. Losartan mediates angiotensin II type I receptor downregulation of TGF-β activators, such as thrombospondin-1, causing a reduction in TGF-β signaling.[40] TGF-β is an actively pursued target in oncology so the antitumor

effects from its inhibition may work in tandem with the benefits of reducing tumor collagen levels. TGF-β inhibition with Losartan led to an increase in drug penetration and subsequent improvement in survival in multiple murine tumors. [40–42] Lorsartan also targets hyaluronan and cancer-associated fibroblasts.[40,41] Nonetheless, the preclinical success was mirrored in a small phase II clinical trial in pancreatic cancer testing the benefits of Losartan in combination with the FOLFIRINOX (leucovorin, 5-fluorouracil, irinotecan, and oxaliplatin) chemotherapy combination, where over 50% of treated patients identified by radiographic imaging were able to have their tumors resected leaving a margin that had no detectable tumor cells.[17,43]

Another mode to limit collagen deposition is through inhibition of lysyl oxidase-like-2 (LOXL2) activity. LOXL2 cross-links collagen to the fibrillar form found in the ECM and an antibody against LOXL2 reduced the number of collagen cross-links and overall tumor burden in murine xenografts.[44] LOXL2 inhibition also caused a decrease in activated fibroblasts and production of growth factors and cytokines involved in cell signaling.[44] Thus, as with TGF-β blockade, the anti-tumor effects of LOXL2 inhibition occur in tandem to the benefits of collagen reduction. Despite the preclinical success there is concern that this approach of blocking matrix synthesis may be therapeutically limited to early tumor stages prior to the establishment of the characteristically dense matrix. For instance, a phase II trial in metastatic pancreatic cancer patients that combined simtuzumab (anti-LOXL2) with gemcitabine failed to improve clinical outcomes, likely due to the advanced stage of the cancer.[45] Several other antifibrotic drugs have been investigated to reduce tumor ECM, including tranilast,[46] pirfenidone,[47] fasudil,[48] and metformin.[49] The expanded

Losartan trial will be pivotal to understand if inhibition of ECM by repurposing low molecular weight, orally available molecules can translate into the clinic.

The alternative approach to deplete tumor collagen is through the use of collagenases. Collagenases were explored in the 1980s to dissolve excess collagen in patients with severe back pain via collagenase injection into spinal discs.[50] The clinical utility of collagenases is validated by the approval of Xiaflex®, a bacterial clostridium histolyticum collagenase, for the treatment of Dupuytren's contracture as an injection against thickening of collagen tissue within the hand. However, the clinical utility of collagenases in improving cancer therapy is much less well established despite collagen being the most abundant tumor ECM component.

In theory, the use of collagenases would be especially attractive for improving drug penetration but unlike hyaluronidase, which degrades linear hyaluronan down to short oligosaccharides, collagenases cleave at distinct sites along the collagen triple helix,[37–40] leaving behind large subunits of approximately 10-95 kDa (Figure 1-3).[51,52] These cleavage products may not effectively separate from collagen fibers resulting in only microscopic local changes to the collagen structure with collagenase therapy.[53] Preclinical work to evaluate the use of collagenases in oncology, however, indicated that collagenase treatment improved drug diffusion and penetration in treated tumors (Tables 1-1-1-6). The challenge for interpreting or comparing results from the studies reviewed in the following sections is that they varied in enzyme exposure (amount and time), route of injection, tumor model, penetration criteria, and type of drug. These variations make it difficult to predict the potential clinical utility of injected collagenases in cancer therapy or to evaluate the promise and limitations of the approach.

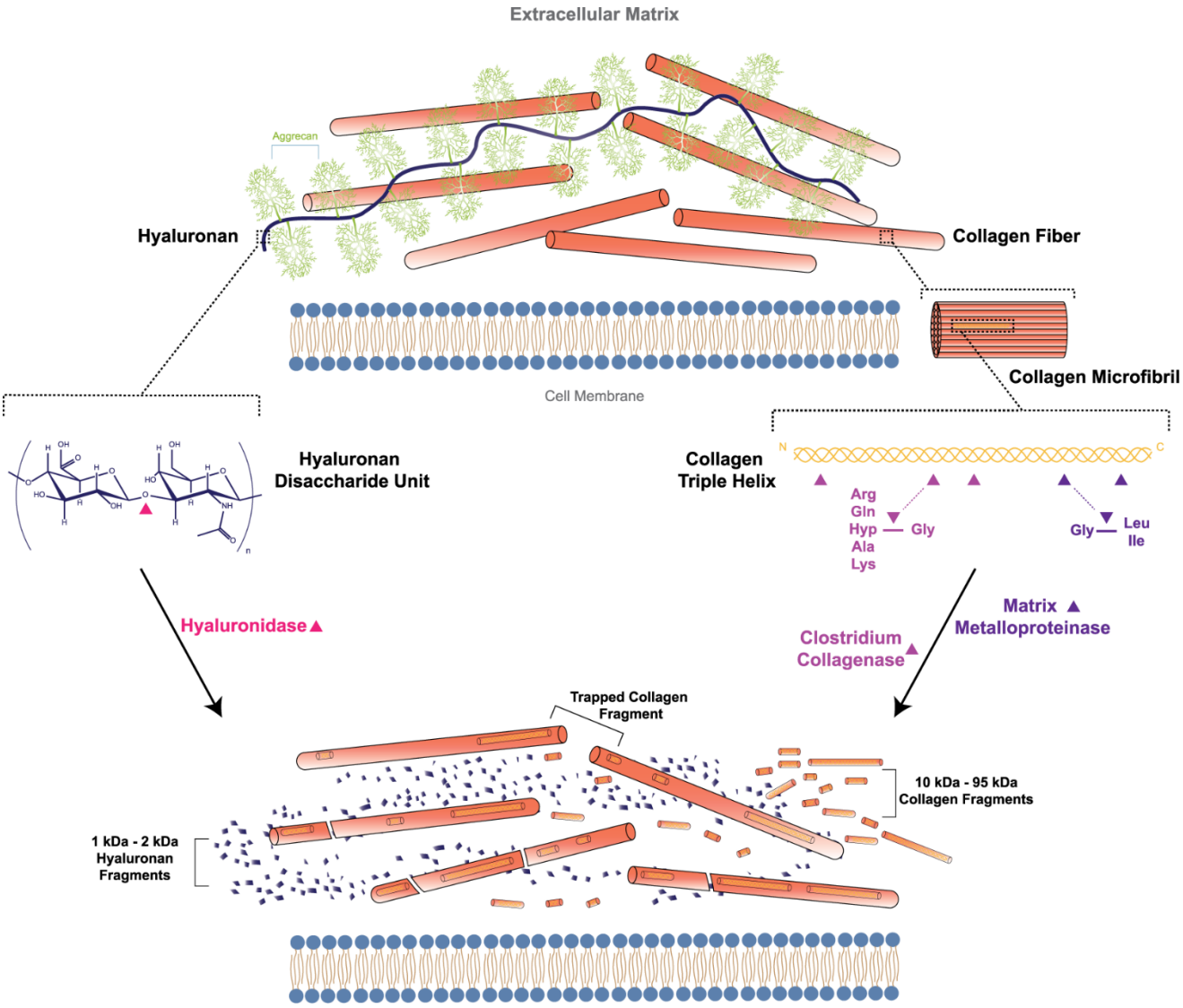

Figure 1-3: Cleavage of extracellular collagen and hyaluronan. Extracellular hyaluronan and collagen are cleaved by hyaluronidase and collagenase, respectively. Hyaluronidase cleaves at hexosaminidic bonds between β-(1,3)-D-glucuronic acid and β-(1,4)-N-acteyl-D-glycosamine, producing efficiently-cleared oligosaccharide fragments. Bacterial and human collagenases (matrix metalloproteinases-1,3,8) cleave at defined sites along the collagen triple helix.[52] Large collagen cleavage fragments may not effectively be removed from collagen fibers.

1.5 Diffusion as a predictor of drug accessibility in tumors

Diffusion is a key factor that controls delivery of therapeutics into the tumor core. The high IFP and torturous ECM within tumors limits the ability of drugs to freely diffuse.[54]

Furthermore, the amount of collagen inversely correlates with tumor diffusivity.[16] Studies examining the effects of collagenase on drug diffusion focus primarily on protein therapeutics. The findings are especially relevant because protein therapeutics are the most successful class of clinically approved macromolecules in recent years[55] and will require improved penetration for the continued clinical success.

Collagenase treatment increased the diffusion of macromolecules in tumors by a modest 2-fold in a majority of studies (Table 1-1). Alexandrakis et al.[56] observed that molecules moving through a Mu89 melanoma tumor undergo both a rapid and slow diffusion. The slower diffusion occurs in parts of the tumor with heightened ECM deposition. Intratumoral (IT) collagenase treatment removed this impediment and caused nonspecific IgG antibodies to shift from slow to more rapid diffusion by 1.3-fold within a tumor. Netti et al.[57] also investigated the role of ECM components on transport in four different tumors. HST sarcoma and U87 glioblastoma tumors had 2-5-fold more collagen relative to tumor mass than the LS174T and MCalV tumors investigated. Higher collagen content in the HST and U87 tumors corresponded with a 2-fold decrease in diffusivity of an IgG antibody. In these tumors, intratumorally injected collagenase doubled the diffusion coefficient for a labeled IgG. Notably, despite the improvement from collagenase treatment, it only restored transport to levels seen in LS174T and MCalV tumors and a larger effect may be required to significantly improve delivery to therapeutically relevant levels.

Eikenes and co-workers[58] used an intravenous (IV) injection of collagenase but also obtained a comparable 2-fold increase in diffusion for a 150 kDa FITC-dextran. Their studies were completed using an osteosarcoma (OHS) tumor model. The change in

diffusion following collagenase treatment persisted for at least 48 hours. This is promising because it would allow time for drugs to traffic into tumors and exploit the increased diffusivity to penetrate into the tumor core.

Magzoub et al. is the only study to obtain an increase in diffusion greater than 2-fold.[59] They reported a 10-fold increase in diffusion for a 500 kDa dextran at a depth of 2 mm into a tumor. While previous work relied on the more conventional dorsal skinfold window chamber tumor model coupled with fluorescence resonance after photobleaching (FRAP) to determine diffusivity (Table 1-1), Magzoub designed a fiberoptic probe to intravitally measure diffusion using a more representative melanoma tumor model. Their innovation enabled photobleaching measurements for diffusion at multiple depths within a tumor. Larger macromolecules do not penetrate deeply into dense tissues thus even a minor absolute change in the penetration could lead to a large relative change in penetration, which may be why the magnitude of this scale has not been replicated elsewhere. This is underscored by the fact that at a more superficial depth or with a smaller particle the magnitude is reduced to what was observed in previous studies. At a depth of 0.5 mm, along the tumor periphery, the increase in diffusion for the 500 kDa dextran was only 2-fold. As well, bovine serum albumin whose mass is an order of magnitude less, had an increase in diffusion of only 2-fold at all depths studied. Enhancements in tumor diffusion are overall promising but do not directly address if a 2-fold increase in diffusivity parallels an increase in total drug within tumors.

Table 1-1: *In vivo* collagenase effect on diffusion

Particle	Amount of enzyme	Duration of treatme	Route of Injection	Source	Tumor Type	Effect	Change in ECM	Ref
IgG	2000 µg	1 hour	Intratumoral	Bacterial collagenase (Sigma)	Mu89 melonoma (dorsal skinfold chamber)	1.2X increase in the percentage of particles undergoing	N/A	56
IgG	30 mg	24 hours	Intratumoral	Clostridium (Biochemical Corp)	HSTS sarcoma, U87 (dorsal skinfold chamber)	2X increase in the diffusion coefficient	N/A	57
150 kDa Dextran	100 µg	24 or 48 hours	Tail vein	Clostridiopeptidase A (Sigma)	OHS osteosarcoma (dorsal skinfold chamber)	2X increase in the diffusion coefficient	N/A	58
500 kDa Dextran, Albumin	2000 µg	3 hours	Intratumoral	Bacterial collagenase (Sigma)	B16F10 melanoma (shoulder blades)	2X increase in the diffusion coefficient (.5 mm depth). 10X increase in tumor diffusion	Reduction by Western blot	59

1.6 Drug Uptake

1.6.1 Drug Uptake: Proteins

Interestingly, collagenase treatment increased uptake of protein therapeutics by roughly the same magnitude as the increase in diffusion. Globally, uptake was enhanced 1.1-2-fold in murine tumors (Table 1-2). Collagenase treatment increased the uptake of a radiolabeled, nonspecific IgG by 2-fold in Choi et al.[60] Choi used an atypical tumor model where they implanted ovarian cancer cells, SKOV-3 or OVCAR-3, in the abdominal wall of rats then affixed a chamber to the peritoneal surface surrounding the exposed tumor. Collagenase solution followed by IgG solution was added to the chamber and allowed to enter the tumor under hydrostatic pressure. Intriguingly, along with boosting total uptake, collagenase treatment also increased the penetration distance of IgG 4-fold beyond the periphery in these ovarian tumors. This added effect points to the ability of collagenases to support the delivery of drugs deeper into the tumor core. Still, the mechanism by which this effect occurred is unclear since collagenase failed to significantly lower tumor interstitial pressure or total collagen content.

Erikson et al.[53] and Eikenes at al.[61] used an identical OHS tumor model and enzyme exposure following an IV injection but obtained a 1.1-fold and 2-fold increase in labeled TP-3 antibody uptake, respectively. The difference in uptake may be accounted for by changes to TP-3 labeling since the method to attach the fluorophore to the antibody can alter antibody pharmacokinetics.[5] Eikenes et al. biotinylated the antibody and quantified it using a fluorescent streptavidin while Erikson directly labeled the TP-3 antibody with a fluorophore. Nonetheless, because TP-3 antibodies are targeted against OHS cells, the combined work confirms that collagenase therapy can enhance uptake of

therapeutically relevant antibodies. Furthermore, when looking at changes to the tumor microenvironment, Eikenes measured a 45% reduction in IFP following treatment and a reduction in collagen by histology (not quantified), whereas Erikson and co-workers opted to measure second harmonic generation (SHG) of collagen and found no significant change in the total collagen amount following treatment. It is possible that due to the lack of change in the SHG signal, Erikson et al. did not achieve the necessary change in IFP to attain a higher increase in uptake. However, it is uncertain how changes to the tumor microenvironment are related to IFP and which modifications to ECM structure are necessary to improve drug infiltration.

Despite the variety of methods employed to degrade collagen, the degree of the effect is roughly 2-fold whether measuring diffusion or uptake. Only two studies reported significant changes in tumor IFP and none demonstrated quantifiable changes to collagen following collagenase treatment so it remains unclear what factors within the tumor microenvironment are good determinants of drug penetration following collagenase treatment (Table 1-2).

Table 1-2: *In vivo* collagenase effect on drug uptake

Particle	Amount of enzyme	Duration of treatment	Route of Injection	Source	Tumor Type	Effect	Change in ECM	Ref
IgG	37.5 U/mL	2 hours	IP Chamber	Bacterial collagenase (Sigma)	SKOV-3, OVCAR-3 ovarian cancer;	2X increase in IgG concentration in the tumor by radiography 4X increase in the penetration distance of IgG beyond the peritoneum	3X decrease in collagen by OH-Pro (not significant). 30% reduction in IFP (not significant)	[60]
IgG (TP-3)	100 µg	24 hours	Tail vein	Clostridiopeptidase A (Sigma)	OHS osteosarcoma	1.10X increase in percent area of imaged tumors exhibiting	No detectable change in imaged tumor SHG intensity	[53]
IgG (TP-3)	100 µg	24 hours	Tail vein	Clostridiopeptidase A (Sigma)	OHS osteosarcoma	2X increase in antibody fluorescence intensity throughout the	45% reduction in tumor IFP	[61]
Gadopentate-dimeglumine	10 µg*	3 hours	Tail vein	Collagenase (Sigma)	NCI-H460 Non-Small Cell Lung Cancer	1.3X increase in MRI contrast in the tumor core	50% reduction in IFP	[62]

**Total dose determined assuming a 25 g mouse*

1.6.2 Drug Uptake: Nanoparticles

Whereas an antibody has a hydrodynamic diameter less than 10 nm, nanoparticles can be upward of 10-times larger. In drug delivery, nanoparticles can encapsulate drugs often lowering drug toxicity, improving targeting, and extending circulation compared to the free drug.[63–65] In cancer, liposomal nanoparticles are the most successful drug carrier, but they rely on passive targeting through leaky endothelial fenestrations found in many types of cancer.[30,63] This phenomenon known as the enhanced permeability and retention (EPR) effect, enables nanoparticles to reach tumor sites. However, nanoparticles are notorious for their entrapment in the tumor periphery and could benefit from the removal of the tumor ECM. [66–68]

Collagenase treatment modestly increased nanoparticle penetration 1.4-2-fold (Table 1-3). The change in uptake is similar to what was observed with antibodies; however, the large diameter of nanosystems remains a barrier to penetration throughout the tumor. This is highlighted in Erikson et al.[53] where uptake of Caelyx™ (liposomal doxorubicin) content in tumors was determined following collagenase treatment. Doxorubicin fluorescence was computed and showed no significant change in payload uptake almost a day following IV injection of collagenase, which can be contrasted with the 2-fold increase of the smaller TP-3 antibody under identical conditions. This absence of an increase in liposome uptake from matrix component degradation is also reported by Kohli and co-workers[30] who inhibited hyaluronan synthase.[30]

Zheng et al.[69] also examined uptake of liposomal doxorubicin. Rather than measure fluorescence of free doxorubicin, they encapsulated a radiolabeled probe into their liposomes and measured global scintillation counts. They reported no improvement

in uptake following IV injection of collagenase. Interestingly, IT injection of collagenase increased liposomal uptake 2-fold, while only using a fraction of the enzymatic dose (scaled based on tumor mass relative to body weight). Although there is no measurement of the amount of enzyme within the tumor, the short serum half-life (6-30 minutes) of collagenases likely resulted in only a small fraction of the enzyme within the tumor 2 hours after IV injection.[70] The difference in collagenase concentration between IT and IV injection mirrored the difference in IFP. The IV injection reduced IFP for only 2 hours following collagenase administration, whereas the localized IT injection allowed the reduction in IFP to persist for 24 hours, granting liposomes more time to enter the tumor via the EPR effect.

Lee et al.[71] also relied on an IT injection of collagenase and found just under a 2-fold increase in uptake of fluorescently labeled 300 nm glycol chitosan particles. Collagenase treatment amplified nanoparticle intensity in the core of A549 alveolar adenocarcinoma tumors and doubled the signal in individual tumor cells following single-cell isolation. There is no report of changes to tumor IFP; however, these improvements were accompanied by a qualitative reduction in collagen by histology which was not quantified. Kato et al.[72] intravenously injected collagenase prior to labeled 150 nm lipoplexes and found a 1.5-fold enhancement in uptake. They injected lipoplexes 1 hour after collagenase treatment since this window corresponded with a 70% decrease in IFP. It is unclear precisely how long the reduction in IFP persisted, the authors only reported that by 24 hours IFP returned to baseline. Dosing lipoplexes 1 hour after collagenase treatment, when the reduction in IFP was greatest, likely allowed for the significant relative change in uptake compared to studies that dosed nanomaterials 24 hours following IV

collagenase treatment (Table 1-3). The authors did not track pharmacokinetic tumor accumulation of the nanoparticles but this dosing schedule could have mitigated the short serum half-life of lipoplexes (under 1 hour)[73] by allowing them to extravasate into the tumor under the reduced IFP.

Another way to exploit transient changes to IFP is to co-deliver the nanoparticle with collagenase. Co-delivery, especially if the enzyme is attached to the drug carrier, may offer improved safety and efficacy through more targeted digestion of collagen at routes of nanoparticle entry.[74] Murty et al.[75] used this approach and found a 1.4-fold increase in penetration of 30 nm collagenase-coated gold nanoparticles 24 hours after administration. Although, there is no quantification of changes to IFP or tumor collagen, attaching the enzyme to the nanoparticle could extend the circulation time of the enzyme, allowing for a more sustained alteration of the tumor microenvironment. Murty et al. used an A549 alveolar adenocarcinoma model to measure uptake of collagenase-coated gold nanoparticles, the same model used by Lee at al.[71] for glycol chitosan nanoparticles (Table 1-3). Attaching collagenase to the gold nanoparticles promoted increased penetration following IV administration of the combination, whereas Lee et al. relied on an IT injection of the enzyme. (Table 1-3).

In summary, collagenase treatment can modestly improve delivery of nanomedicines and their payload. Tumor IFP appears to be one important criteria for nanoparticle penetration, but its importance compared to other aspects of the tumor microenvironment is still uncertain.

Table 1-3: *In vivo* collagenase effect on nanoparticle uptake

Particle	Amount of enzyme	Duration of treatment	Route of Injection	Source	Tumor Type	Effect	Change in ECM	Ref
Caelyx®	100 µg	24 hours	Tail vein	Clostridiopeptidase A (Sigma)	OHS osteosarcoma	No change in the percent area of imaged tumors exhibiting labeled liposome fluorescence	No detectable change in imaged tumor SHG intensity	53
Doxil	25 or 125 µg*	20 hours	Intratumoral + Intravenous	Collagenase 2 (Invitrogen)	SCC-4 tongue sarcoma	2X increase in radiography intensity of labeled liposomes in extracted tumors at 0.5% dose (IT)	No detectable change in imaged tumor SHG intensity 35-40% reduction in IFP (under 2 hours IV) (over 2 hours IT)	69
Glycol Chitosan Nanoparticles (300 nm)	11 or 220 U/mg	72 hours	Intraturmoral	Collagenase Type 1 (Gibco)	A549 alveolar adenocarcinoma	1.8X increase in the fluorescence intensity of labeled nanoparticles in extracted tumors	Visual reduction in tumor collagen by histology (not quantified)	71
Lipoplexes with CpG plasmid (150 nm)	300 µg	4 hours	Intravenous	Clostridium type 1 (Wako Pure Chemical)	LLC lung carcinoma	1.5X increase in the fluorescence intensity of labeled lipoplexes in extracted tumors	65% reduction in IFP (1 hr after collagenase injection)	72
Collagenase coated Gold nanoparticles (30 nm)	<300 µg*	24 hours	Intravenous	Clostridium collagenase (Sigma)	A549 alveolar adenocarcinoma	1.4X increase in the percent injected dose of collagenase-labeled gold nanoparticles by ICP-OES quantification	N/A	75

**Total dose determined assuming a 25 g mouse*

1.6.3 Drug Uptake: Gene therapy

Gene therapy has long been viewed as a promising tool to combat human cancers.[76,77] However, as with other drugs, it is crucial to ensure that nucleic acids get to their intracellular targets especially since many of these products are susceptible to extracellular degradation and rapid elimination. Reduction of tumor collagen can open routes of intracellular delivery for genetic drugs. In mice, improvement in gene delivery with collagenase treatment ranges from 2-10-fold (Table 1-4). For instance, Kato et al. used their 150 nm lipoplexes described earlier to deliver luciferase plasmids in a Lewis lung carcinoma tumor model.[72] Following intravenous injection of collagenase, lipoplex uptake increased 1.5-fold while luciferase expression was 2-fold higher throughout the tumor. Despite the significant difference in size between the lipid carrier and the plasmid, the similarity in effect suggests that the penetration of the carrier may be critical for the penetration of the contents in gene therapy. The magnitude here also echoes the effect observed for liposomal doxorubicin contents discussed earlier. [53]

Cemazar et al.[78] bypassed the need for a carrier by directly injecting luciferase and green fluorescent protein (GFP) plasmids into various tumors following IT collagenase treatment. They applied electric pulses to aid in gene transfer after administering the plasmid but found no significant changes in gene delivery with collagenase treatment despite a 75% decrease in the area density of collagen. However, treatment with both collagenase and hyaluronidase resulted in a 10-fold increase in the percent transfected area of GFP up to 15 days post administration and a 10-fold increase in functional luciferase within the tumor 2 days after administration. The extent of the effect observed is one of the largest reported following ECM digestion and suggests that the

administration of two enzymes active against the major extracellular components of the ECM, hyaluronan and collagen, may be needed for large improvements in the gene titers within the tumor.

Kuriyama et al.[79] also employed a combination therapy for improved gene therapy in the U-87 glioblastoma mouse model. A collagenase/dispase mixture administered IT improved the delivery of a herpes simplex virus (HSV) coding for thymidine kinase measured by tumor growth. Dispase exhibits extracellular proteolytic activity against both fibronectin and collagen.[80] There was no quantification of the change in viral delivery, but collagenase/dispase treatment followed by gene delivery reduced tumor weight and volume by over 80% compared to a PBS control. Even though there is uncertainty around the amount of virus inside the tumor, this study begins to address the downstream question of the antitumor efficacy of collagenase pretreatment.

McKee at al.[81] computed changes to HSV penetration as well as subsequent effectiveness in limiting tumor growth with collagenase matrix reduction. They found that when a GFP encoding HSV was co-injected IT with collagenase there was a 3-fold increase in viral distribution measured by quantifying the spread of GFP intensity away from the injection site. In addition, collagenase-treated tumors exhibited increased presentation of HSV antigen in tumors 2 days following treatment and decreased overall tumor growth. There was a 2-fold increase in the time for the tumor to grow ten-times its original size compared to treatment with the oncolytic virus alone. They employed second harmonic generation imaging of collagen to describe the importance of collagen in limiting viral penetration. The viral particle penetration was inversely related to collagen density. The relative change in collagen observed with treatment is, however, not reported.

Notably, these gene therapy studies employed an IT delivery of collagenase and with the exception of the luciferase lipoplexes, the virus or plasmid was also delivered IT (Table 1-4). It remains unanswered how collagenase treatment would affect gene delivery in an IV setting. Irrespective of the approach taken, further quantification of changes in collagen is needed to understand the potential of matrix removal strategies in solid tumor gene-therapy.

1.6.4 Drug Uptake: Imaging agent

Beyond augmenting the therapeutic treatment of tumors, collagenases may also aid in tumor diagnosis and evaluation. Hassid et al.[62] showed that IV collagenase could increase the concentration of a gadolinium-based MRI contrast agent, GdDTPA, in an orthotopic non-small cell murine lung cancer tumor. They measured a 1.33-fold increase in GdDTPA steady state concentration in the tumor core during an IV infusion performed 3 hours following collagenase treatment (Table 1-2). GdDTPA was also more homogeneously distributed throughout the tumor compartment. The authors propose that this increase is likely due to the 65% reduction in IFP observed in treated tumors 5 hours after collagenase therapy. Although the overall effect is modest, using a contrast agent could be a beneficial tool to identify tumors that are most responsive to collagenases, to stratify patients that are more favorable to matrix reduction and to reveal a beneficial window for drug dosing post collagenase therapy.

Table 1-4: *In vivo* collagenase effect on gene delivery

Particle	Route of Injection	Amount of enzyme	Duration of treatment	Source	Tumor Type	Effect	Change in ECM	Ref
Lipoplexes with CpG plasmid (150 nm)	Intravenous	300 µg	4 hours	Clostridium type 1 (Wako Pure Chemical)	LLC lung carcinoma	2X increase in luciferase activity in tumor tissue lysate	65% reduction in IFP	[72]
pEGFP-N1, pCMVLuc plasmid	Intratumoral	30 µg	24 hours	Collagenase (Roche Diagnostics)	LPB; fibrosarcoma	10X increase in the percent of GFP positive areas in imaged tumors (combination treatment with hyaluronidase, no effect collagenase alone) 10X increase in luciferase activity in tumor lysates	75% decrease in area density of collagen by histology	[78]
Ad-HSV-tk	Intratumoral	10 µg	24 hours	Collagenase/ dispase (Sigma)	U87, U251 glioblastoma	6X reduction in tumor volume 50 days post administration of virus with collagenase/dispase	N/A	[79]
VP16-GFP HSV	Intratumoral	0.2 µg	30 minutes	Bacterial collagenase (Sigma)	Mu89 melanoma (dorsal skinfold chamber)	3X increase in viral distribution by fluorescence away from injection site	N/A	[81]

Traditional 2-D cell culture lacks a suitable architecture and ECM to reliably study the effects of matrix breakdown.[84,85] 3-D tumor spheroids are the preferred *in vitro* model for collagenase therapy since they mimic several aspects of the avascular portions of a tumor, including epithelial tight junctions, an inhibitory ECM, cellular heterogeneity, and a proliferating and quiescent region along with a necrotic core.[86–88] The use of tumor spheroids is contentious as a means to evaluate drug delivery systems; however drug penetration studies in tumor spheroids have demonstrated a 2- to 11-fold increase in particle delivery following collagenase treatment, which is on the same order as what is observed *in vivo* (Table 1-5). However, as with *in vivo* experiments, spheroid studies seldom report quantifiable changes to tumor collagen with collagenase treatment.

Eikenes et al.[58] found that despite a 2-fold increase in diffusion of a 150 kDa dextran *in vivo,* there was no significant change in dextran diffusion *in vitro* in tumor spheroids. However, Elkenes observed that the larger 2 mDa dextran showed an almost 2-fold increase in diffusion following collagenase treatment in the same OHS spheroids. This suggests that spheroids may be useful predictors for the diffusion of larger particles, but the diffusion of lower molecular weight drugs may not be sufficiently inhibited by the spheroid ECM to observe the effects of collagenase treatment.

Goodman et al.[89] and Cui et al.[90] both measured the penetration of various nanoparticles as a function of their diameter and observed that collagenase treatment increased penetration in a size-dependent manner. Goodman et al. found a 7, 12, 3, and 1.5-fold increase in fluorescence in the spheroid core for 20, 40, 100 and 200 nm fluorescently labeled polystyrene nanoparticles, respectively. The effect of collagenase treatment on particle uptake peaks for 40 nm particles but is much less pronounced for

the 100 and 200 nm particles. When collagenase was attached to the surface of the 100 nm particle there was a 4-fold further increase (totaling ~12-fold) in fluorescence signal beyond the spheroid periphery compared to an equivalent particle given with free collagenase.

Cui et al.[90] coated albumin nanoparticles with collagenase and found a 6 and 27% increase in penetration for 100 and 200 nm particles, respectively. Spheroids were imaged after a 96-hour exposure to collagenase-coated nanoparticles to determine the localization of the nanoparticles. It is important to note that the 200 nm particles exhibited approximately 2-fold greater collagenase activity than the 100 nm particles, which could account for the larger percent increase in localization. The authors did not quantify the total fluorescent signal in spheroids which makes it difficult to compare the magnitude of change to what was seen by the nanoparticles in Goodman et al..[89] However, the authors noted that only the 100 nm collagenase-coated nanoparticles displayed increased signal in the spheroid core (unquantified) which supports the importance of particle size for deep penetration within spheroids. These studies replicate the enhancement in nanoparticle penetration observed *in vivo* by Murty et al.[75] (Table 1-3) when collagenase is covalently attached to the nanoparticle.

Spheroids were also evaluated as models for determining enhancements in gene therapy following ECM clearance. In 9L rat glioma tumor spheroids, collagenase therapy showed no improvement in the delivery of an AAVP tumor-targeting phage carrying a luciferase gene.[91] However, the combination of collagenase and hyaluronidase increased luciferase activity almost 3-fold in these tumor spheroids. The magnitude is smaller than what was observed *in vivo* with luciferase and eGFP plasmids[78] but aligns with the finding

that digestion of multiple ECM components can provide greater improvement in macromolecular delivery (Table 1-4).

Although the improvements in drug penetration with spheroids are consistent with those *in vivo*, their use is not without caveats. The relationship between spheroid collagen content and drug uptake is unclear. Spheroid morphology and response to external stimuli are extremely sensitive to the method used to produce the 3-D cells.[87] In addition, spheroid penetration studies are limited to tumor cells, which can form spheroids at appropriate sizes to adequately restrict drugs. Spheroids have also not demonstrated the ability to measure changes in penetration of small molecule and protein therapeutics following ECM breakdown. More quantitative studies are needed using standardized methods for growth and viability and that show that outcomes in spheroids replicate *in vivo* before spheroids can be considered fully vetted tools for assessing drug penetration.

1.7 Overall outlook; needs and benefits

It is undetermined if the moderate improvements in drug penetration observed *in vivo* with collagenase treatment in animals will translate to patients. There are major concerns regarding the toxicity of injected collagenases due to the potential for increased tumor metastasis,[92–100] degradation of collagen in healthy tissues,[71,101] and immune reactions against bacterial collagenases.[75] For instance, collagenases that could improve drug delivery when administered at 100-300 µg/mouse resulted in fatalities when injected at greater than 500 µg/mouse.[61,72] It is debatable whether the potential efficacy is enough to overcome such a narrow therapeutic window.

Table 1-5: *In vitro* collagenase effect in tumor spheroids

Particle	Amount of enzyme	Duration of treatment	Source	Tumor Type	Size (µM)	Effect	Ref
2MDa, 150 kDa Dextran	1-10 mg/mL	1 hour	Clostridiopeptidase A (Sigma)	OHS osteosarcoma	150-250	70% increase in the diffusion coefficient of a 2 mDa Dextran. No change for the 150 kDa particle (even after 18 hours)	58
Polystyrene beads	0.004-1 mg/mL	5 hours	Clostridium Type I (Sigma)	SiHa cervical carcinoma	400-500	12X increase in the fluorescence intensity in spheroid core for 40 nm particle; 7X for 20 nm, 3X for 100 nm; 1.5X for 200 nm; 4X for 100 nm collagenase coated nanoparticles	89
Collagenase coated albumin nanoparticles	N/A	96 hours	Clostridium Type I (Sigma)	C8161+ melanoma cocultured and HFF (human foreskin derived fibroblasts)	300-400	5% increase in imaged total area of labeled particles in spheroids for 100 nm particle; 27% for 200 nm	90
AAVP Bacteriophage vector	100 µg	1 hour	Clostridium Type I (Sigma)	9L Glioma	N/A	2.6X increase in luciferase expression. 40% decrease in cell viability (67% in combination with hyaluronidase)	91

1.7.1 Efficacy: hyaluronidase versus collagenase

Hyaluronidase experiments offer a good benchmark for understanding the translational capacity of collagenases. Several studies compared injected collagenases to injected hyaluronidases to determine which was superior at increasing drug penetration. Despite collagenases only cleaving collagen into large fragments which may become trapped in the ECM (Figure 1-3), collagenases were generally equal to or better than hyaluronidases. For instance, hyaluronidase treatment reduced diffusion by about 2-fold at all depths of a melanoma tumor for a 2 kDa dextran while collagenase treatment had the opposite effect.[59] Collagenase and hyaluronidase both doubled the diffusion coefficient of a larger 150 kDa dextran in an osteosarcoma tumor, but the effect did not persist beyond 2 days for hyaluronidase treatment whereas the increased diffusivity remained higher for at least 2 days in collagenase treated tumors.[58] For antibodies of similar size, hyaluronidase decreased the portion of labeled IgG antibodies undergoing rapid diffusion within melanoma tumors by 40%, whereas collagenase increased it by 20%.[56] A similar result revealed that hyaluronidase treatment reduced uptake of a TP-3 antibody by 10%, but collagenase treatment enhanced it by 10%.[53] Interestingly, hyaluronidase treatment increased uptake of liposomal doxorubicin by 4% despite collagenase treatment having no effect in the same model.[53] In another study, both collagenase and hyaluronidase increased delivery of glycol chitosan nanoparticles by about 2-fold in an alveolar adenocarcinoma.[71] Of note, the authors mentioned that the brightest signal of the labeled particle in tumors came from the collagenase-treated group. Additionally, in the tumor microenvironment, hyaluronidase treatment showed no change in IFP and had a minimal effect on IgG transport despite the removal of 90% of the

exposed tumor HA in an ovarian cancer model while collagenase improved uptake 2-fold with only minimal changes to tumor collagen.[60] The lack of change in collagen could be due to insufficient clearance of hydrolyzed collagen fragments from fibrillar bundles.

Gene delivery appears to be the one area where collagenase is not clearly superior to hyaluronidase. Collagenase treatment alone was found to not sufficiently improve gene therapy and had to be used in combination with hyaluronidase to enhance uptake.[78,91] In multiple *in vivo* tumors although the combination was superior, hyaluronidase treatment attained a lesser but significant improvement in delivery of a luciferase plasmid in three (SA-1, EAT, and B16) of the four (LPB) tumors investigated.[78] In 9L glioma tumor spheroids, hyaluronidase alone was no better than collagenase at improving delivery of an AAVP phage.[91]

Hyaluronidases have been more extensively studied than collagenases and are generally observed to enhance drug penetration and reduce IFP in tumor models.[35] The benefits of hyaluronidase treatment appear to translate clinically, therefore based on the experiments which showed collagenase treatment is a better driver of drug penetration than hyaluronidase treatment, collagenases could have the same, if not better, clinical efficacy.[18,19] Importantly, there are large differences between the ECM turnover of HA and collagen. In parts of the body, HA has a rapid half-life of under 2 days while collagen has a significantly slower half-life of several months to upward of 15 years.[37,102] Although tumors can reduce ECM turnover,[103] the difference in half-life of collagen and HA could explain why collagen reduction had a more robust effect. Even minor changes in collagen structure could have a pronounced effect on drug penetration since collagen content is unable to recover. In the phase II PEGPH20 clinical trial, hyaluronidase was administered

twice per week in a typical 4-week cycle.[104] Due to the slower turnover of collagen, long-circulating collagenases could be dosed less frequently reducing the overall medical burden of the therapy. The slow turnover of collagen does, however, increase safety concerns around the effect of removing collagen in healthy tissues.

1.7.2 Collagenase Safety

Despite a short serum half-life of 6-30 minutes,[70] intravenous injection of bacterial collagenases at amounts greater than 500 µg (0.5%) is lethal to mice due to abdominal and pulmonary hemorrhaging and necrosis of the lungs.[61,72,101] This toxicity is an important concern for injectable collagenase treatments. At a systemic dose below this, the enzyme did not demonstrate lethality nor drug accumulation in other body compartments while increasing drug penetration in tumors (Tables 1-1-1-4). Following IT administration of collagenase there was no significant toxicity in any major organ as well as no change in drug biodistribution in tissues outside of the tumor.[69,71] The lack of organ toxicity and change in biodistribution also held true after IV collagenase.[71] At a dose of 300 µg, there were no observed changes to the delivery of lipoplexes or the luciferase plasmid cargo in any organs outside of the tumor compared to animals without collagenase treatment.[72] Collagenase-coated nanoparticles reported no injury to the liver or spleen, the major organs for nanoparticle accumulation (as quantified by histology) or an abnormal elevation in any biochemical blood markers.[75]

There are concerns that treatment of tumors with collagenases might increase metastases of malignant cells from the parent tumor. This has not been observed. Six weeks following collagenase injection, there were no signs of increased metastasis in treated animals.[78,81] More data on tolerability in large animals at higher doses (>0.5%)

are required to satisfy the safety concerns surrounding collagenase injection. Nevertheless, current data, using low collagenase doses shown to be effective, suggest little off-target toxicity and no tumor metastasis.

The immunogenicity of bacterial collagenases is another safety concern. From Xiaflex® human safety trials, a majority of patients exhibited anti-collagenase antibodies by the third injection.[70] All patients developed antibodies by the fourth injection and 10-20% of the antibodies were found to be neutralizing, which would interfere with subsequent treatments and potentially cross react with human matrix metalloproteinases.[70] Perhaps this effect can be mitigated in the same manner as hyaluronidase by switching to a PEGylated human collagenase.[34]

1.8 Ongoing needs to validate matrix reduction therapies to improve cancer treatment

1.8.1 Therapeutic requirements

The current literature indicates that collagenases can be both effective and tolerated at low doses in mice but to solidify these findings we must better understand the changes to the tumor matrix subsequent to collagenase treatment, particularly the clearance of collagen fragments, the rebound of collagen fibers to pretreatment levels, and the functionality of tumor blood vessels; use more relevant tumor models which broaden the solid tumor types that are treated with collagenases; and move beyond unspecific bacterial collagenases. First, few studies quantified changes to tumor collagen content or organization following collagenase treatment. Those that did quantify found little to no effect in collagen that correlates with changes in probe penetration (Tables 1-1-1-4).

Small (12 kDa) degradation fragments of collagen can separate from fibers and be directly measured in plasma whereas larger fragments require additional proteolytic cleavage.[102,105] The dose of collagenase used to improve drug infiltration may not allow adequate cleavage of collagen to liberate larger fragments.

For instance, one study validating the use of SHG to measure tumor collagen showed that an IT collagenase dose of 10 mg,[106] which is substantially greater than the doses used in a majority of studies measuring drug penetration, was required to observe dramatic changes in tumor SHG intensity. Lower collagenase doses may only exhibit minor changes to tumor collagen. This makes it difficult to know whether a change in total collagen or a change in collagen structure is needed or for how long that change must persist in order to observe increased probe penetration. In addition, there is little understanding of how collagenase treatment reduces tumor mechanical stress and normalizes drug perfusion. Changes in tumor IFP offer a surrogate for the robustness of the effect of collagenase treatment in some instances but a more complete understanding of what happens to collagen, the ECM architecture, and tumor pressure after treatment is needed.

Second, the dorsal skinfold window chamber tumor model is the most widely used because it allows for intravital imaging. The problem is that this model is limited to tumors which can grow in that environment where they may not exhibit a canonical array of tumor behaviors in that atypical microenvironment.[82] As such, traditional orthotropic and spontaneous tumors would serve as better models to assess the benefits of collagenase treatment. In these models, it is essential to demonstrate that an increase in particle penetration causes an increase in overall survival. The few studies that seek to address

this show decreases in tumor volume but do not unequivocally show improved *in vivo* survival. Performing IV over IT injections of collagenase should also be prioritized since the need for defined tumor boundaries for a successful IT injection may limit the tumors that are candidates for matrix reduction therapies.

Third, studies discussed here use bacterial collagenase which exhibits activity on a variety of collagens.[107,108] Collagen I is the most abundant in vertebrates, but there are 28 different types of collagen identified.[9] Several types of collagen including collagen I, II, III, IV, V, and IX are implicated in cancer progression.[9,10] Therefore, it could be advantageous to tailor the collagenase to the tumor or create a mixture of collagenases that would digest collagens in many different tumor types. In this regard, matrix metalloproteinases (MMP), in particular, should be further explored for ECM degradation because they would limit the immunogenicity from a bacterial collagenase as well as offer a library of proteinases to better match the collagenase to the type of tumor collagen.

1.8.2 Matrix metalloproteinases

There are 23 different MMPs which target various aspects of the ECM.[109] The three collagenases, MMP-1 (human collagenase 1), MMP-8 (human collagenase 2), and MMP-13 (human collagenase 3) and two gelatinases, MMP-2 (gelatinase A) and MMP-9 (gelatinase B), would be the most useful because of their ability to cleave native collagen and its gelatin fragments.[109] MMP-1, MMP-8, and MMP-9 were shown to increase delivery of oncolytic viruses when transfected into tumor cells (Table 1-6). For instance, tumor cells engineered to express MMP-1 or MMP-8 displayed improved penetration of a virus into the tumor core and increased overall viral load 3-fold compared to control tumors *in vivo*.[110] The enhancement in viral delivery was therapeutically efficacious by slowing

overall tumor growth. A complementary study demonstrated complete survival in mice bearing BxPC-3 pancreatic cancer xenografts over 7 weeks when co-injected with an oncolytic virus along with a nonreplicating virus carrying an MMP-8 gene. Mice given the oncolytic virus alone exhibited only 20% survival over the same period.[111]

The primary caveats with MMPs are that they have limited yields when produced recombinantly and certain ones are postulated to be linked to metastasis.[92,94–97] Bacterial expression of MMPs requires purification from insoluble inclusion bodies and lengthy refolding protocols.[112–114] In addition, bacterial expression is limited to truncated versions of the proteinases, often lacking their collagen binding domain.[115,116] Mammalian and insect expression systems can produce full-length MMP protein with a proper glycosylation pattern, but yields generally do not exceed a few milligrams per liter of culture.[117] Even with the expression limitations, MMPs may offer a precision in ECM degradation that cannot be achieved with the bacterial collagenases used in previous studies. Production constraints create a bottleneck for advancing the use of MMPs for improved delivery in academic laboratories but the potential therapeutic upside warrants deriving methods for increased throughput.

MMPs have long been implicated for their role in promoting tumor metastasis by supporting extravasation and subsequent intravasation of tumor cells.[118] However, after failure of MMP inhibitors in the clinic,[92] there is a greater appreciation for the nuanced roles of MMPs at various stages in tumor progression. For example, MMP-8 has been shown to limit the invasiveness of breast cancer cells.[119] In addition, patients with higher MMP-8 expression presented a lower incidence of lymph node metastasis.[119] In mice, lung tumors engineered to overexpress MMP-8 showed no evidence of increased

metastasis or tumor progression.[111] MMP-3, 9, and 12 have also exhibited antitumor activities, such as reduced tumor cell migration and invasiveness in murine cancers.[120,121] Furthermore, considering that bacterial collagenase experiments showed no tumor metastases despite their broad activity for various collagens, MMP therapies may be much safer than the current wisdom would indicate.[69,71,75]

1.8.3 Combination therapies

In addition to broadening the collagenase repertoire, combinations of enzyme digestion treatments should be further studied with the caveat that total depletion of all biopolymers in the ECM may be counterproductive. Collagenase and hyaluronidase combinations have already allowed for improvements in gene therapy.[78,91] Additional combinations of ECM degrading enzymes could allow for a more complete clearance of the inhibitory tumor ECM. Synergies could be achieved using collagenases and mammalian gelatinases, since the gelatinases can break down large collagen fragments produced when collagen is enzymatically cleaved,[102] enabling improved clearance of collagen and further opening the ECM to drugs. Selecting the appropriate enzyme or combination may allow for quantifiable changes in total collagen, which have alluded researchers thus far. Combinations involving collagenases with collagen[40] or hyaluronan synthesis inhibitors[29,30,41] should also be attempted to further improve ECM drug penetration into tumors. Intravenous collagenases could first be used to clear the tumor ECM followed by collagen synthesis inhibitors to sustain this effect for an extended period, starving the tumor of the benefits of a dense ECM while allowing more drug to enter.

Table 1-6: MMPs used to improve drug delivery

Particle	Duration	Source	Tumor Type	Effect	Change in ECM	Ref
HS Vector MGH2	7 days	MMP-1 and MMP-8 expressing HSTS26T	HSTS26T Sarcoma	5-10X increase in viral immunostaining at tumor center 1.3X decrease in tumor growth	No detectable change in imaged tumor SHG intensity	[110]
Adwt300 virus	Up to 50 days	MMP-8 expressing A549 and BxPC-3 cells	A549 alveolar adenocarcinoma BxPC-3 pancreatic cancer	Increase in viral distribution by viral immunostaining (unquantified) 3X decrease in tumor volume (days 30-50) Complete survival of animals (BxPC-3)	3X decrease in visible collagen by histology	[111]
HSV-eGFP	21 days	MMP-9 expressing SK-N-AS	SK-N-AS Neuroblastoma	3X increase in GFP positive cells (Spheroids) Increase tumor vector distribution by viral immunostaining (unquantified)	N/A	[121]

1.8.4 Additional therapeutic areas

Although the focus of this review is on the benefits of collagenase treatment in cancer, collagenases could be beneficial in other diseases which feature abundant collagen deposition. These areas could offer insights involving pharmacokinetics, pharmacodynamics, and biodistribution of collagenases which could inform tumor studies. The benefits of collagenases in disease are reviewed elsewhere.[122,123] In short, collagenases could be most beneficial in orthopedics, wound healing, and fibrosis. With early collagenase trials in patients to treat back pain and the approval of Xialfex®, there is a wealth of clinical data available on how collagenases behave near joints and bones.[124,125] In homeostatic repair, collagenases are able to clear debris from necrotic

tissues and promote dermal cell migration.[126] As such, collagenases are used clinically to enhance healing in burn injury.[127] Collagenases were also explored in fibrosis to clear extracellular deposits. In a rat model of liver cirrhosis, MMP-8 and MMP-13 transfected into hepatic cells showed a significant reduction in liver cirrhosis compared to the control.[128,129]

1.9 Conclusion

The increased exploration using macromolecules, nanoparticles, and viruses to treat cancer motivates the need for ways to improve penetration of these agents into tumors. The data for injected collagenase treatment suggest it to be relatively safe and modestly efficacious (Tables 1-1-1-6). However, before that potential can be fully realized, investigators will have to explicate how collagenase treatment affects the amount and structure of tumor collagen and how changes in collagen relate to alterations in the tumor microenvironment. This information could be used to understand precisely what changes to the ECM are needed to enhance drug delivery as well as enable an appropriate selection of enzyme combinations and matrix metalloproteinase subtypes to maximize drug uptake in tumors. Making these rational improvements could digest a path forward for matrix reduction therapy as a clinical modality to enhance the delivery of drugs, macromolecules, and nanoparticles into solid tumors.

2 Chapter 2: Sulfated liposomes for targeted anticancer therapy

2.1 Introduction

Advances in liposome drug development have culminated in over ten approved liposomal therapies.[63,130] Despite steady progress in the field, the sub-optimal release of drug cargo limits the safety and efficacy of liposomal therapies. As a result, considerable efforts have focused on triggerable liposomes that liberate contents by employing external (ultrasound, light, heat) or local (pH, enzymes) cues to facilitate liposomal content release. External stimuli control where drug content is released through the precise application of the stimuli. This approach can be applied to the primary tumor but fails to target metastatic nodes which are often responsible for patient mortality.[64] Local cues, exploiting aspects of the tumor microenvironment such as low pH or the overexpression of enzymes including matrix metalloproteinases[131] and phospholipases,[132] allow for directed release of liposomal cargo. Enzymatically-triggered systems, in particular, could have utility at sites of metastasis since many target enzymes are substantially upregulated due to their roles in tumor cell migration and invasion. For instance, extracellular sulfatases have up to 70-fold higher expression in tumor cells compared to healthy tissue making them attractive targets for a triggered release system.[133]

Human sulfatases are a highly conserved class of enzymes that are responsible for the cleavage of sulfate esters yielding a hydroxyl group. Two extracellular sulfatases, SULF1 and SULF2 (SULFs) are overexpressed in a variety of tumors including lung squamous cell carcinoma, pancreatic adenocarcinoma, hepatocellular carcinoma, and invasive breast carcinoma.[134–137] In many cases, overexpression correlates with a more aggressive tumor and reduced patient survival.[138] The SULFs are involved in the removal

of the 6-O sulfate of heparan sulfate proteoglycans (HSPGs) at the cell surface.[139] HSPGs are key structural components of the extracellular matrix and are ubiquitously found across several cells. In addition to structural integrity, HSPGs are pivotal in cell signaling because of their ability to bind various receptors, enzymes, growth factors, chemokines and cytokines based on the HSPG sulfation pattern.[140] Consequently, HSPGs and SULFs are implicated in tumor development and progression.[140] SULFs are involved in proliferative signaling (Wnt ligands, FGF),[141] migration (CXCL12),[142] and angiogenesis (VEGF, endostatin)[143] – all players in tumor progression. The consensus in the field is that the SULFs promote tumorigenesis by lowering the affinity of HSPGs for Wnt ligands via sulfate removal. Wnt is then free to bind its Frizzled receptor which leads to cell proliferation.[138,140] Thus, the overexpression of SULFs on tumor cells compared to normal tissue, make SULFs a rational target for the selective release of drugs from nanoparticles.

Our group has synthesized a series of inverse-charge zwitterionic lipids with a flipped charge orientation compared to naturally occurring lipids since the cationic amine is at the bilayer interface and the anion extends into the aqueous phase. These were prepared with diverse anionic headgroups including carboxylate, phosphate, and sulfonate.[63] Removal of the anionic headgroup will produce a cationic particle that can interact with negatively charged cell membranes. This could facilitate increased uptake or transient membrane destabilizing and allow for enhanced delivery of the therapeutic cargo. We hypothesize that liposomes containing a lipid with a terminal sulfate and quaternary amine headgroup (AS) can be engineered to selectively deliver contents to cells that overexpress sulfatases due to enzymatic removal of the negatively charged sulfate, creating a cationic particle (Figure 2-1).

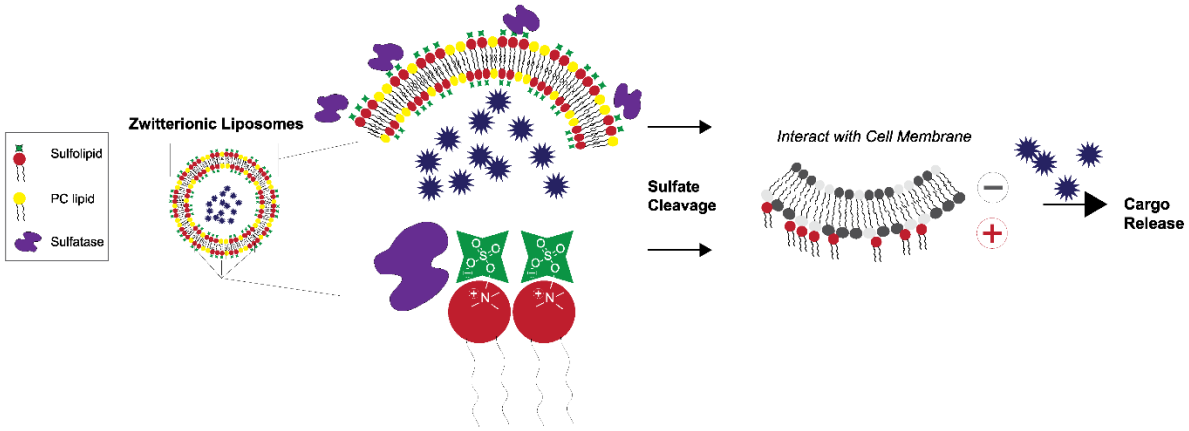

Figure 2-1: Schematic of content release from sulfated lipid nanoparticles. In the presence of extracellular sulfatases, the terminal sulfate will be cleaved yielding a cationic liposome which can interact with the negatively charged cell membrane facilitating liposomal uptake and downstream content release.

2.2 Results

2.2.1 Gene Expression

To verify overexpression of SULFs in tumors compared to normal tissue, Illumina HiSeq expression from the TCGA PANCAN dataset was analyzed for SULF expression (Figure 2-2). Expression data confirmed that both SULF1 and SULF2 are overexpressed in a variety of tumors. The Log_2 difference in expression varied based on the tumor type, with breast, colon and lung carcinomas exhibiting the largest differences in SULF expression between normal and tumor tissue. The difference is more pronounced for SULF1 than SULF2. Still, SULF enhancement in multiple tumor tissues supports the use of these enzymes as triggers for nanoparticle drug delivery.

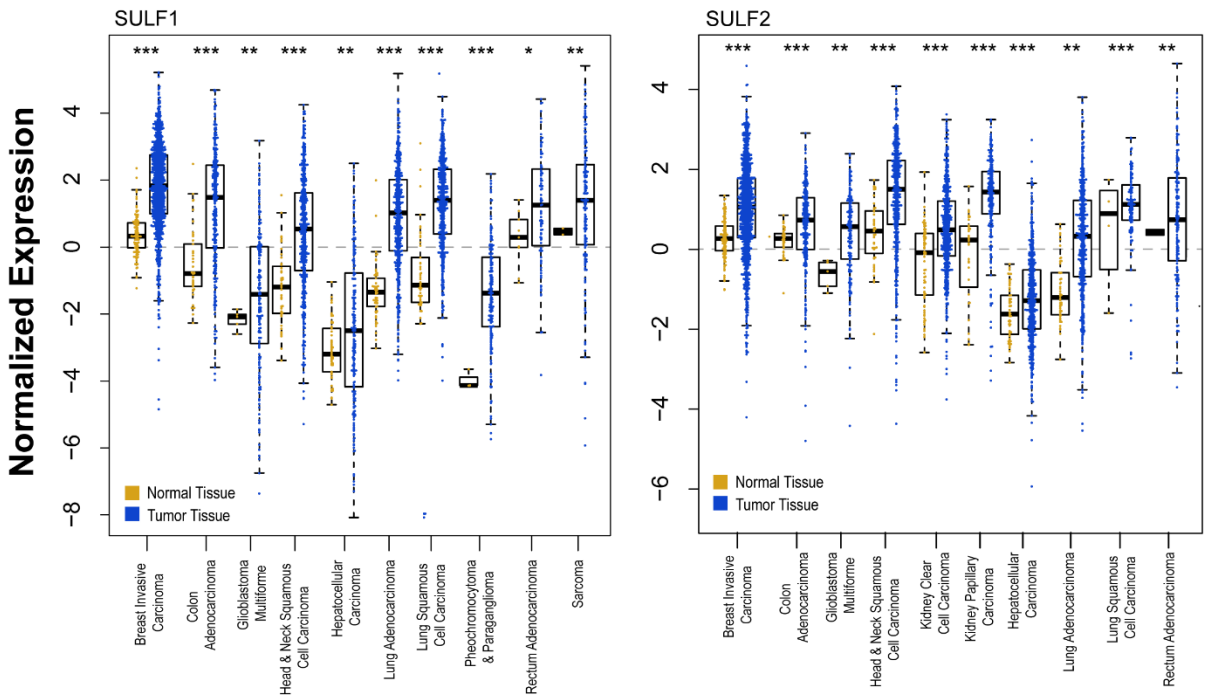

Figure 2-2: Gene expression of SULF1 (left) and SULF2 (right) from TCGA PANCAN dataset. Log_2 differences in normalized gene expression show that the two SULFs are overexpressed in a variety of tumor types. *p<0.05, **p<0.01, ***p>5 x 10^{-5}, t-test.

2.2.2 Synthesis

Upon verifying the overexpression of SULF1 and SULF2 in tumor tissues we looked to synthesize a series of novel sulfolipid substrates (Figure 2-3). Initially, a sulfate headgroup precursor was generated through sulfation of bromopropanol or hydroxylphenethyl bromide with sulfurtrioxide–pyridine to afford the sulfate precursor 1 and 1a respectively. Subsequently, 3-(dimethylamino)-1,2-propanediol was acylated with a variety of lipid tails and the resulting products (2a–f) were alkylated with bromopropylsulfate (1) at the amine to afford the final products (3a–f) containing a quaternary amine and terminal sulfate. An aromatic inverse sulfolipid was also produced by quaternization of 2d with 1a. Upon sulfation, most of the lipids (3b–3f, 4) precipitated

at 60ºC to yield pure products. Additional recrystallization was performed to remove minor impurities. DOAS (3a) failed to precipitate in DMF and was purified by silica gel chromatography.

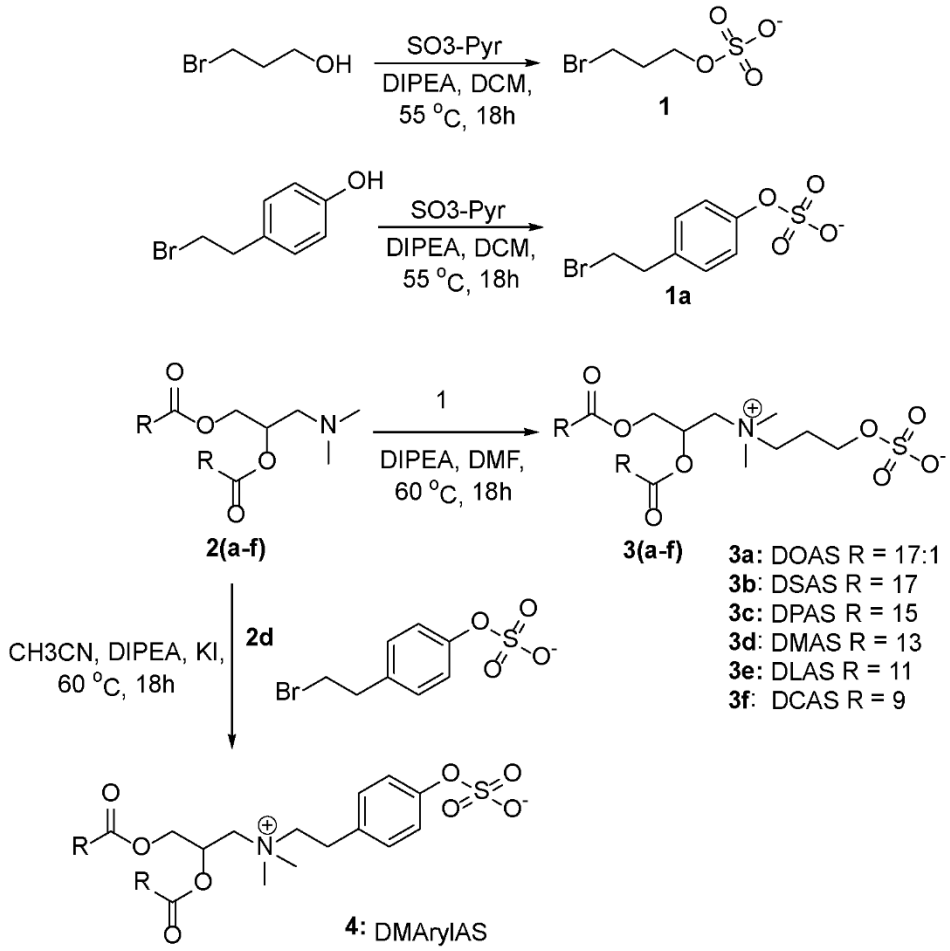

Figure 2-3: Reaction scheme for the synthesis of inverse sulfolipids

2.2.3 Phase transition temperature

The phase transition temperature for each of the sulfolipids was determined by differential scanning calorimetry. Each of the pure lipids had exceptionally high transition temperatures (Tm) (Figure 2-4). The Tm determined for each lipid is 38, 89, 83, 76, 67,

56 and 87ºC for DOAS (3a), DSAS (3b), DPAS (3c), DMAS (3d), DLAS (3e) DCAS (3f), and DMArylAS (5), respectively. The elevated Tm observed with the AS series of lipids are higher than those observed for previously synthesized inverse lipids.[144–146] Phase transition temperatures of all lipids are 30–60ºC higher than phosphatidylcholine (PC) lipids of equivalent chain length and highlights the role of headgroup interactions on the gel to liquid lipid transition. To the best of our knowledge, this is the first report of a cis-unsaturated lipid (DOAS) with a transition temperature above 25ºC.

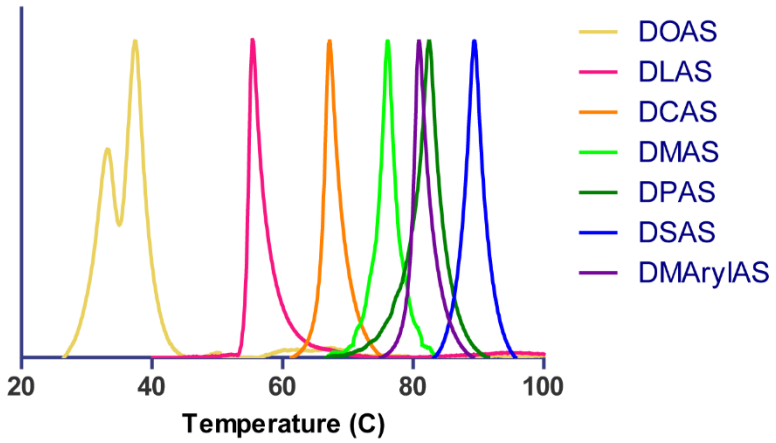

Figure 2-4: Transition temperature of AS lipids. AS lipids display high phase transition temperatures as a result of the interactions from the zwitterionic headgroup.

2.2.4 SULF Activity

Next, sulfolipids were assessed for their propensity for sulfatase cleavage. Initially, SULF2 was collected from the conditioned media of MCF-7, a common approach for assaying human sulfatases.[147] SULF2 activity from conditioned media was verified using a known probe, methylumbelliferyl sulfate (MU-S). As expected, MCF-7 cells secreted activate sulfatases to a significantly greater extent than other cells grown under identical

conditions (Figure 2-5). Due to the poor aqueous solubility of the lipids, sulfatase activity was assessed using the sulfate head precursors 1 and 1a. Unlike, MU-S whose sulfate cleavage can be monitored by fluorescence, sulfate cleavage was monitored by turbidimetry by the formation of barium sulfate precipitates from liberated sulfate ions in the presence of free barium. Surprisingly, there was no sulfate cleavage of the newly synthesized sulfate groups (Figure 2-5). Despite SULF possessing aryl sulfatase activity, it was unable to cleave the aromatic sulfate (1a) even with increasing the enzyme dose.

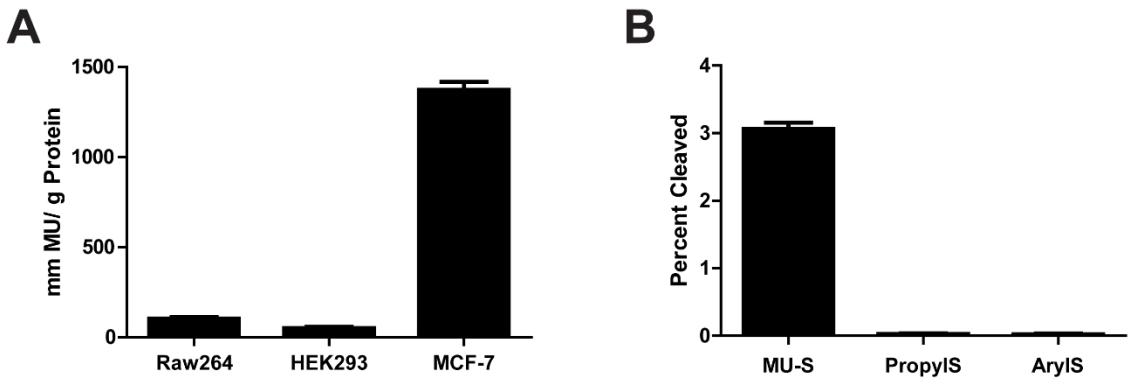

Figure 2-5: SULF2 enzymatic activity. A) SULF2 activity was determined from the conditioned media of Raw264, HEK293, and MCF-7 cells. MCF-7 cells showed the greatest SULF2 activity against Mu-S. B) The terminal sulfate from inverse sulfolipid headgroups, PropylS and ArylS, is not cleaved by SULF2.

2.2.5 Sulfate pH sensitivity

Although the sulfolipid headgroups were not SULF substrates, the terminal sulfate may be sensitive to acid hydrolysis. Liposomes traffic into cells via the endosomal pathway into late endosomes or lysosomes.[148,149] Lysosomal escape is essential for the delivery of encapsulated contents. The low pH environment of the lysosome could facilitate cleavage of the terminal sulfate, yielding a cationic lipid which could facilitate

lysosomal escape by interacting with the anionic lipids of the lysosomal compartment. DMArylAS was utilized to test the acid lability of the sulfolipids because the aromatic ring could help stabilize the phenoxide intermediate in sulfate removal. DMArylAS was placed in a solvent mixture of chloroform:methanol:acetic acid:water (65:15:10:4) to allow for maximal solubility of the compound and the liberation of the sulfate was monitored by C13 NMR (Figure 2-6). The carbon harboring the sulfate becomes more shielded upon removal of the sulfate as indicated by a shift in the NMR peak from 121.9 ppm to 118.2 ppm. By 1 hour there is evidence of sulfate cleavage with almost completed sulfate removal by 48 hours. The promising result supported further evaluation of these sulfolipids as drug carriers.

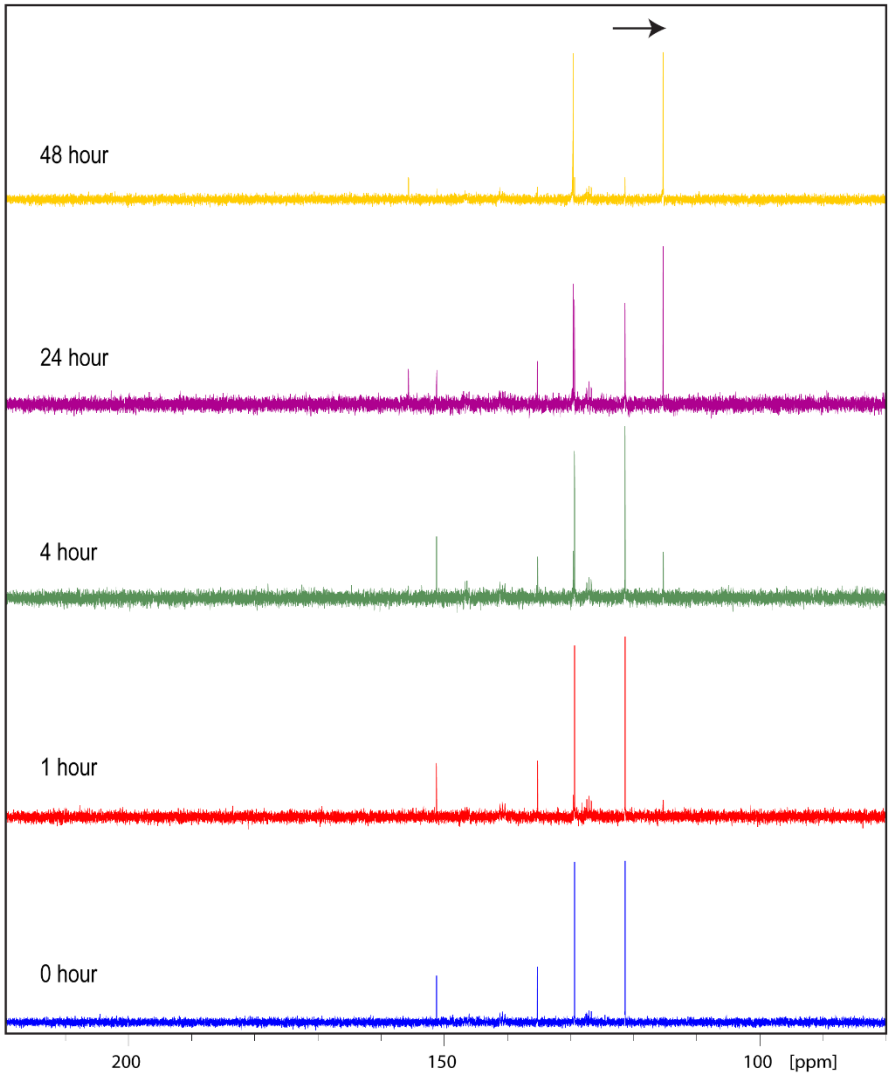

Figure 2-6: DMArylAS sulfate acid sensitivity. Carbon NMR in chloroform:methanol:acetic acid:water (65:15:10:4). The acidic environment facilitates detectable cleavage of the sulfate within 1 hour (red). Complete cleavage is achieved by 48 hours (yellow). Spectrum scaled to focus on aromatic carbons.

2.2.6 Vesicle Formation

To evaluate these lipids as drug carriers, we determined their ability to form liposomal vesicles. Formation of vesicles would allow for encapsulation and protection of drug payload. In addition, liposomal formation would increase aqueous solubility of these

sulfolipids to further access their response to pH and sulfatase. We focused our efforts on three lipids, DOAS (3a) and DMAS (3d) due to their lower transition temperatures and the ability of analogous PC lipids to form stable vesicles and DMArylAS (4) because of the acid sensitive sulfate. Transmission electron microscopy (TEM) of the DOAS formulation revealed small (~100 nm) worm-like structures and spirals (Figure 2-7). TEM of DMAS showed stacked micron-sized particles.

We attempted to promote bilayer formation by including lipids that might induce positive curvature such as tocopherol (TC) and PEGylated tocopherol (TC-PEG). TEM images of each formulation showed dramatically different structures with DMAS:TC generating large (1 mm) amorphous looking structures with poorly defined edges, while DMAS:TC-PEG generated sheet-like structures. We tested other additives (e.g. salts or sucrose), and coformulations with helper lipids (e.g. cholesterol and other long chain lipids) but these sulfolipids were unable to form vesicles.

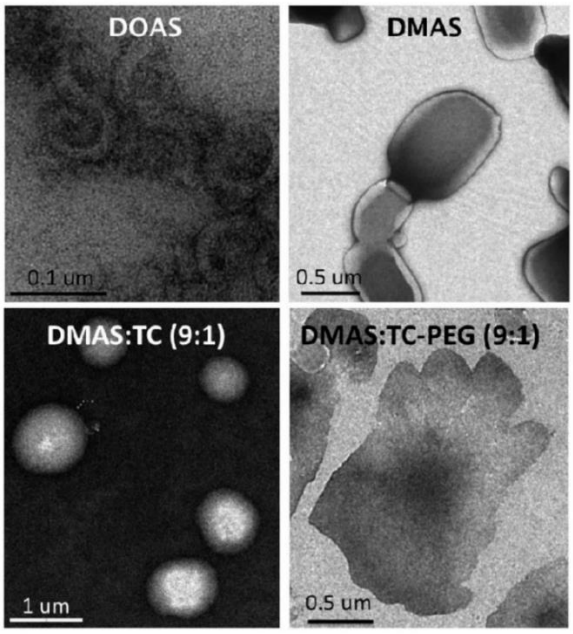

Figure 2-7: TEM images of inverse sulfolipids. Sulfolipids are poorly hydrated and form amorous structures alone and with additives.

2.3 Discussion

We synthesized a series of novel inverse-charge zwitterionic sulfolipids with exceptionally high transition temperatures. Phase transition temperatures of all lipids are 30–60ºC higher than PC lipids of corresponding chain length. The high transition temperature observed for these lipids suggests that the sulfate– amine interactions in the headgroup have a significant effect on the gel to liquid phase transition. This effect is likely due to intermolecular charge-charge interactions with neighboring lipid headgroups. The inability to form stable vesicles using sulfolipids stems from these ionic interactions at the aqueous-bilayer interface. In aqueous solutions, the sulfated quaternary amine lipids appear to form bilayer sheets instead of stable vesicular structures.

The sulfate group of these lipids is not susceptible to cleavage by extracellular sulfatases. Previously synthesized inverse lipids from our group with a phosphate anion

were substrates for phosphatase removal of the terminal anion, yielding a cationic lipid.[144] Phosphatases have a broader substrate specificity to allow for phosphate scavenging .[150] Conversely, sulfatases show a strong preference for their natural substrates and have a more limited substrate specificity.[151] Despite SULF2 displaying aryl sulfatase activity, the difference in specificity between phosphatases and sulfatases could explain the difference in cleavage between the two classes of inverse lipids. The AS lipids could be useful for lysosomal escape due to removal of the sulfate from the low pH environment or from the collection of more promiscuous lysosomal sulfatases.[151] However, the inability for these lipids to form vesicles is a significant barrier to their utility in drug delivery.

Chemical modifications to the AS lipid structure could aid in vesicle formation and sulfate cleavage. For example, using a tertiary amine to limit charge-charge interactions to a given pH range when the amine is protonated could aid in forming liposomes. Furthermore, placing a bulkier aromatic spacer between the amine and sulfate may promote vesicle formation by limiting intermolecular charge-charge interactions as well as improve recognition by sulfatases.

2.4 Conclusion

We synthesized a novel class of inverse-charge sulfated lipids. Although these lipids were unable to form vesicles or serve as SULF substrates, these sulfolipids exhibited exceptional biophysical properties with some of the highest transition temperatures reported. These lipids join a family of inverse lipids with properties that differ significantly from naturally-occurring phospholipids. This class of lipids can serve as a tool to better evaluate lipid biophysical properties. For example, they have already facilitated additional

investigation to understand the intermolecular interactions of adjacent lipids within lipid monolayers.[152,153]

2.5 Materials and methods

2.5.1 Instrumentation

NMR measurements were performed on a Bruker (Billerica, MA) 300MHz Advance system and analyzed using TopSpin software. MALDI-TOF measurements were performed on a Bruker Daltonics MicroFlex LT system (Billerica, MA). High Performance flash chromatography (HPFC) was carried out using a Grace Reveleris Flash System (Columbia, MD) with prepacked silica gel columns. Elemental analysis was performed by the Microanalytical Laboratory at the University of California Berkeley using an ICP Optima 7000 DV instrument. Differential Scanning Calorimetry (DSC) measurements were obtained using a high temperature MC-DSC 4100 calorimeter from Calorimetry Sciences Corp. (Lindonk, UT). Fluorescence spectroscopy was measured on a FluoroLog-3 spectrofluorimeter (Horiba Jobin Yvon) equipped with a temperature-controlled stage (LFI-3751) or a SpectraMax M5 Micoplate Reader (Sunnyvale, CA) and data was collected through FluorEssence or SoftMax pro software, respectively. TEM images were obtained using a FEI Tecnai 12 transmission electron microscope at the University of California Berkeley Robert D. Ogg Electron Microscope Laboratory.

2.5.2 Materials

Phospholipids and additives were obtained from Avanti Polar Lipids (Alabaster, AL). PD-10 sephadex columns were obtained from GE Healthcare (San Francisco, CA).

All cell culture products were purchased from the UCSF Cell Culture Facility. All other reagents were purchased from Sigma–Aldrich (St. Louis, MO).

2.5.3 Synthesis

Lipids were prepared in a two-step synthesis (Figure 2-3) starting with the acylation of 3- (dimethylamino)-1,2-propanediol as previously reported.[145] Sulfolipids were produced through amine quaternization with a sulfated precursor.

2.5.4 Synthesis of compound 1 and 1 a

Synthesis of 1-bromo-3- propanesulfate (1) and 4-hydroxyphenethyl-sulfate (1a) was performed by stirring 1 mmol of 1-bromo-3-propanol or 4-hydroxyphenethyl-bromide, respectively, at 0.2 M in dichloromethane (DCM) as 4 mmol sulfurtrioxide-pyridine complex (45%) and 1 mmol diisopropyl ethylamine was added. The reaction was then heated to 40°C overnight under nitrogen. The reaction was concentrated and taken up in DCM to afford a solid, which was removed by filtration. The filtrate was purified by silica gel flash chromatography (0-10% methanol in DCM). The products eluted as a diisopropyl ethylamine salt in a 1:1 ratio as determined by NMR.

2.5.5 Synthesis of 2a-f

3- (dimethylamino)-1,2-propanediol (0.5 mmol) was solubilized in chloroform where (1.5 mmol) of the desired fatty acid was added followed by dimethylaminopyridine (DMAP) (0.2 mmol) and 1-Ethyl-3-(3-dimethylaminopropyl)carbodiimide (EDC) (4 mmol). The reaction proceeded overnight at room temperature, concentrated then washed 3X in 1 N HCL. The organic phase was dried over sodium sulfate and concentrated by rotary

evaporation followed by silica gel flash chromatography (0-10% methanol in DCM) to yield a pure product.

2.5.6 Synthesis of 3a-f

The diacyl tertiary amine lipid (2a-f) (1 mmol) was quaternized with 1-bromo-3-propanesulfate (1) (3.5 mmol) and 2 mmol diisopropyl ethylamine in dimethylformamide at 0.15 M. The reactions were heated to 60°C overnight under nitrogen. A precipitate formed in the reactions with saturated lipid tails (distearoyl (3b), dipalmitoyl (3c), dimyristoyl (3d), dilauryl (3e) and dicapryloyl (3f)) and these solutions were then heated to 80°C for 2 hours before cooling to room temperature. The precipitate reformed and was filtered and washed with DMF to yield a white solid. Quaternization of the unsaturated lipid (dioleoyl (3a)) was performed in the same manner but did not result in a precipitate. The reaction mixture was concentrated and taken up in DCM and purified by silica gel flash chromatography (0-10% methanol in chloroform with 0.1% NH_4OH)

2.5.7 Synthesis of 4

The diacyl tertiary amine lipid (2d) (1 mmol) was quaternized with 4-hydroxyphenethyl-bromide (1a) (3.5 mmol), 2 mmol diisopropyl ethylamine in dimethylformamide, and 0.05 mm potassium iodide at 0.15 M in acetonitrile. The reactions were heated to 60°C overnight under nitrogen. A precipitate formed in the reaction and these solutions were then heated to 80°C for 2 hours to solubilize all the solid. Mixture was cooled to 60°C where a precipitate reformed and was filtered and washed with acetonitrile to yield a white solid.

2.5.8 Chemical Characterization

Compound 1 – Yield (74%). 1H NMR (CDCl3): δ 1.44 (d, 6H, DIPEA), 1.51 (d, 6H, DIPEA), 1.53 (t, 3H, DIPEA), 2.24 (t, 2H), 2.24 (t, 2H), 3.13 (m, 2H, DIPEA), 3.54 (t, 2H), 3.69 (m, 2H, DIPEA), 4.19 (t, 2H). 13C NMR (CDCl3): δ 12.4 (DIPEA), 17.3 (DIPEA), 18.6 (DIPEA), 30.2, 32.7, 42.8 (DIPEA), 54.5 (DIPEA), 65.3.

Compound 1a: Yield (60%). 1H NMR (CDCl3): δ 1.40 (d, 6H, DIPEA), 1.51 (d, 6H, DIPEA), 1.53 (t, 3H, DIPEA), 3.07 (m, 2H, DIPEA), 3.12 (t, 2H), 3.54 (t, 2H), 3.69 (m, 2H, DIPEA), 7.14 (d, 2H), 7.31 (d, 2H). 13C NMR (CDCl3): δ 12.4 (DIPEA), 17.3 (DIPEA), 18.6 (DIPEA), 33.0, 39.0, 42.8 (DIPEA), 54.5 (DIPEA), 121.9, 129.0, 135.4, 151.7.

Compound 3a (DOAS) – Yield: 45%. 1H NMR (CDCl3): δ 0.89 (t, 6H), 1.29 (m, 40H), 1.59 (m, 4H), 2.02 (m, 8H), 2.26 (m, 2H), 2.32 (m, 4H), 3.21 (s, 3H), 3.28 (s, 3H), 3.49 (m, 2H), 3.68 (t, 2H), 3.94 (d, 1H), 4.12 (t, 2H), 4.51 (d, 1H), 5.35 (m, 4H), 5.64 (m, 1H). 13C NMR (CDCl3): δ 14.12, 22.68, 24.70, 24.80, 27.22, 27.24, 29.10, 29.16, 29.20, 29.22, 29.28, 29.32, 29.34, 29.54, 29.78, 31.91, 33.89, 34.19, 51.18, 51.63, 63.37, 65.81, 129.70, 130.05, 172.80, 173.23. MALDI-TOF calculated for [C44H83NO8S] (m/z): 785.58, observed: 787.39. Elemental analysis for [C44H83NO8S]: C, 67.22; H, 10.64; N, 1.78; S, 4.08. Found: C, 67.22; H, 10.90; N, 1.68; S, 4.33

Compound 3b (DSAS). Yield: 42%. 1H NMR (CDCl3:MeOD (20:1)): δ 0.76 (t, 6H), 1.14 (m, 56H), 1.49 (m, 4H), 2.06 (m, 2H), 2.24 (m, 4H), 2.99 (s, 3H), 3.03 (s, 3H), 3.49 (m, 2H), 3.57 (t, 2H), 3.93 (d, 1H), 4.00 (t, 2H), 4.34 (d, 1H), 5.48 (m, 1H). 13C NMR (CDCl3): δ 13.60, 22.31, 24.30, 24.38, 25.28, 28.77, 29.00, 29.16, 29.33, 31.57, 33.49, 33.75, 50.51, 51.25, 57.60, 62.95, 63.54, 63.83, 65.18, 172.65, 173.23. MALDI-TOF calculated

for [C44H87NO8S] (m/z): 789.62, observed: [M+H] 791.16. Elemental analysis for [C44H87NO8S]: C, 66.79; H, 11.21; N, 1.77; S, 4.05. Found: C, 66.58; H, 11.54; N, 1.74; S, 4.65. Note: Elemental analysis of sulfur is believed to be high due to free sulfate.

Compound 3c (DPAS) – Yield: 71%. 1H NMR (CDCl3:MeOD (20:1)): δ 0.79 (t, 6H), 1.17 (m, 48H), 1.52 (m, 4H), 2.09 (m, 2H), 2.26 (m, 4H), 3.01 (s, 3H), 3.05 (s, 3H), 3.51 (m, 2H), 3.61 (t, 2H), 3.95 (d, 1H), 4.03 (t, 2H), 4.35 (d, 1H), 5.51 (m, 1H). 13C NMR (CDCl3): δ 13.95, 22.57, 22.85, 24.56, 24.63, 29.00, 29.04, 29.22, 29.26, 29.43, 29.55, 29.57, 29.59, 31.82, 33.74, 34.03, 50.82, 51.34, 57.98, 63.22, 63.79, 63.90, 64.22, 64.39, 65.48, 172.86, 173.41. MALDI-TOF calculated for [C40H79NO8S] (m/z): 733.55, observed: [M+H] 734.88. Elemental analysis for [C40H79NO8S]: C, 65.35; H, 10.97; N, 1.91; S, 4.36. Found: C, 65.17; H, 11.33; N, 1.95; S, 4.79.

Compound 3d (DMAS) – Yield: 71%. 1H NMR (CDCl3:MeOD (20:1)): δ 0.82 (t, 6H), 1.20 (m, 40H), 1.53 (m, 4H), 2.14 (m, 2H), 2.29 (m, 4H), 3.05 (s, 3H), 3.10 (s, 3H), 3.56 (m, 2H), 3.67 (t, 2H), 3.99 (d, 1H), 4.06 (t, 2H), 4.38 (d, 1H), 5.53 (m, 1H). 13C NMR (CDCl3): δ 13.89, 22.51, 22.81, 24.50, 24.57, 28.97, 29.19, 29.35, 29.49, 31.76, 33.68, 33.97, 50.66, 51.22, 63.09, 63.61, 63.88, 64.47, 65.37, 172.75, 173.31. MALDI-TOF calculated for [C36H71NO8S] (m/z): 677.49, observed: [M+H] 678.59. Elemental analysis for [C36H71NO8S]: C, 63.68; H, 10.69; N, 2.06; S, 4.72. Found: C, 63.52; H, 10.92; N, 1.98; S, 5.35. Note: Elemental analysis of sulfur is believed to be high due to free sulfate.

Compound 3e (DLAS) –. Yield: 69%. 1H NMR (CDCl3:MeOD (20:1)): δ 0.77 (t, 6H), 1.15 (m, 32H), 1.50 (m, 4H), 2.07 (m, 2H), 2.24 (m, 4H), 3.00 (s, 3H), 3.05 (s, 3H), 3.49 (m, 2H), 3.60 (t, 2H), 3.95 (d, 1H), 4.01 (t, 2H), 4.35 (d, 1H), 5.49 (m, 1H). 13C NMR (CDCl3): δ13.79, 22.44, 22.76, 24.42, 24.50, 28.85, 28.89, 29.05, 29.07, 29.10, 29.24, 29.26,

29.37, 29.40, 31.67, 33.59, 33.88, 50.57, 51.10, 63.03, 63.53, 63.81, 64.30, 65.31, 172.70, 173.29. MALDI-TOF calculated for [C32H63NO8S] (m/z): 621.43, observed: [M+H] 622.91. Elemental analysis for [C32H63NO8S]: C, 61.80; H, 10.21; N, 2.25; S, 5.16. Found: C, 61.52; H,9.85; N,2.13; S, 5.03.

Compound 3f (DCAS) – Yield: 65%. 1H NMR (CDCl3): δ0.90 (t, 6H), 1.29 (m, 24H), 1.60 (m, 4H), 2.27 (m, 2H), 2.35 (m, 4H), 3.21 (s, 3H), 3.29 (s, 3H), 3.70 (m, 3H), 3.96 (d, 1H), 4.13 (t, 3H), 4.51 (d, 1H), 5.64 (m, 1H). 13C NMR (CDCl3): δ14.10, 22.70, 24.74, 24.84, 29.19, 29.36, 29.49, 31.91, 33.94, 34.25, 51.10, 51.64, 63.39, 63.61, 63.84, 64.56, 65.84, 172.83, 173.25. MALDI-TOF calculated for [C28H55NO8S] (m/z): 565.37, observed: [M+H] 566.72. Elemental analysis for [C28H55NO8S]: C, 59.44; H, 9.80; N, 2.48; S, 5.67. Found: C, 59.32; H, 9.67; N, 2.46; S, 5.63.

Compound 4 (DMArylAS) – Yield: 35%. 1H NMR (CDCl3): δ 0.74 (t, 6H), 1.13 (m, 40H), 1.52 (m, 4H), 2.27 (m, 4H), 2.89 (m, 2H), 3.06 (s, 6H), 3.40 (m, 2H), 3.59 (m, 2H), 3.96 (m, 1H) 4.35 (m, 1H), 5.50 (m, 1H), 6.99 (m, 4H). 13C NMR (CDCl3): δ13.89, 22.7, 24.50, 28.0, 29.8, 31.9, 33.7, 51.7, 63.4, 65.9, 66.60, 121.9, 124.8, 130.4, 131.5, 151.7, 173.31. MALDI-TOF calculated for [C41H73NO8S] (m/z): 739.51, observed: [M+H] 741.177. Elemental analysis for [C41H73NO8S]: C, 66.54; H, 9.94; N, 1.89; S, 4.33. Found: C, 66.3; H,9.85; N,1.97; S, 4.25.

2.5.9 Gene Expression

SULF1 and SULF2 Illumina HiSeq expression from the TCGA PANCAN dataset was imported from the Cancer Genome browser. Data was imported R to generate box plots showing normal versus tumor expression across all the various cancers.

2.5.10 Cell Culture

MCF-7 cells were grown in RPMI-1640 supplemented with 10% FBS and 1 µg/ml insulin. Cells were grown in a T175 flask and once confluent cells were washed 3X with OptiMEM. Fresh OptiMEM (18 mL) was added to each T175 flask and the cells were allowed to grow for 3-4 days. The media was collected and concentrated using an amicon 10K spin filter. Sulfatase activity was determined by measuring the conversion of MU-S to MU by fluorescence (excitation 320, emission 449). Aliquots of the active solution were frozen and thawed as needed.

2.5.11 Barium Sulfate Assay

Samples were diluted into 50 mM HEPES, 2.5 mM $CaCl_2$, 250 mM NaCl to a final concentration of 20 mM with SULF conditioned media at 1 mg/mL. The reaction was allowed to proceed for 4 hours at 37ºC then quenched by dilution into carbonate buffer, pH 11. A 60 µl of each sample was added to 140 µl of 50% perchloric acid and heated at 140°C in a glass tube for 12 min. After cooling to room temperature, 0.8 ml of 0.4 M trisodium citrate solution was added to each sample then vortexed. Barium working solution (4 mM barium acetate, 2.5 mM PEG 6000) was placed on a stir plate and 0.25 ml from the stirring barium working solution was transferred to each tube and immediately vortexed. Samples were left at room temperature for 1 hour then vortexed and transferred to 96-well plate to measure the absorbance at 600 nm. Percent cleavage was determined by comparison to a sodium sulfate standard curve.

2.5.12 Elemental Analysis

A total of 5–10 mg of dry lipid was submitted to Microanalytical Laboratory at the University of California Berkeley for elemental analysis determinations using an ICP Optima 7000 DV instrument.

2.5.13 Differential Scanning Calorimetry

DSC experiments were based upon a protocol described previously.[154] Lipids films were prepared in glass tubes from a 20 mg/mL stock solution in 25% methanol in chloroform by concentrating the lipids under vacuum. The lipid films were then rehydrated at 20 mM in 10 mM HEPES buffer. In all experiments, the lipids were heated to 90°C for 10 min and sonicated with heating for 10 minutes, then 250 µL of lipid was transferred to a reusable Hestelloy sample ampoule using a glass syringe. Data were collected over a range of 10-110°C at 1°C/min with the relevant buffer as the reference. The CpCalc 2.1 software package was used to convert the raw data into a molar heat capacity. The data was then exported to Excel and GraphPad Prism for processing. Samples were scanned through a heat-cool-heat cycle and data was collected from the second heating cycle.

2.5.14 Transmission electron microscopy

A 2.0 µL drop of liposomes in 140 mM NaCl, 10 mM HEPES pH 7.4 were adsorbed for 1 minute on a glow-discharged carbon-coated copper grid (Ted Pella, Redding, CA) and water was wicked off. Then, 2 microliters of a 1% uranyl acetate negative stain solution were added then left to stain for 1 minute and wicked off. The grid was then washed with deionized water 3X and the water was removed by wicking. Grids were

imaged with a FEI Tecnai T12 TEM (FEI company, Hillsboro, OR) at 120kV. Data were acquired with a 4 x 4 Gatan UltraScan CCD camera (Gatan, Pleasanton, CA).

3 Chapter 3: Sterol-modified PEGs for improved liposomal stability

3.1 Introduction

Liposomes are amongst the leading class of nanoparticle therapeutics. They can extend drug circulation *in vivo* by promoting a serum half-life of almost 2 days.[155,156] This is achieved through the incorporation of polyethylene glycol (PEG) anchored to a 1,2-distearoyl glycerol-3-phosphoethanolamine lipid (DSPE) which limits liposome aggregation, the adherence of serum proteins, and recognition of immune cells.[157]

These pharmacokinetic benefits are dependent on DSPE-PEG lipids successfully incorporating into the lipid bilayer. However, there are conflicting reports of the miscibility of DSPE-PEG when mixed with 1,2-distearoyl glycerol-3-phosphocholine (DSPC). On one side, in lipid-monolayer-coated-microbubbles it was found by electron and fluorescence microscopy that DSPE-PEG2000-biotin is immiscible with DSPC.[158] In addition, Lozano et al.[159] showed that DSPC and DSPE-PEG2000 coexisted as a two-phase system and were almost completely immiscible in lipid monolayer mixtures. On the opposing side, Chou and Chu[160] found that the two lipids were actually fully miscible in lipid monolayers and that addition of DSPE-PEG caused the monolayer to become more compressible. In addition, Dos Santos et al.[161] showed that liposomes containing DSPC and DSPE-PEG2000 exhibited similar pharmacokinetics in mice with and without cholesterol which is predicted to help stabilize interactions between DSPC and DSPE-PEG.[159] Considering the conflicting information, there is a need for substitutes to DSPE-PEG which can unequivocally mix favorably with DSPC lipids.

As a result, we synthesized two cholesterol-anchored PEGs to create alternatives to DSPE-PEG that can be miscible with DSPC within lipid bilayers. Cholesterol mixes favorably with DSPC[162] and is commonly used in liposomes to improve bilayer stability. Previous sterol-modified lipids exhibited almost identical properties to conventional linear phospholipids,[163] which further supports the use of cholesterol as a suitable anchor without the loss of PEG functionality. Here, we present the biophysical properties of two sterol-anchored PEGs and evaluate their utility in liposomal drug delivery.

3.2 Results

3.2.1 Synthesis

We synthesized two sterol-modified PEG-2000 (2000 kDa) molecules using standard approaches (Scheme 1). Glycerol-mimetic backbones were produced by reacting PEG-nitrophenylcarbonate with 3-methylamino-1,2-propanediol or 2-methyl-2-amino-1,3-propanediol, to produce compounds **4** and **6**, respectively. PEG2K-2-methyl-2-amino-1,3-propanediol was reacted with cholesteryl hemisuccinate (**3**) through EDC coupling to yield a dicholesteyl hemisuccinate PEG (**DiCHEMS-PEG**) (**7**). For the other sterol-modified PEG, cholesterol was first derivatized using tert-butylbromoacetate in the presence of sodium hydride. The column purified product (**1**) was deprotected using formic acid to yield compound **2**, which was coupled to **4** in the presence of EDC to provide a dicholesterol PEG (**DiCHOL-PEG**) (**5**). DiCHEMS-PEG and DiCHOL-PEG were purified by dialysis with the DiCHOL-PEG requiring additional purification on a silica column.

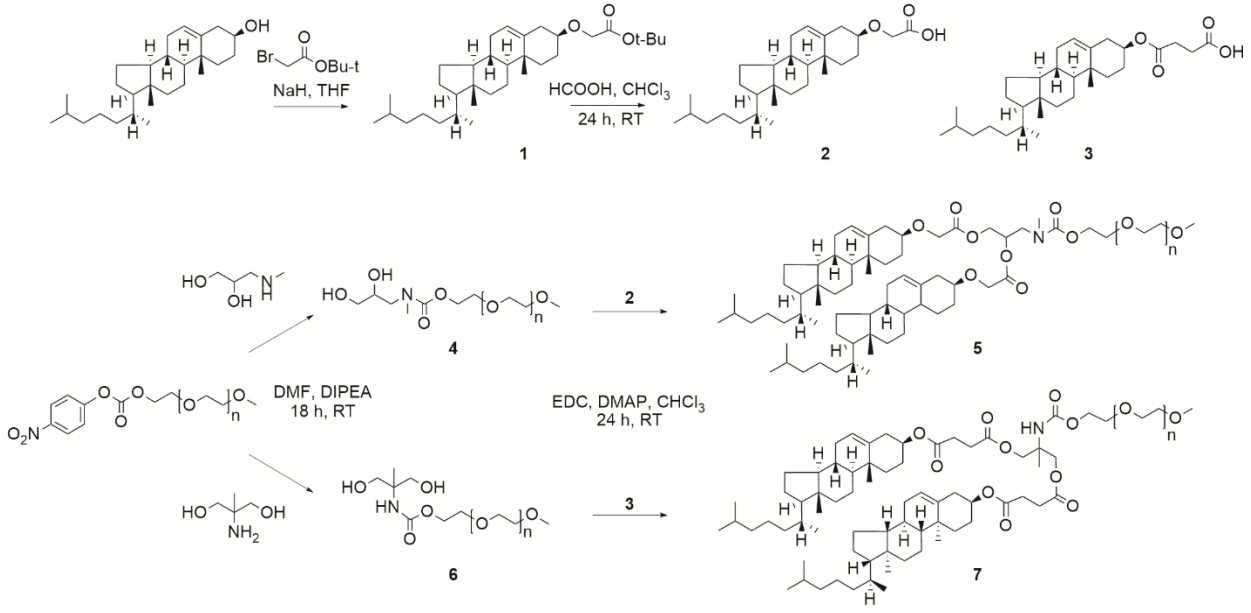

Figure 3-1: Synthetic scheme for synthesis of sterol-anchored PEG lipids.

3.2.2 Anisotropy

To determine the fluidity of bilayers comprised of sterol-anchored PEG, DSPC lipid nanoparticles were produced with increasing amounts of PEG. Fluorescence anisotropy of 1,6- diphenyl-1,3,5-hexatriene (DPH) was measured and compared to DSPE-PEG and an equivalent amount of cholesterol (Figure 3-2). Pure DSPC undergoes a phase transition at 55ºC marked by a dramatic reduction in anisotropy. The addition of increasing amounts of cholesterol eliminates this transition represented by an increase in anisotropy at a temperature of 55ºC and greater, flattening the overall anisotropy trace (Figure 3-2A). Alternatively, increasing amounts of DSPE-PEG in DSPC vesicles lowered the entire anisotropy curve likely due to the presence of DSPE-PEG micelles when used at 15% or greater since PEG micelles increase DPH fluidity and lower anisotropy (Figure 3-2B).[164] Anisotropy of DiCHOL-PEG and DiCHEMS-PEG in DSPC vesicles displayed behavior closer to cholesterol than DSPE-PEG (Figure 3-2 C,D). There is a gradual increase in

anisotropy at or above the transition temperature of DSPC with increasing amounts of sterol-anchored PEG lipids. Higher percentages of DiCHOL-PEG caused a limited loss in anisotropy at 45ºC and above but the effect was not as pronounced as DSPE-PEG and did not replicate with DiCHEMS-PEG. The overall anisotropy similarity to cholesterol for both the sterol-anchored PEG molecules suggests that these lipids could exhibit both stabilizing effects of cholesterol along with the protective effect of a PEG coating.

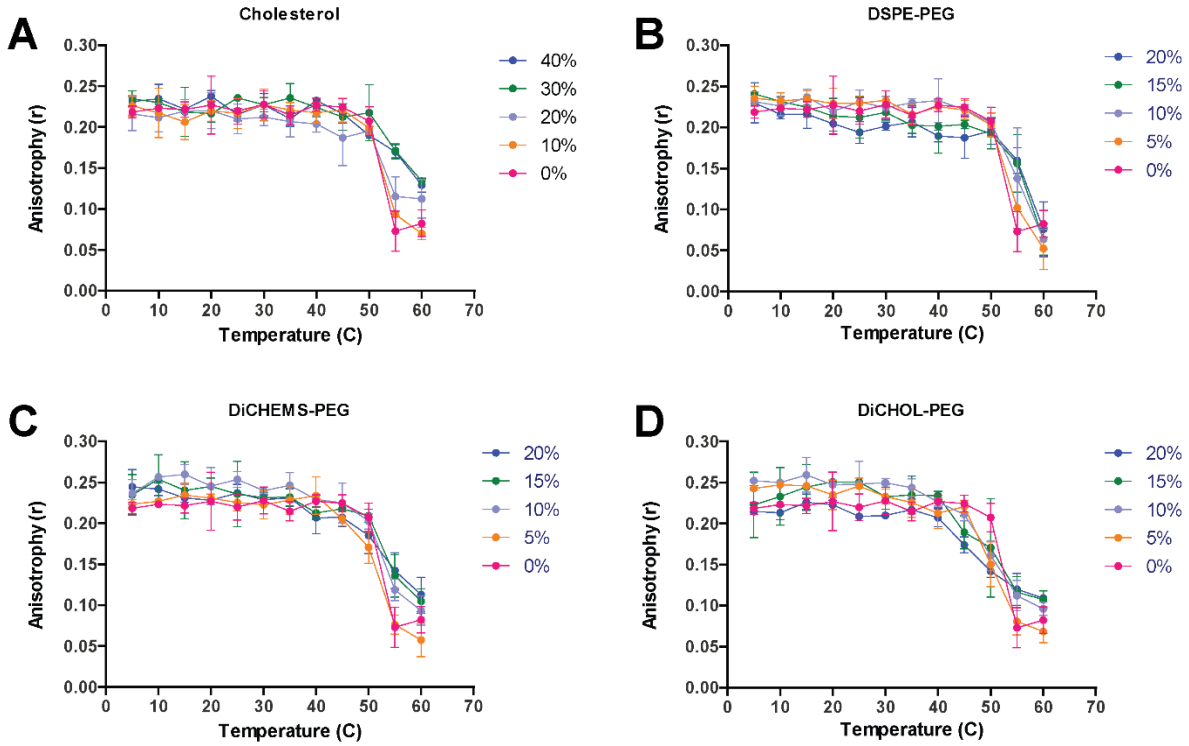

Figure 3-2: DPH fluorescence anisotropy of DSPC vesicles with increasing amounts of cholesterol. (A), DSPE-PEG (B), DiCHEMS-PEG (C) and DiCHOL-PEG (D). Sterol-anchored PEG exhibits similar anisotropy traces to pure cholesterol in DSPC vesicles. Free cholesterol mole percent in the bilayer is equivalent to double the DiCHEMS-PEG or DiCHOL-PEG mole percent. Errors bars represent mean ± SD.

3.2.3 Leakage

Importantly, for these lipids to be used successfully they would need to retain the ability to encapsulate drugs. Liposomes containing 5% DSPE-PEG, DiCHEMS-PEG, or DiCHOL-PEG were evaluated for bilayer stability through encapsulation of carboxy fluorescein (CF). The DSPE-PEG liposomes also contained 10% cholesterol to match the total cholesterol present with the DiCHEMS-PEG and DiCHOL-PEG liposomes. Following CF encapsulation, free CF was separated from liposomes by size-exclusion chromatography. Liposomes were placed in serum and CF leakage was measured over a week at 37ºC (Figure 3-3). All liposomes exhibited an initial burst release of CF within the first 24 hours before equilibrating in serum. DSPC containing 5% DiCHEMS-PEG or DiCHOL-PEG released approximately 12% of encapsulated CF within 7 days which was comparable to the conically stable DSPC:Cholesterol (60:40) liposome formulation. Leakage was also comparable to DSPC:Cholesterol:DSPE-PEG (85:10:05) with 10% cholesterol.

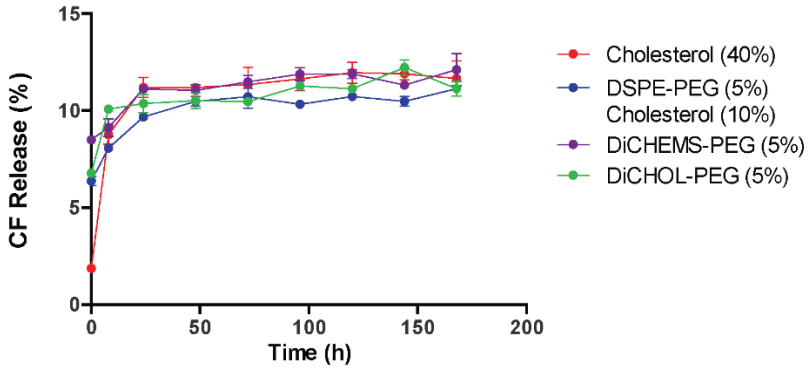

Figure 3-3: CF leakage from liposomes. DiCHEMS-PEG and DiCHOL-PEG liposomes exhibit similar CF leakage in serum as cholesterol containing liposomes. Error bars represent mean ± SD.

3.2.4 TEM

To verify the morphology of sterol-anchored PEG molecules, transmission electron spectroscopy was performed. Formulations containing 5% DiCHEMS-PEG or DiCHOL-PEG with DSPC formed vesicles similar to that of DSPC:Cholesterol:DSPE:PEG formulations (Figure 3-4)

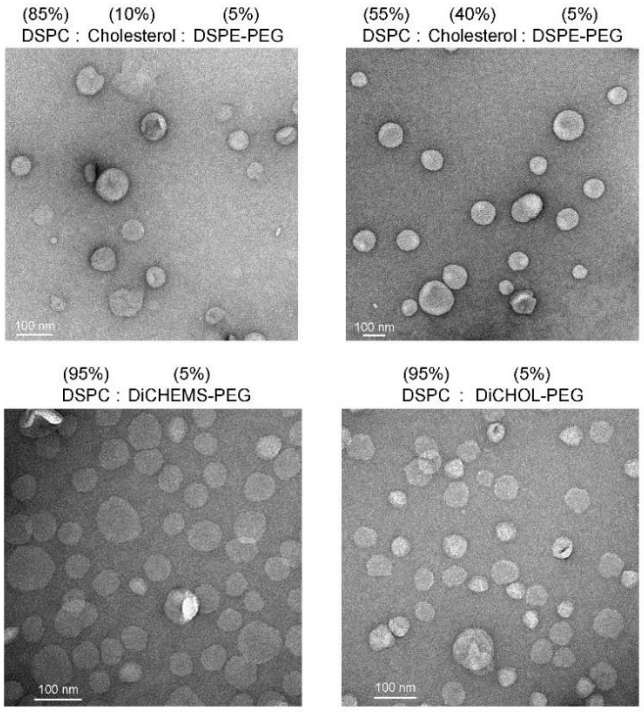

Figure 3-4: TEM images of liposome formulations. DiCHOL-PEG and DiCHEMS-PEG (bottom) form vesicles when mixed with DSPC comparable to DSPC:Cholesterol:DSPE:PEG liposomes (top).

3.2.5 Protein Binding

Next, we investigated if the sterol-anchored PEG lipids could prevent non-specific protein binding. DiCHOL-PEG and DiCHEMS-PEG displayed no differences in protein binding than the DSPC:Cholesterol:DSPE:PEG liposomes investigated (Figure 3-5).

Liposomes were mixed with plasma or fluorescently labeled BSA and the amount of bound protein was determined following size exclusion chromatography to remove any unassociated proteins. Plasma binding studies suggested that the DSPC:Cholesterol:DSPE:PEG formulation containing 10% cholesterol bound the least amount of plasma protein (Figure 5A). However, when non-specific binding was quantified using labeled albumin there was no significant differences between the groups (Figure 5B).

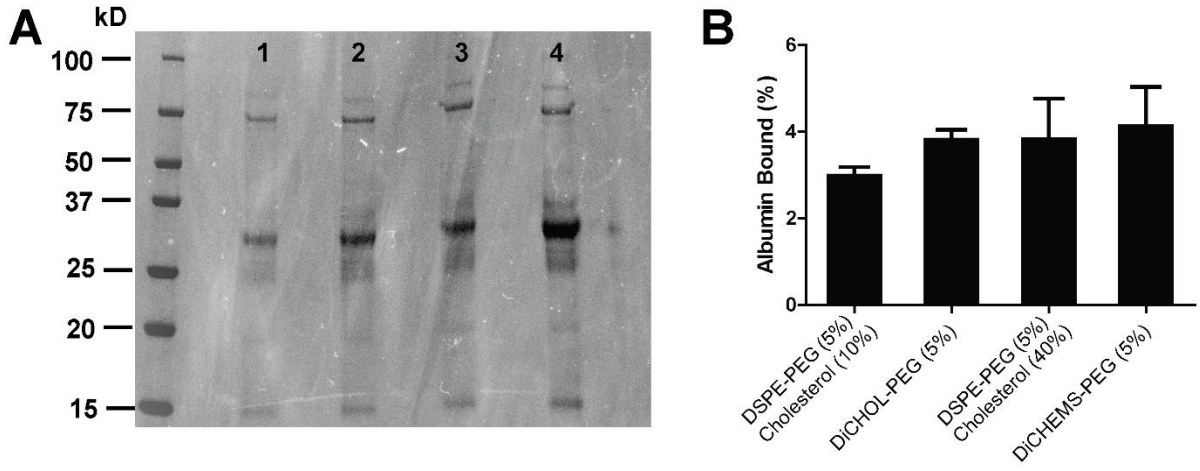

Figure 3-5: Normalized liposome protein binding. Liposome formulations exhibit minimal differences in non-specific protein binding. A) Normalized binding of liposomes to plasma proteins show only minor differences in plasma adhesion. 1, DSPC:Cholesterol:DSPE-PEG (85:10:05); 2, DSPC:DiCHOL-PEG (95:05); 3, DSPC:Cholesterol:DSPE-PEG (85:10:05); 4, DSPC:DiCHEMS-PEG (95:05) B) Percent albumin binding shows no significant changes in the levels of albumin associated with the liposomes. Protein content normalized to liposome concentration. Error bars represent mean ± SD, n=3/group.

To determine how protein binding may affect behavior *in vivo,* we measured cellular uptake in the presence and absence of apolipoprotein 3 (apoE3). ApoE3 can absorb onto the surface of neutral liposomes to facilitate hepatic clearance.[165] Only the DiCHEMS-PEG showed an increase in uptake in the presence of apoE3 (Figure 3-6). In

addition, the DiCHEMS-PEG had the largest cellular uptake compared to all other liposome formulations. DiCHOL-PEG exhibited slightly higher uptake compared to DSPE-PEG liposomes but the differences were not significant.

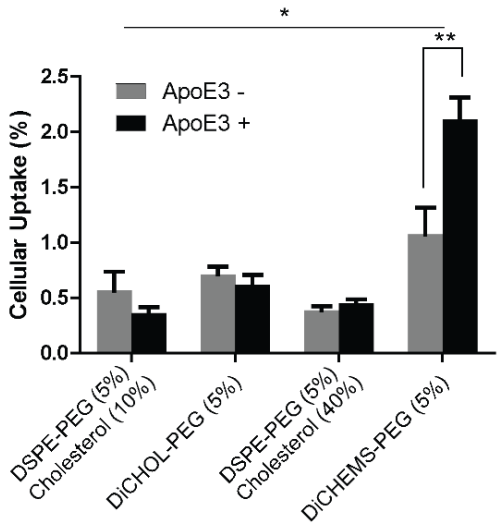

Figure 3-6: ApoE3 cellular uptake. Liposomes containing DiCHEMS-PEG exhibit increased cellular uptake in the presence of ApoE3. Error bars represent mean ± SD, n=4 wells/group. *p<0.05 ANOVA with Tukey's post-hoc test; **p<0.01, *t*-test.

3.2.6 Pharmacokinetics

We then attempted to understand how the biophysical properties of the sterol-anchored PEGs would affect liposome circulation. Liposomes were produced within ±10 nm in diameter to limit deviations in pharmacokinetics based on size. Percent of dose remaining was measured 24 hours post injection (Table 2-1). Interestingly, DSPC liposomes containing 5% DiCHEMS-PEG or DiCHOL-PEG were more rapidly cleared from circulation than DSPC liposomes with 5% DSPE-PEG (Table 1). There was only approximately 3% of the dose remaining for the sterol-anchored PEGs, whereas DSPC liposomes with 5% DSPE-PEG had at least 14% of the dose remaining.

Table 3-1: Size and percent dose remaining of DSPC vesicles containing DSPE-PEG with cholesterol, DiCHEMS-PEG or DiCHOL-PEG.

Formulation	Size (nm)	% Dose at 24 hr
DSPC:Cholesterol:DSPE-PEG (55:40:05)	100 ± 3	14 ± 2.48
DSPC:Cholesterol:DSPE-PEG (85:10:05)	94 ± 4	22 ± 2.48
DSPC:DiCHOL-PEG (95:05)	95 ± 4	3 ± 0.22
DSPC:DiCHEMS-PEG (95:05)	93 ± 5	2.4 ± 1.15

Values represent mean ± SD. n=3 per group

3.3 Discussion

We synthesized and characterized two sterol-anchored PEG molecules with similar biophysical properties as potential alternatives to DSPE-PEG. Bilayer fluidity determined by fluorescence anisotropy of DiCHEMS-PEG or DiCHOL-PEG vesicles was similar to that of bilayers containing pure cholesterol. Formulations with either lipid encapsulated contents with only 12% release over 7 days in serum. Neither of the sterol-anchored PEGs strongly associated with plasma proteins. However, the DiCHEMS-PEG showed increased cellular uptake on cultured cells in the presence of apoE3. It displayed four-times more cellular uptake with ApoE3 than any of the other formulations examined. The primary structural difference between the two lipids is the use of cholesteryl hemisuccinate or cholesterol as the sterol anchor. Although cholesteryl hemisuccinate is conventionally used as a reactive form of cholesterol,[154,166,167] it contains an ester linkage

on the free hydroxy of cholesterol, where that ester carbonyl is believed to interfere with bilayer packing.[168] Therefore, in the DiCHEMS-PEG formulation the cholesterol may be more accessible to protein adhesion. This structural difference could account for the increase in apoE3-driven uptake observed with the DiCHEMS-PEG lipid.

The two cholesterol modified lipids also differed in the aminopropyl moiety that anchored the cholesterol to the PEG. For the DiCHEMS-PEG, cholesteryl hemisuccinate was anchored to the 1 and 3 positions of the glycerol-like backbone with the PEG attached to the amine at the 2 position. Whereas in the DiCHOL-PEG, the cholesterol esters were attached to the 1 and 2 positions with the PEG anchored to the methylamino group at the 3 position. It is not evident how these positional changes would influence the behavior of the appended 2000 MW PEG chain.

Regardless, DSPC liposomes containing DiCHEMS-PEG or DiCHOL-PEG exhibited accelerated plasma clearance with only about 3% of the respective dose remaining in mouse plasma 24 hours following IV injection. In the case of the DiCHEMS-PEG, the sterol-anchor may facilitate the recognition of liposomes by lipophilic ApoE proteins since they are known to interact with cholesterol, triglycerides, and lipoproteins.[169,170] As a result, the ApoE3 accumulation could increase the hepatic clearance of liposomes which likely contributed to the reduced circulation. The DiCHOL-PEG showed slightly greater uptake in cells than DSPE-PEG which suggests it may also be cleared more rapidly due to increased cellular recognition.

3.4 Conclusion

We synthesized two novel sterol-anchored PEG molecules, DiCHEMS-PEG and DiCHOL-PEG that exhibit unique biophysical properties. They form stable vesicles in the presence of DSPC, are capable of encapsulating drugs, and show little nonspecific protein adhesion. These lipids are cleared more rapidly in mice than lipids containing DSPE-PEG in part due to increased ApoE recognition and hepatic clearance. The increased ApoE recognition could, however, be utilized for targeted delivery of liposomes to hepatocytes.[169] These lipids offer a potential alternative to DSPE-PEG in lipid vesicles as well as could be used to help clarify the complex relationship between DSPE-PEG, DSPC, and cholesterol in lipid bilayers to better understand the criteria for immiscibility.

3.5 Materials and methods

3.5.1 Instrumentation

NMR measurements were performed on a Bruker (Billerica, MA) 300MHz Advance system and analyzed using TopSpin software. MALDI-TOF measurements were performed on a Bruker Daltonics MicroFlex LT system (Billerica, MA). Elemental analysis was performed by the Microanalytical Laboratory at the University of California Berkeley using an ICP Optima 7000 DV instrument. Particle size and zeta measurements were carried out using a Nano-ZS Dynamic Light Scattering Instrument from Malvern (Westborough, MA). Fluorescence spectroscopy was measured on a FluoroLog-3 spectrofluorimeter (Horiba Jobin Yvon) equipped with a temperature- controlled stage (LFI-3751) or a SpectraMax M5 Micoplate Reader (Sunnyvale, CA) and data was collected through FluorEssence or SoftMax pro software, respectively.

3.5.2 Materials

1,2-Distearoyl-sn-glycero-3-phosphocholine (DSPC), 1,2-distearoyl-sn-glycero-3-phosphoethanolamine-N- [methoxy(polyethylene glycol)-2000] (DSPE-PEG) were obtained from Avanti Polar Lipids (Alabaster, AL). tert-Butylbromoacetate and cell culture materials were purchased from Fisher Scientific (Hanover Park, IL). [Methoxy(polyethylene glycol)-2000]- Nitrophenyl Carbonate (mPEG-NPC) was purchased from Laysan Bio Inc (Arab, AL). 1,1′-Dioctadecyl-3,3,3′,3′-tetramethylindotricarbocyanine iodide (DiR) was purchased from Biotium (Freemont, CA) PD-10 sephadex columns were obtained from GE Healthcare (San Francisco, CA). Heat-inactivated fetal calf serum was purchased from General Electric (Logan, UT). Mouse plasma was purchased from Pel Freez Biologicals (Rogers, Arkansas). All other reagents were purchased from Sigma–Aldrich (St. Louis, MO).

3.5.3 Synthesis

Disterol-PEG derivatives were synthesized from acylation of an amino-propanediol backbone previously reported[171] and as outlined in Figure 1.

3.5.3.1 Synthesis of compound 1

Compound **1** and **2** were synthesized as done previously.[172] Cholesterol (7 mmol), dissolved in anhydrous THF (12 mL) was treated with 60% NaH dispersion in mineral oil (15 mmol) and tert-butylbromoacetate (18 mmol) was added dropwise at 0°C. The reaction was quenched by addition of methanol (3.0 mL) at 0°C after 24 hours under inert atmosphere and stirred for 30 min before concentration by rotary evaporation. The resulting solid was dissolved in chloroform and washed three times with water. Organic

phases were combined, dried over anhydrous sodium sulfate and filtered. The filtrate was purified by silica column chromatography with 10% ethyl acetate in n-hexane.

3.5.3.2 Synthesis of compound 2

Compound 2 (2 mmol) was first dissolved in chloroform (2 mL) with formic acid slowly added while stirring (3.0 mL). After stirring overnight at room temperature, the reaction mixture was concentrated by rotary evaporation. Chloroform (15mL) was added 3X and concentrated to remove residual formic acid which yielded a pure product.

3.5.3.3 Synthesis of compound 4

3-Methylamino-1,2-propanediol (0.8 mmol) was dissolved in dimethylformamide (DMF) (1 mL) and stirred under inert atmosphere. mPEG-NPC (0.4 mmol) was dissolved in DMF (3 mL) and added dropwise. The reaction was allowed to stir for 30 minutes before the dropwise addition of DIPEA (0.5 mmol). After overnight stirring the mixture was dialyzed against water for 24 hour with four changes in a 2K MWCO tube. The resulting sample was lyophilized and recrystalized with diethylether to yield a pure product.

3.5.3.4 Synthesis of compound 5

Sterol addition to **4** was completed as done previously.[145] **4** (0.5 mmol) was solubilized in 5 mL chloroform. **2** (1.5 mmol) was added followed by dimethylaminopyridine (DMAP) (0.2 mmol) and 1-Ethyl-3-(3-dimethylaminopropyl)carbodiimide (EDC) (4 mmol). The reaction proceeded overnight at 40º C then dialyzed in a 2K MWCO tube in chloroform:methanol (50:50) with four solvent changes into 100% methanol over 24 hours. Sample was concentrated by rotary evaporation, dissolved in water and dialyzed over 24 hours at 4º C. Lyophilization

produced an off-white solid that was purified by silica column chromatography in 10% ethylacetate in n-hexane with the product eluted in 5% methanol in chloroform.

3.5.3.5 Synthesis of compound 6

Compound **6** was synthesized in the same manner as **4** with using 2-methyl-2-amino-1,3-propanediol as the template.

3.5.3.6 Synthesis of compound 7

Sterol addition to **6** was completed in the same manner as **4** using commercial available cholesteryl hemisuccinate (**3**). Following lyophilization the compound did not require further purification.

3.5.4 Chemical Characterization

Compound 1. Yield: 30%. ^{1}H NMR ($CDCl_3$): δ 0.70 (s, 3H), 0.87 (d, 6H), 0.93 (d, 3H), 1.02 (s, 3H), 1.02-1.63 (m, 21H), 1.49 (s, 9H), 1.94 (m, 5H), 2.35 (m, 2H), 3.21 (m, 1H), 4.03 (s, 2H), 5.37 (d, 1H)

Compound 2. Yield: Quantitative. ^{1}H NMR ($CDCl_3$): δ 0.70 (s, 3H), 0.87 (d, 6H), 0.93 (d, 3H), 1.02 (s, 3H), 1.02-1.63 (m, 21H), 1.94 (m, 5H), 2.35 (m, 2H), 3.31 (m, 1H), 4.18 (s, 2H), 5.37 (d, 1H)

Compound 4. Yield 70%. ^{1}H NMR (D_2O): δ 2.92 (s,2H), 3.32 (s, 3H), 3.46 (m, 2H), 3.58 (m, 6H), 3.60 (s, 190H), 3.89 (t, 3H), 4.19 (m, 1H)

Compound 5: Yield: 50%. ^{1}H NMR ($CDCl_3$): δ 0.68 (s, 6H), 0.85 (d, 12H), .86 (d, 6H), .98 (s, 6H), 1.01-1.6 (m, 40H), 1.89 (m, 6H), 2.37 (m, 4H), 2.96 (s, 3H), 3.23 (m, 2H), 3.38 (s, 3H), 3.45 (m, 6H), 3.63 (s, 210H), 3.81 (t, 3H), 4.06 (s, 4H), 4.13 (m, 2H), 4.19 (m,1H),

4.26 (m, 2H), 4.42 (m,1 H), 5.34 (s, 2H). ^{13}C NMR ($CDCl_3$): 11.9, 18.7, 19.3, 21.4, 22.6, 24.1, 28.1, 31.9, 35.6, 36.6, 39.6, 42.2, 50.0, 56.5, 58.9, 70.9, 72.1, 122.1, 140.5, 170.6. MALDI, MW_{AVG}= 3.0 kDa, PDI=1.03. Elemental analysis for [C154H281NO53]: C, 61.76; H, 9.46; N, 0.47; Found: C, 60.31; H, 9.03; N, 0.25. Carbon values are lower due to hydroscopic nature of PEG.

Compound 7: Yield: 70%. ^{1}H NMR ($CDCl_3$): δ 0.67 (s, 6H), 0.85 (d, 12H), 0.90 (d, 6H), 1.0 (d, 6H), 1.03-1.65 (m, 40H), 1.61-1.93 (m, 10H), 2.31 (d, 4H), 2.39 (m, 1H), 2.62 (m, 4H), 3.24 (s, 3H), 3.50 (m, 6H), 3.64 (s, 205H), 3.81 (t, 3H), 4.20 (m, 6H), 4.60 (m, 2H), 5.23 (m, 2H). ^{13}C NMR ($CDCl_3$): 11.7, 18.8, 19.2, 21.0, 22.7, 23.8, 27.9, 29.2, 31.7, 35.9, 36.4, 38.2, 39.3, 42.0, 50.0, 56.5, 58.8, 70.4, 71.9, 74.1,122.6, 139.7, 171.6. MALDI, MW_{AVG}= 3.1 kDa, PDI= 1.01. Elemental analysis for [C158H289NO54]: C, 61.88; H, 9.50; N, 0.46; Found: C, 61.54; H, 9.39; N, 0.47

3.5.5 Elemental Analysis

A total of 5–10 mg of dry lipid was submitted to Microanalytical Laboratory at the University of California Berkeley for elemental analysis determinations using an ICP Optima 7000 DV instrument.

3.5.6 Carboxyfluorescein (CF) release

The carboxyfluorescein encapsulating protocol was completed as done previously.[145] A lipid film (5 μmol) was rehydrated in 10 mM Tris, 100 mM carboxyfluorescein (CF), pH 7.4 to a final concentration of 10 mM lipid. Each sample was heated at 60ºC for 1 hour and subsequently sonicated at 60ºC for 10 min. Liposomes were then extruded 11-13 times through a 100 nm polycarbonate membrane. Free CF

was removed by size exclusion chromatography with a PD-10 sephadex column. Liposomes were incubated in 200 µL of 105 mM NaCl, 10 mM HEPES pH 7.4 containing 30% (v/v) fetal bovine serum, 0.02% sodium azide at 37ºC for one week. Leakage was measured on a SpectraMax M5 microplate reader with excitation at 485 nm and emission at 518 nm. Percent leakage values were obtained by normalization to the fluorescence of the samples after lysis of liposomes using 0.1% Triton. Leakage measurements were run in triplicate.

3.5.7 Fluorescent anisotropy

Lipids were dissolved in chloroform, dried to form a thin film, and placed under high vacuum overnight. The films were hydrated with 140 mM NaCl, 10 mM HEPES at 60°C and vortexed to obtain a lipid concentration of 5 mM. Each sample was heated at 60ºC for 1 hour and subsequently sonicated at 60ºC for 10 minutes. Liposomes were then extruded 11-13 times through a 100 nm polycarbonate membrane. Liposomes were diluted 8-fold with PBS and 6 µl of 1,6- diphenyl-1,3,5-hexatriene in tetrahydrofuran (0.15 mg/ml) was added to the sample. The mixture was incubated at 65°C for 1 hour to allow DPH to integrate into the bilayer. Liposomes were heated or cooled in 5°C increments from 5–65°C, with a 3–10 minute equilibration between transitions and anisotropy was detected by DPH fluorescence (Ex. 350 nm, Em. 430 nm).

3.5.8 Liposome size and charge

Zeta and size measurements were obtained with 200 µM liposomes in 140 mM NaCl, 10 mM HEPES using a Malvern Nanosizer. All samples were run in triplicate.

3.5.9 Transmission electron microscopy.

TEM was performed as done previously.[171] Liposomes were buffer exchanged into 140 mM ammonium carbonate, 10 mM HEPES, pH 8. A 2.0 µL drop of liposomes were adsorbed for 60 seconds on a glow-discharged carbon-coated copper grid (Ted Pella, Redding, CA) and water was wicked off. Then, 2 µL of a 1% uranyl acetate negative stain solution were added and left to stain for 60 seconds and wicked off. The grid was then washed with deionized water three times and the water was removed by wicking. Grids were imaged with a FEI Tecnai T12 TEM (FEI company, Hillsboro, OR) at 120kV. Data were acquired with a 4 x 4 Gatan UltraScan CCD camera (Gatan, Pleasanton, CA).

3.5.10 Albumin labeling

A 10 mg/mL solution of bovine serum albumin with 0.4 mg/mL fluorescein isocyanate in 100 mM carbonate buffer, pH 8 was allowed to stir for 3 hours at room temperature. Albumin was separated from unreacted fluorescein by size-exclusion chromatography on a PD-10 column to yield labeled albumin.

3.5.11 Protein binding

Liposomes were mixed at 5 mM with sterile filtered fluorescently labeled albumin (10 mg/mL) or mouse plasma in 140 mM NaCl, 10 mM HEPES, 0.5 mM EDTA, 1mM DTT for 5 hours at 37°C. Samples were centrifuged at 120,000 x*g* in a Beckman TL-100 ultracentrifuge to pellet the liposomes and any bound protein. After the supernatant was removed, liposomes were resuspended into binding buffer and analyzed for associated proteins. Samples were run in triplicate and normalized based on liposome concentration.

3.5.12 Cell Uptake

Cell uptake was performed as done previously.[169] HeLa cells were plated onto 12 well plates and grown to 70-80% confluency. Media was removed and cells were washed 3X with PBS before being incubated in reduced serum media containing 100 µmol liposomes and 1 ug/mL ApoE3 for 5 hours at 37ºC with gentle rocking. Following the incubation, the media was removed and the cells were washed 3X with PBS then lysed using RIP-A at 4ºC and spun down at 12,000 RPM for 20 minutes. The supernatant was removed and uptake was determined by liposome fluorescence compared to the total initial concentration added initially.

3.5.13 Pharmacokinetic studies

Mouse pharmacokinetics was conducted at Murigenics (California) in male CD-1 mice of 20-30 g following standard procedures. Mice were injected with 60 µmol/kg of lipid via tail vein with serum collected 24 hours later. Plasma was shipped under dry ice and analyzed for fluorescence compared to a standard curve of liposomes with spiked amounts of plasma. Each liposome sample was injected into groups of three mice.

4 Chapter 4: Recombinant expression of matrix metalloproteinases from E. coli

4.1 Introduction

Matrix metalloproteinases (MMPs) are one of the key regulators of the extracellular space surrounding cells.[118] They maintain cellular homeostasis by influencing cell signaling, mechanochemical transduction, cell growth/migration, and cell-differentiation.[173] The MMP family includes 23 different proteins in vertebrates which have a similar protein sequence consisting of an N-terminal inhibitory sequence followed by a catalytic domain, a flexible hinge and lastly a C-terminal hemopexin region (Figure 4-1). Despite the similarity in structure, MMPs target a wide range of extracellular proteins including collagen, gelatins, aggrecan, entactin, tenascin, perlecan, decorin, laminin, and fibronectin.[109]

Due to their breadth of functions, aberrant MMP activity can lead to dire cellular consequences including bone deficits, inflammation, and angiogenic defects.[173] Most notably, greater MMP activity has been linked to increased tumor metastasis and a worse tumor prognosis.[10,92–100] The association between MMPs and cancer captured the clinical focus of these enzymes. This led to the development of inhibitors against various MMPs in hopes of improving cancer outcomes. These inhibitors demonstrated little efficacy and high musculoskeletal toxicity in clinical trials.[92,174,175] The failure of MMP inhibitors generated a greater appreciation for the complex roles of MMPs in modulating the ECM and raised questions surrounding the precise conditions where MMPs may contribute to tumor progression.

Although the clinical enthusiasm surrounding MMP inhibition may have been misplaced, there are a series of ailments marked by increased ECM deposition including,

fibrosis,[176] cancer,[10] Dupuytren's,[124] Peyronie's disease,[125] and disc degeneration,[177] which could all benefit from ECM clearance. Therefore, it may be therapeutically relevant to augment by supplementation or induction rather than to inhibit the native activity of MMPs in targeting the ECM. MMPs are largely untested in these areas but before they can be used therapeutically, the enzymes will need to be produced at sufficient levels to enable *in vivo* experiments.

Recombinant expression from bacteria requires elaborate extraction from bacterial inclusion bodies and subsequent refolding with limited yields.[112,178,179] In addition, recombinant expression in bacteria is limited to the catalytic domain of the proteins without the flexibility and substrate specificity provided by the hinge and hemopexin domains.[115,178] Mammalian and insect expression systems allow for purification of full length protein but such systems are costly, time consuming, and provide yields around 1 mg/L of culture.[117] MMPs will also need to demonstrate that they can be functional in long circulating formulations after intravenous injection to allow enzymes sufficient time to extravasate into the target tissue and reduce ECM deposits.

Here, we highlight approaches and limitations in producing recombinant MMPs in bacteria and demonstrate tools to enable translational experimentation. We direct our focus on MMP-8 (Collagenase 2) since it has activity for a variety of ECM components[13] and has been the most explored MMP for reducing the extracellular matrix.[110,111,129]

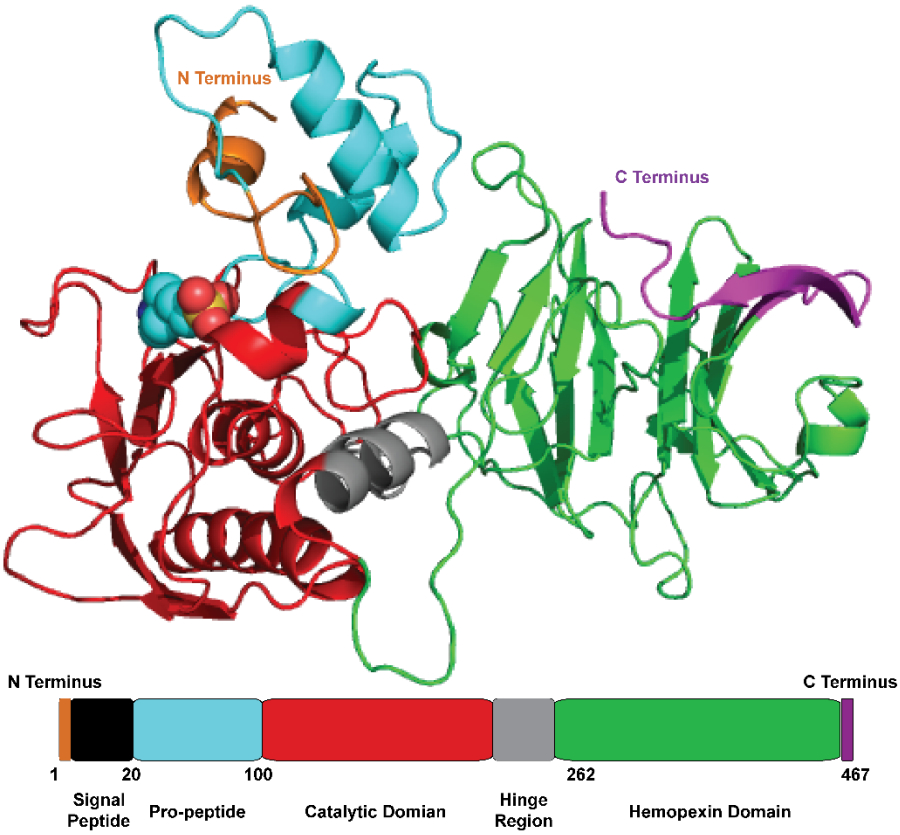

Figure 4-1: MMP-8 homology model. A homology model of human MMP-8 was produced in PyMol using MMP-13 as a reference. The structure highlights the key elements common to MMPs: (N to C Terminus) a signal peptide for extracellular secretion; a pro-peptide which must be cleaved to enable enzymatic activity; a catalytic domain which performs the protein hydrolysis; a flexible hinge region to enable binding to and cleaving substrate; and a hemopexin domain responsible for binding to fibrillar collagen during proteolysis.

4.2 Results

4.2.1 Periplasmic Expression

Periplasmic expression of full length and truncated (M100-G262) MMP-8 (Figure 4-1) was attempted by cloning both versions into a pET22B expression vector behind a pelB localization sequence for periplasmic secretion (Figure 4-2A). In 20 mL cultures,

purification from the periplasmic space by osmotic shock yielded truncated MMP-8 with a mass of approximately 19 kDa whether expressed at 16 or 25ºC. To determine whether the periplasmic extraction provided MMP-8 in an active form, activity was measured using a fluorescent gelatin peptide at both expression temperatures. Enzyme activity was significantly higher when culturing bacteria at 16ºC suggesting that growing the bacteria at a slower rate allowed for improved protein production and folding into an active orientation (Figure 4-2A).

Surprisingly, when scaling up to production of 1 L and greater, periplasmic expression did not provide any MMP-8 (Figure 4-2C). In addition, periplasmic extraction did not provide any full-length MMP-8 regardless of the temperature or scale of production. Altering the amount of IPTG, incubation length, and temperature did not improve the results. Our inability to successfully scale to larger cultures dictated the need to investigate alternative methods to produce MMP-8.

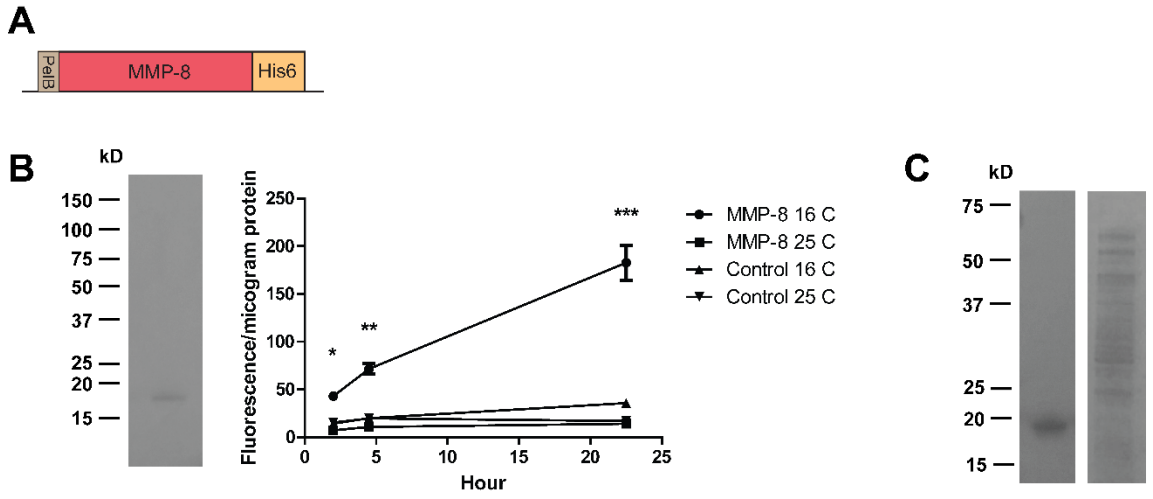

Figure 4-2: Periplasmic expression of truncated MMP-8. Full length and truncated MMP-8 were cloned and extracted from the periplasmic space of BL21(DE3) cells. A) Schematic of the constructs used for expression. B) Truncated MMP-8 can be extracted

from periplasmic space by osmotic shock (left) while retaining activity (right). Activity is greater when produced at 16ºC rather than 25ºC. C) SDS-Gel comparing periplasmic protein extract when bacteria cells are grown at 20 mL (left) or 1 L (right) scale. Increased culture size eliminated periplasmic secretion of MMP-8. *p<0.001, **p<0.001, ***p<0.001; One-way ANOVA with Tukey's post-test.

4.2.2 Column Refolding and Purification

After failure to produce MMP-8 at large volumes by periplasmic expression, production was attempted using a modified column refolding protocol.[112] In summary, freshly transformed MMP-8 containing bacteria were grown overnight with downstream extraction from the insoluble inclusion bodies where the isolated protein was refolded on a NiNTA-charged column (Figure 4-3). Constructs were cloned to remove the pelB leader and incorporate a *GGS* space between the protein and His_6 tag (Figure 4-4A). Column refolding using a stepwise titration from 8 M to 0 M urea yielded pure truncated MMP-8. It appears that adequate space to refold was required for the enzyme when bound to the column since maximum yields of 900 µg/liter culture were achieved when urea extracted protein was diluted onto multiple joined columns (Figure 4-3). The HisTrap HP columns can accommodate upwards of 40 mg of His_6 protein per milliliter resin, but the truncated MMP-8 was refolded optimally at 1 mg of protein per milliliter of resin.

Truncated MMP-8 structure was confirmed by Western blot and MALDI-TOF (Figure 4-4A, B). To determine whether the protein could cleave ECM components, activity was first determined by gelatin zymography, a gel-based staining technique which revealed gelatin removal at the expected protein mass of approximately 19 kDa (Figure 4-4B). In addition, dose dependent activity over a 24-hour period was measured using a gelatin fluorophore (Figure 4-4C). This procedure was successful for purification of truncated MMP-8 from 1 L bacterial cultures but not the full-length protein.

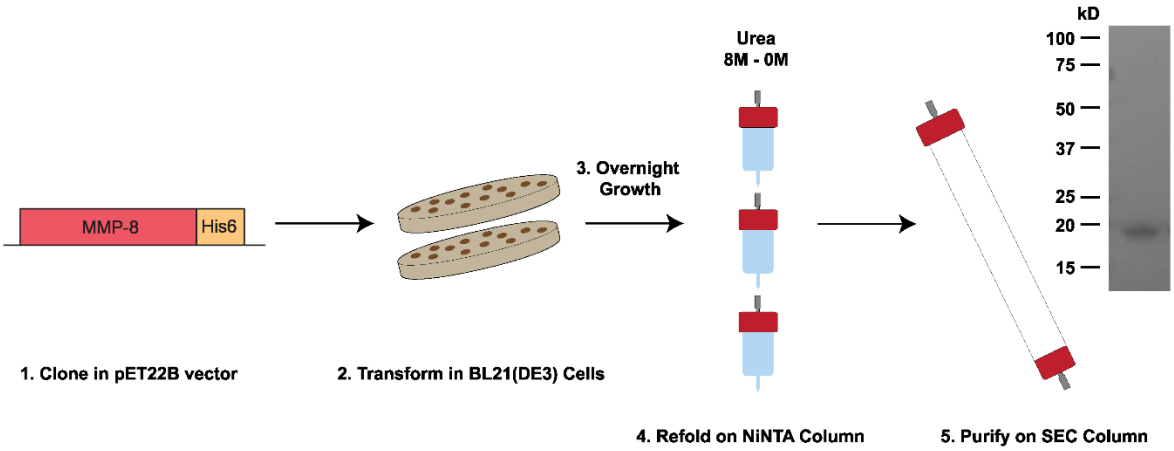

Figure 4-3: MMP column refolding procedure. MMPs were produced by: (1) cloning the enzyme into pET expression vectors; (2) transformation into BL21(DE3) cells and grown overnight on ampicillin resistant plates; (3) refolding on multiple NiNTA columns through a stepwise titration from 8M to 0M urea; and (4) isolation by SEC.

Full-length MMP-8 displayed no expression in BL21(DE3) cells while the urea extracted fraction from SHuffle® cells displayed full length protein along with its activated form lacking the pro-domain (Figure 4-4D). The added chaperone proteins present in SHuffle® cells compared to BL21(DE3) cells likely improved stability of the produced protein. However, following His_6-NiNTA purification and column refolding, the protein underwent post-production degradation and only recovered a band corresponding to the mass of truncated protein (Figure 4-4D). The result was consistent across cell growth conditions despite altering the amount of IPTG, incubation length, and temperature. MMPs can undergo autoproteolysis[180] which may explain the result but addition of EDTA, which is known to chelate Zn^{+2} and Ca^{+2} required for MMP activity, did not prevent proteolysis before or after refolding (Table 4-1). The inability to recombinantly produce full-length MMP-8 aligns with what is reported by other researchers.[115,117]

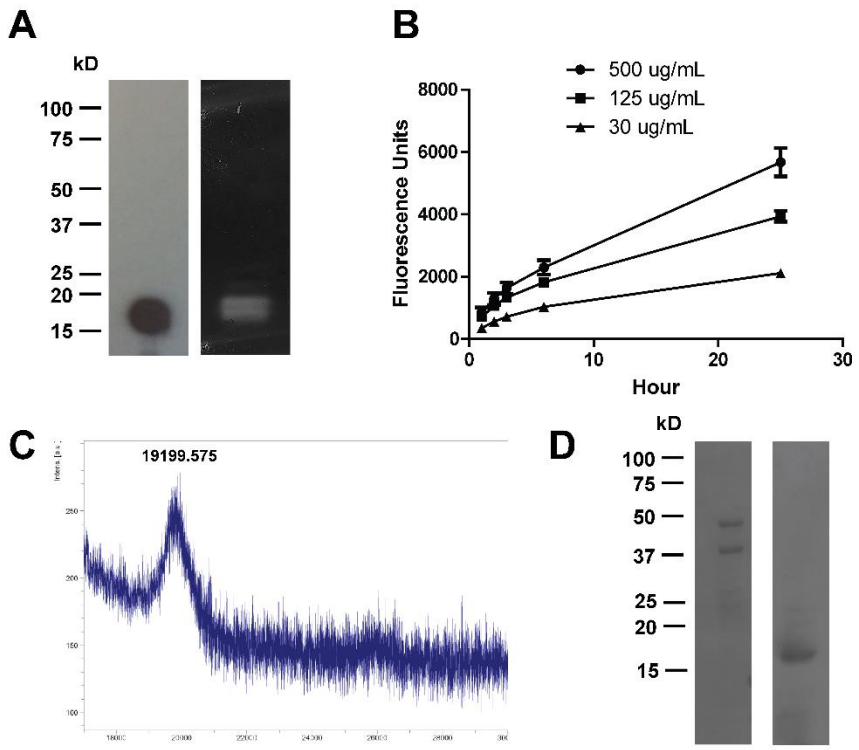

Figure 4-4: Truncated MMP-8 purification and characterization. MMP-8 was purified using a column refolding protocol described above. A) Enzyme structure was confirmed by western blot (left) and gelatin zymography (right). B) Purified protein displayed dose depend activity. C) MALDI-TOF confirmed protein mass (Expected 19121) and matched results from zymography and western blotting. D) Full length MMP-8 SDS gel before (left) and after (right) column refolding. Two bands correspond to the protein with (top) and without (bottom) the pro-peptide. The full-length construct undergoes post production degradation after refolding.

4.2.3 mKate Fusion Proteins

Although the column refolding protocol produced active truncated MMP-8, it occurred at low yields and was unsuccessful for the full-length protein. Fusing well-solubilized proteins to proteins which are difficult to express can aid in the solubilization and increase overall yields.[181] mKate, a soluble and highly expressed protein in E. coli, was fused to the N and C terminus of truncated and full-length MMP-8 with a *GGGS* linker

in a pET15B vector (Figure 4-5A). In addition to serving as a protein chaperone, mKate's fluorescent properties would enable tracking and quantification of MMP-8 within the ECM.

Expression of C and N-terminal mKate fusions for truncated MMP-8 did not allow purification from the soluble portion of the cell; the fusion proteins remained in the inclusion bodies (Figure 4-5B). There was no expression of the full-length protein fusions in any cellular fraction. Constructs were re-cloned to include a more flexible *GSAGSAAGSGEF* linker between mKate and MMP-8 to improve spacing for the fusion protein to refold (Figure 4-5A). The increased linker flexibility allowed for expression of full-length MMP-8-mKate fusions in BL21(DE3) cells (Figure 4-5B), however all fusion proteins were still shunted to the insoluble portion of the cell in bacteria.

C and N-terminal truncated MMP-8 fusions were extracted from the bacterial inclusion bodies using the column refolding protocol described above to determine if the fusion protein could be successfully purified. Column refolding from small 20 mL cultures yielded purified N and C terminal fusions (Figure 4-5C). The N-terminal fusion exhibited higher activity than the C terminal fusion likely due to the proximity of mKate to the catalytic site of MMP-8 (Figure 4-5D). The activity of the N-terminal fusion was similar to the unmodified MMP-8 and it also displayed a comparable emission spectrum to that of mKate, highlighting that these fusions could be used to track MMP-8 while liberating ECM (Figure 4-5E). Importantly, when scaling up to 1 L cultures all of the mKate fusions underwent post-production degradation to yield two bands corresponding to isolated mKate and truncated MMP-8 (Figure 4-5F). The degradation was present when using either the *GGGS* or *GSAGSAAGSGEF* linkers for both C and N-terminal fusions.

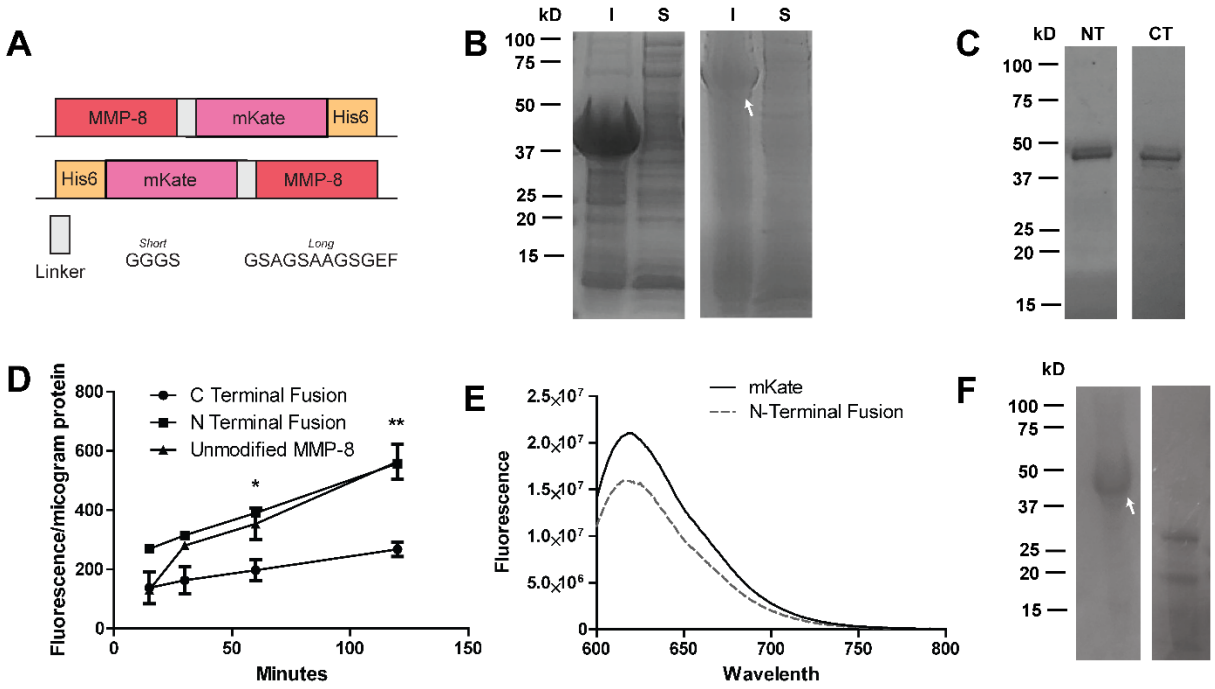

Figure 4-5: MMP-8-mKate fusion protein expression and characterization. A) Schematic of constructs used for expression detailing N and C-terminal fusions in addition to the linkers tested. B) Truncated (left) and full-length (right) MMP-8-mkate are expressed in the insoluble (I) rather than soluble (S) portion of bacteria. Gel is representative for all truncated MMP-8 fusions (left) and full-length fusions using the longer linker (right). C) Column refolding allowed for purification of N-Terminal (NT) and C terminal (CT) truncated MMP-8 fusion proteins. D) CT displays lower enzymatic activity than NT and unmodified truncated MMP-8. E) Fluorescence emission spectrum (Ex. 588) of mKate (top) and NT. The fusion protein exhibits a similar fluorescence emission spectrum. F) Representative gel of the autoproteolytic cleavage event following purification of fusion proteins from larger cultures. The fusion protein is intact following the urea extraction step (left) but is cleavage into individual proteins after column refolding (right). *p<0.01,**p<0.01 One-way ANOVA with Tukey's post-hoc test.

4.2.4 Liposome Attachment

Alongside improving expression and purification of MMP-8 it was important to determine if the protein could be formulated for improved *in vivo* delivery. Recombinantly produced proteins undergo rapid clearance when administered *in vivo*.[182] Attaching therapeutic proteins to a long circulating nanoparticle can aid in extending the half-life

beyond a few minutes in mice. Bacterial collagenases have been successfully attached to lipid nanoparticles while still retaining activity[74,75] but there is no published evidence doing so with MMPs. We sought to attach MMPs to liposomes both covalently and noncovalently to determine if this could be a viable approach (Figure 4-6).

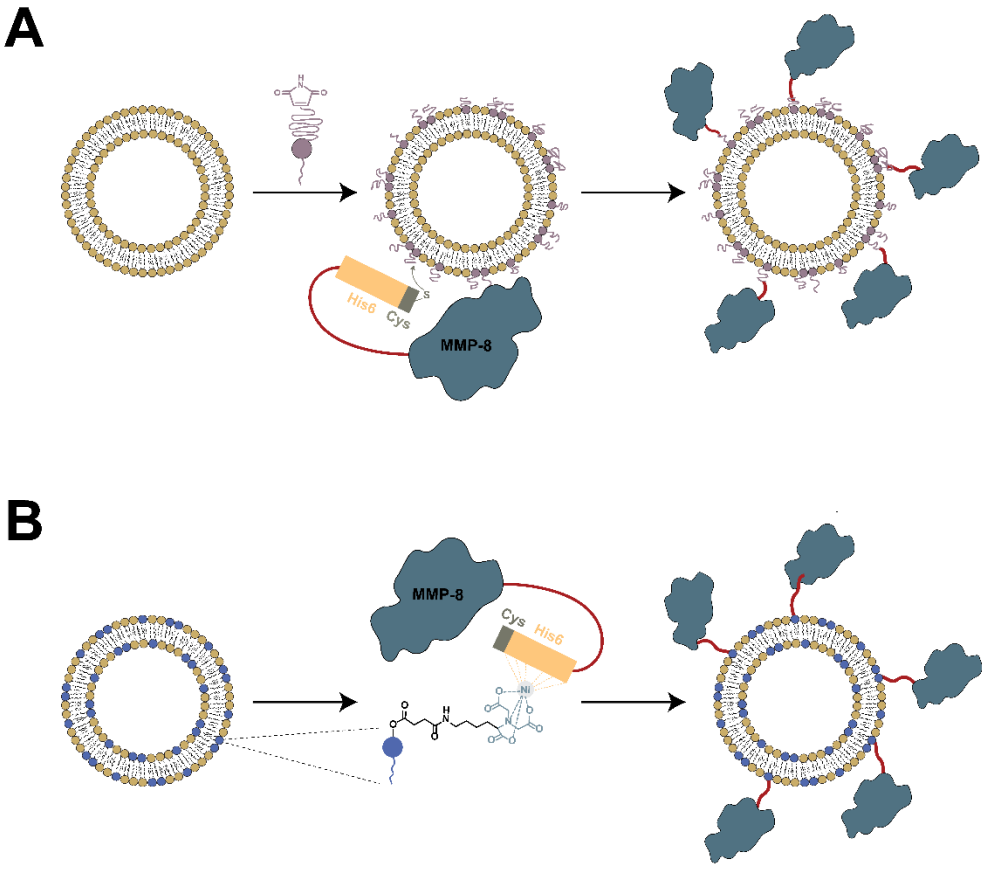

Figure 4-6: Schematic of attaching MMP-8 to the liposome surface. MMP-8 was attached to liposomes both covalently (top) and non-covalently (bottom). For covalent conjugation, a reactive DSPE-PEG2K-maleimide lipid was incorporated into the lipid bilayer and later reacted with a terminal cysteine on MMP-8. For non-covalent attachment, liposomes were produced containing a DGS-NiNTA lipid, which interacted with the His_6 tag of the protein for successful association to the liposome surface.

A terminal cysteine was cloned into pET22B truncated MMP-8 to enable conjugation to liposomes. MMP-8 was reacted with a DSPE-PEG2K-Maleimide lipid while

incorporated into a liposome formulation equivalent to that of the FDA approved Doxil®. A total of 70-80% of the enzyme was attached to the liposome surface. Conjugation of the DSPE-PEG2K-Maleimide lipid was confirmed by Western blot compared to the unreacted enzyme. The Western blot demonstrated a 3 kDa increase in mass for the MMP-8-DSPE-PEG2K-maleimide lipid compared to MMP-8 alone (Figure 4-7B).

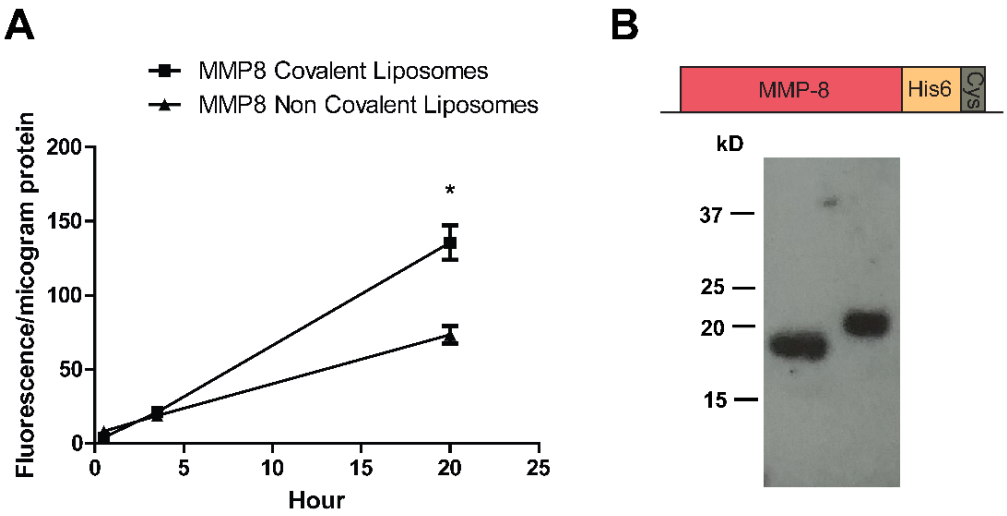

Figure 4-7: Liposome associated MMP-8. A) Activity of truncated MMP-8 covalently and noncovalently bound to the liposome surface. Covalent attachment to a DSPE-PEG2K-Maleimide lipid allowed for increased activity. B) Western blot verification of conjugation to DSPE-PEG2K-maleimide lipid as indicated by a 3 kDa increase in mass (right) compared to the unmodified MMP-8 (left). *p<0.01, *t*-test.

MMP-8 was also associated with liposomes by utilizing a His_6-NiNTA interaction. A DGS lipid containing a NiNTA headgroup was incorporated into liposomes and allowed to interact with His_6 tagged MMP-8. Approximately 80-90% of the MMP-8 associated with the liposomes. Attaching MMP-8 to the liposome covalently through DSPE-PEG2K-Maleimide and noncovalently via the DGS-NiNTA lipids produced enzyme-containing particles that retained enzymatic activity. The two formulations exhibited comparable

activity over four hours but the covalent formulation had significantly greater activity by 20 hours (Figure 4-7A). Attaching the enzyme to the end of a 2 kDa PEG likely limited the steric hinderance from the liposomes enabling more effective enzymatic activity. Notably, the enzymatic activity was approximately ten-fold lower than the unmodified enzyme likely due to the bulkiness of the liposomes. the enzymatic activity was approximately ten-fold lower than the unmodified enzyme likely due to the bulkiness of the liposomes.

4.2.5 Other MMPs

To determine if the purification methods extended to other MMPs beyond MMP-8 we attempted to purify MMP-1, MMP-9, and MMP-13. The collagenase and gelatinase activity of MMP-1 (Collagenase 1), MMP-13 (Collagenase 3) and MMP-9 (Gelatinase 2) make them attractive for ECM degradation. MMP-1, MMP-13, and MMP-9 were cloned into pET22B expression vectors with a C-terminal His_6 tag (Figure 4-8). MMP-1 and MMP-13 were extracted from the insoluble portion of the SHuffle® cells to reveal proteins at an appropriate mass (Figure 4-8). However, these proteins were unable to be successfully purified. Similar to MMP-8, after column purification both proteins underwent post-production degradation, highlighting that challenges in MMP expression are shared amongst several members of the protein family. MMP-9, which is almost double the size of other MMPs investigated, showed very low levels of expression in the Shuffle® cells.

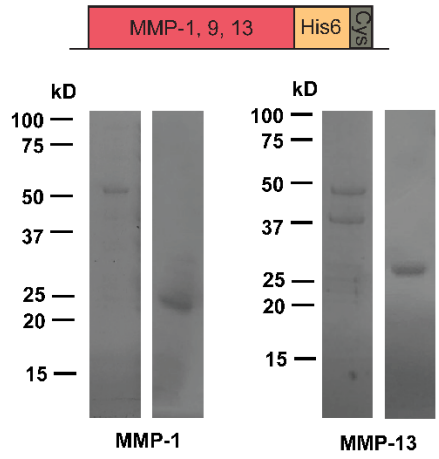

Figure 4-8: Expression of additional MMPs. Constructs used for expression (top). Representative SDS-gels illustrating protein before (left) and after (right) column refolding. Similar to MMP-8, MMP-1 and MMP-13 undergo autoproteolytic cleavage following purification. MMP-9 had only minimal expression.

4.3 Discussion

MMPs are notoriously difficult to express recombinantly in bacteria and have limited yields in conventional eukaryotic expression systems.[178] Here we demonstrated several approaches to produce MMPs in *E Coli*. The two primary limitations of MMP expression observed are an absence of scaling between small and large cultures and the post-production degradation of full-length MMPs with purification. In protein expression, results from small-scale protein production generally correlate with results when scaling up.[183] However, protein expression and solubility are greatly influenced by culture conditions, growth rate and aeration which do not always scale with culture size.[183] MMPs are toxic to bacterial cells,[112] therefore those cells producing high levels of protein are at a growth disadvantage compared to cells producing less protein. This difference is intensified during the course of protein production when bacterial cells are growing exponentially. In

our experience, growing cells more slowly generally improved protein yields perhaps by mitigating the difference between growth of high and low MMP expressing cells. For example, periplasmic expression at 16ºC produced protein with higher activity than 25ºC (Figure 4-2), likely due to the slower replication at the lower temperature. This discrepancy may account for the differences observed between small and larger cultures because of the increased aeration and growth achieved in larger culture volumes.

Degradation following refolding and purification was commonly observed with all full-length MMPs and MMP-8-mKate fusion proteins. The result is likely due to the inherent instability of the protein and susceptibility to autocleavage.[180] Interestingly, for the mKate fusions, degradation even occurred despite the limited space between the two proteins when using a short *GGGS* linker. To combat the issues with culture-scaling and degradation, we attempted to include several additives during various steps of the refolding and purification but did not observe any appreciable changes to purification of active protein (Table 4-1).

Table 4-1: Investigated additives to improve MMP production and purification.

Additive	Production Step	Desired Effect	Result
Lysozyme- 0.1%	Lysis	Improve protein lysis to allow more proteins to be extracted from cells	No Change
Triton- 0.01-1%	Lysis	Improve protein lysis to allow more proteins to be extracted from cells	No Change
Tween- 0.01-.1%	Lysis	Improve protein lysis to allow more proteins to be extracted from cells	No Change

Additive	Production Step	Desired Effect	Result
Glucose- 2%	Bacteria Growth	Ensure bacteria have a sufficient energy source for growth and protein production	No Change
Glycerol- 5-20%	Dialysis	To stabilize the protein following column refolding	No Change
Polyethylene Glycol- 10-20%	Dialysis	To precipitate unfolded proteins	No Change
EDTA – 5 mM	Dialysis Urea Extraction	Inhibit potential autoproteolytic activity	No Change

Despite the difficulties in purification of MMPs we were able to successfully produce active truncated MMP-8 from the periplasmic space, and from inclusion bodies alone and as an mKate-fusion. Furthermore, we were able to attach the enzyme to the surface of liposomes while retaining enzymatic activity. To the best of our knowledge this is the first example to illustrate the ability to purify human collagenases from the periplasm as well as the first to utilize a column refolding protocol for purification of MMP-8. A lot still has to be done to optimize the yields and stability of MMPs with these procedures, including improving the fraction of protein that refolds and insuring protein stability during production and purification.

Only a small fraction of total protein refolds when purified from inclusion bodies.[183] Repeatedly, our systems would yield 30 mg/L of unfolded protein but under 1% would refold and the remainder would either precipitate or elute in the void during SEC. Optimizing the ratio of resin to protein increased the percentage of refolded protein to a

maximum of 3% or about 900 µg by providing the protein more room to refold (Figure 4-3). However, because this improvement may be capped, novel cocktails of protease inhibitors, polymers or substrate (to serve as a scaffold for refolding) might also aid in augmenting the ratio of refolded protein.

Increasing the amount of active protein should be done in tandem with increasing the downstream stability because higher concentrations of active protein may cause greater auto-proteolysis. Cocktails of additives used to improve the fraction of refolded protein might also be used to bolster MMP stability. The improved expression of full-length MMPs in SHuffle® cells over BL21(DE3) points to the benefits of endogenous protein folding stabilizers, such as the protein chaperones present in SHuffle® cells, on MMP stability and expression. Site-directed mutagenesis to identify problematic amino acid sequences may further help in protecting full-length constructs from premature degradation.

Although outside the scope of the work presented here, it is worth noting that even with the low yields, MMP production may be better achieved in costlier mammalian systems especially for full-length enzymes. The difficulties in expression observed with MMP-8 and replicated with MMP-1 and MMP-13, suggest that any success in purifying one of these enzymes could be applied to other collagenases.

4.4 Conclusion

MMPs are notoriously difficult to express recombinantly in bacteria. They are insoluble and unstable. Several contemporary papers published solely on detailing methods to produce MMPs[113,117,184] highlights the large need to further enhance their

production. We have demonstrated new approaches and limitations in the expression of MMP-8 and point to the downstream potential of fluorescently labeled and nanoparticle bound MMP-8 to track and improve enzymatic delivery. In total, we have created a foundation to enable further experimentation on whether MMPs can be therapeutically advantageous at removing heightened ECM deposits found in several diseases.

4.5 Materials and methods

4.5.1 Instrumentation

MALDI-TOF measurements were performed on a Bruker Daltonics MicroFlex LT system (Billerica, MA). Particle size and zeta measurements were carried out using a Nano-ZS Dynamic Light Scattering Instrument from Malvern (Westborough, MA). Fluorescence spectroscopy was measured on a FluoroLog-3 spectrofluorimeter (Horiba Jobin Yvon) with data collection using FluorEssence software or on a SpectraMax M5 microplate reader with data collection using SoftMaxPro.

4.5.2 Materials

Terrific Broth (TB), and isopropyl β-D-1-thiogalactopyranoside (IPTG) were purchased from VWR (Radnor, PA). Nickel Sepharose high performance resin prepacked in 5 mL HiTrap columns (HisTrap FF), PD-10 desalting columns, and Superdex 75 size exclusion chromatography (SEC) column were purchased from GEHealthcare (Piscataway, NJ). EDTA-free protease inhibitor solution was purchased from BiMake (Houston, TX). Amicon spin filters were purchased from Millipore (Billerica, MA). MMP-8 antibody (PA5-28246) was purchased from Thermo Fisher (Waltham, MA). SDS and zymogram materials and buffers were purchased from BioRad (Hercules, CA).

EnzChek™ Gelatinase/Collagenase Assay Kit was purchased from Life Technologies (Carlsbad, CA). BL1(DE3) competent cells, T7 Express Shuffle® Cells, Gibson Assembly Mastermix, and T4 DNA ligase were purchased from New England Biolabs (Ipswich, MA). All lipids were purchased from Avanti Polar Lipids (Alabaster, AL). MMP-1 (3834572), MMP-8 (30915305), MMP-9 (4054882) and MMP-13 (30915315) cDNA were purchased from GE Dharmacon (Lafayette, CO). All other reagents were purchased from Sigma–Aldrich (St. Louis, MO).

4.5.3 Plasmid Construction

Plasmids were cloned using standard techniques, including Gibson assembly with sequence verified upon completion. Plasmids were constructed using the following primers for MMP-1 (BC013875), MMP-8 (BC074989), MMP-9 (BC006093), and MMP-13 (BC074807):

Construct	#	Sequence (5'-3')
pET22B MMP-8	1	GAGCAGAAATGGAAGCGTCTTCAGGGAGAACATGGCCATCGCCGGCTGGGCAG (Vector-R) AATAAATGGCTTAACTGTAGATATGGCCACCACCACCACCACCACTGAGATCC (Vector-F) CTCCTCGCTGCCCAGCCGGCGATGGCCATGTTCTCCCTGAAGACGCTTCCATTTCTGCTC (cDNA-F) ATCTCAGTGGTGGTGGTGGTGGTGGCCATATCTACAGTTAAGCCATTTATTGCCTCTTGC (cDNA-R)
pET22B MMP-8 (M100-G262)	2	TTGGGGTTTCCTGGGGTTAACATGGCCATCGCCGGCTGGGCAG (Vector-R) AGGCCATCTATGGACACCACCACCACCACCACTGAGATCC (Vector-F) CTCCTCGCTGCCCAGCCGGCGATGGCCATGTTAACCCCAGGAAACCCC (cDNA- F) ATCTCAGTGGTGGTGGTGGTGGTGTCCATAGATGGCCTGAATGCCATCGATGTC (cDNA-R)
pET22B MMP-8 - GGS	3	GGAGGTTCTCACCACCACCACCACCACTGAGATCC (F- Phospho) GCCATATCTACAGTTAAGCCATTTATTGCCTCTTGC (R - Phospho)
pET22B MMP-8 (M100-G262) GGS	4	GGCGGTTCTCACCACCACCACCACCACTGAGATCC - (F- Phospho) TCCATAGATGGCCTGAATGCCATCGATGTC (R - Phospho)
pET22B MMP-8 - PelB Removal	5	ATGTATATCTCCTTCTTAAAGTTAAACAAAATTATTTCTAGAGGGGAATTG (R-Phospho) ATGTTCTCCCTGAAGACGCTTCCATTTCTGCTC (F-Phospho)
pET22B MMP-8 (M100-G262) PelB Removal	6	ATGTATATCTCCTTCTTAAAGTTAAACAAAATTATTTCTAGAGGGGAATTG (R-Phospho) ATGTTAACCCCAGGAAACCCCAAGTGGGAA (F-Phospho)

Construct	#	Sequence (5'-3')
pET15B mKate-MMP-8	7	CATCACAGCAGCGGCATGTCTGAACTGATCAAAGAGAACATGCACATGAAGTTATACATG (mKate-F) TAAGAGCAGAAATGGAAGCGTCTTCAGGGAGAACATCGAGCCGCCGCCGCCTTTATGG (mKate-R) CATAAAGGCGGCGGCGGCTCGATGTTCTCCCTGAAGACGCTTCCATTTCTGCTCTTACTC (MMP-8 -F) GTTCTCTTTGATCAGTTCAGACATGCCGCTGCTGTGATGATGATGATGATGGCTGCT (MMP-8 R)
pET15B mKate-MMP-8 (M100-G262)	8	CATCACAGCAGCGGCATGTCTGAACTGATCAAAGAGAACATGCACATGAAGTTATACATG (mKate-F) AGTGCGTTCCCACTTGGGGTTTCCTGGGGTTAACATCGAGCCGCCGCCGCCTTTATGG (mKate-R) GGCCATAAAGGCGGCGGCGGCTCGATGTTAACCCCAGGAAACCCCAAGTGGGAA (MMP-8-F) GTTCTCTTTGATCAGTTCAGACATGCCGCTGCTGTGATGATGATGATGATGGCTGCT (MMP-8-R)
pET15B - MMP-8-mKate	9	GGCGGAGGTGGCGGATCGATGTCTGAACTGATCAAAGAGAACATGCACATGAAGTTATAC (mKate-F) CTTAGTGGTGATGATGGTGATGGCTTGAGCCTTTATGGCCCAGTTTAGAGGGCAGGTCGC (mKate -R)TTTAACTTTAAGAAGGAGATATACCATGTTCTCCCTGAAGACGCTTCCATTTCTGCT (MMP-8-F) TTCAGACATCGATCCGCCACCTCCGCCATATCTACAGTTAAGCCATTTATTGCCTCTTGC (MMP-8-R) AAGGCTCAAGCCATCACCATCATCACCACTAAGGATCCGGCTGCTAACAAAGCCCGAAAG (Vector-F) GGAGAACATGGTATATCTCCTTCTTAAAGTTAAACAAAATTATTTCTAGAGGGGAATTG (Vector-R)
pET15B -MMP-8-mKate (M100-G262)	10	GGAGGCGGTGGCGGATCGATGTCTGAACTGATCAAAGAGAACATGCACATGAAGTTATAC (mKate-F) CTTAGTGGTGATGATGGTGATGGCTTGAGCCTTTATGGCCCAGTTTAGAGGGCAGGTCGC (mKate-R) TGTTTAACTTTAAGAAGGAGATATACCATGTTAACCCCAGGAAACCCCAAGTGGGAA (MMP-8-F) CAGTTCAGACATCGATCCGCCACCGCCTCCATAGATGGCCTGAATGCCATCGATGTCA (MMP-8-R) AAGGCTCAAGCCATCACCATCATCACCACTAAGGATCCGGCTGCTAACAAAGCCCGAAAG (Vector-F) GGTTAACATGGTATATCTCCTTCTTAAAGTTAAACAAAATTATTTCTAGAGGGGAATTG (Vector-R)
pET15B mKate-MMP-8 Long Linker	11	GCATCCGGAGCTTCTGGTATGTCTGAACTGATCAAAGAGAACATGCACATGAAGTTATA (F-Phospho) CGCTCCAGATCCTTCAAAGCCATATCTACAGTTAAGCCATTTATTGCCTCTTGC (R-Phospho)
pET15B mKate-MMP-8 (M100-G262) Long Linker	12	GCATCCGGAGCTTCTGGTATGTCTGAACTGATCAAAGAGAACATGCACATGAAGTTATA (F-Phospho) CGCTCCAGATCCTTCAAAGCCATATCTACAGTTAAGCCATTTATTGCCTCTTGC (R-Phospho)
pET15B - MMP-8-mKate Long Linker	13	GCGGGTTCTGGAGAATTTATGTTCTCCCTGAAGACGCTTCCATTTCTGCTC (F-Phospho) TGCGGAGCCAGCAGAACCTTTATGGCCCAGTTTAGAGGGCAGGTCGCT (R-Phospho)
pET15B -MMP-8-mKate(M100-G262) Long Linker	14	GCGGGTTCTGGAGAATTTATGTTAACCCCAGGAAACCCCAAGTGGGAAC (F-Phospho) TGCGGAGCCAGCAGAACCTTTATGGCCCAGTTTAGAGGGCAGGTCGCT (R-Phospho)
pET22B MMP-8 (M100-G262) GGC	15	GATCCGGCTGCTAACAAAGCCCGAAAG (F-Phospho) CTAACAGCCACCGTGGTGGTGGTGGTGAGAACCTC (R-Phospho)

Construct	#	Sequence (5'-3')
pET22B- MMP-1	16	TCAACTGCAGGAAAAATGGAGGTTCTCACCACCACCACCACCACGGTGGCTGTTAG (Vector-F) TGTGCATATGTATATCTCCTTCTTAAAGTTAAACAAAATTATTTCTAGAGGGGAATTG (Vector-R) TAACTTTAAGAAGGAGATATACATATGCACAGCTTTCCTCCACTGCTGCTGC (cDNA-F) GGTGGTGGTGAGAACCTCCATTTTTCCTGCAGTTGAACCAGCTATTAGCTTTCTGG (cDNA-R)
pET22B- MMP-9	17	GCAGTGCCCTGAGGACGGAGGTTCTCACCACCACCACCACCACGGTGGCTGTTAG (Vector-F) GGGGCCATATGTATATCTCCTTCTTAAAGTTAAACAAAATTATTTCTAGAGGGGAATTG (Vector-R) TTTTGTTTAACTTTAAGAAGGAGATATACATATGGCCCCCAGACAGCGCCAGTC (cDNA-F) GTGGTGGTGGTGGTGAGAACCTCCGTCCTCAGGGCACTGCAGGATGTCATAG (cDNA-R)
pET22B- MMP-13	18	TTCCATTTTGTGGTGTGGAGGTTCTCACCACCACCACCACCACGGTGGCTGTTAG (Vector-F) GGCAGCATATGTATATCTCCTTCTTAAAGTTAAACAAAATTATTTCTAGAGGGGAATTG (Vector-R) TTTGTTTAACTTTAAGAAGGAGATATACATATGCTGCCCCTTCCCAGTGGTGGTGAT (cDNA-F) TGGTGGTGGTGGTGAGAACCTCCACACCACAAAATGGAATTTGCTGGCATGACGCG (cDNA-R)

4.5.3.1 pET22B pelB-MMP-8 periplasm construct

Full length and truncated MMP-8 (M100-G262) for periplasmic expression were cloned from MMP-8 cDNA using primer sets **1** and **2** by Gibson cloning. Primers were designed for insertion of MMP-8 into a pET22B vector with a C-terminal poly-histidine tag.[185] All PCR reactions were performed with Herculase II Fusion DNA polymerase (Agilent). Following PCR amplification, products were gel purified and combined following the Gibson master mix protocol. All plasmids were confirmed by DNA sequencing.

4.5.3.2 pET22B MMP-8-GGS-His_6 with PelB Removal

PelB header and a GGS spacer were placed between the enzyme and the poly-histidine tag to allow for MMP-8 expression from inclusion bodies using primers **3-6**. Primers were phosphorylated to allow for self-ligation following PCR reactions. All PCR reactions were performed with Herculase II Fusion DNA polymerase (Agilent). Following

PCR amplification, products were gel purified and ligated using T4 DNA ligase (New England Biolabs). All plasmids were confirmed by DNA sequencing.

4.5.3.3 pET15B MMP-8-mKate Fusions

mKate was fused to the N Terminus (Primers **7** and **8**) and C Terminus (Primers **9** and **10**) of truncated (M100-G262) and full-length MMP-8 with a *GGGS* linker by Gibson cloning. PCR products were produced using a pET15B mKate template.[182] All PCR reactions were performed with Herculase II Fusion DNA polymerase (Agilent). Following PCR amplification, products were gel purified and combined following the Gibson master mix protocol. All plasmids were confirmed by DNA sequencing.

4.5.3.4 pET15B MMP-8-mKate Fusions; *GSAGSAAGSGEF* linker

A flexible *GSAGSAAGSGEF* linker was placed between mKate and MMP-8 using phosphorylated primers **11-14** for both C- and N- terminal fusions. All PCR reactions were performed with Herculase II Fusion DNA polymerase (Agilent). Following PCR amplification, products were gel purified and ligated using T4 DNA ligase (New England Biolabs). All plasmids were confirmed by DNA sequencing.

4.5.3.5 pET22B truncated MMP-8 GGS-His_6-GGC

A terminal *GGC* was added to the pET22B truncated (M100-G262) MMP-8-GGS-His_6 construct described above. The terminal reactive cysteine was designed to allow for conjugation of MMP-8. All PCR reactions were performed with Herculase II Fusion DNA polymerase (Agilent). Following PCR amplification, products were gel purified and ligated using T4 DNA ligase (New England Biolabs). The resulting plasmid was confirmed by DNA sequencing.

4.5.3.6 pET22B MMP-1, MMP-9, MMP-13

MMP-1, MMP-9 and MMP-13 were cloned from cDNA using primer sets **16**, **17**, and **18,** respectively. by Gibson cloning. MMP-1, MMP-9, and MMP-13 were cloned into a pET-22B vector using the pE22B-MMP-8-GGS-His_6-GGC as a template. All PCR reactions were performed with Herculase II Fusion DNA polymerase (Agilent). Following PCR amplification, products were gel purified and combined following the Gibson master mix protocol. All plasmids were confirmed by DNA sequencing.

4.5.4 Periplasmic MMP-8 Expression

Full-length and truncated pET22b-PelB-MMP-8 was transformed into BL21-Codon Plus (DE3)-RIPL and T7 Express Shuffle® *E. coli* cells and grown overnight on ampicillin plates. A streak of colonies was grown overnight in Terrific Broth then inoculated at 1% into a larger culture containing 100 mg/mL ampicillin. Cultures were allowed to grow overnight with an induction using 0.5 mM IPTG at A_{280}=0.7-1.0. Cells were centrifuged at 10,000 x*g* for 30 minutes at 4ºC. Protein was extracted via osmotic shock as previously described.[185] The pellet was resuspended in hypertonic, 100 mM Tris, 20% sucrose, pH 7.4 with protease inhibitor then placed on ice for 20 minutes. Cultures were spun down at 30,000 x*g* for 30 minutes and supernatant was saved. The leftover pellet was resuspended in hypotonic ice-cold deionized water containing protease inhibitor and spun down at 30,000 x*g*. The supernatant from the hypertonic and hypotonic solutions were combined and analyzed by SDS-page.

4.5.5 Isolation of inclusion bodies

Full-length and truncated pET22b-MMP-8-GGS and MMP-8-mKate fusion proteins were transformed into BL21-Codon Plus (DE3)-RIPL and T7 Express Shuffle® *E. coli* cells and grown overnight on ampicillin plates. A streak of colonies was grown overnight in Terrific Broth then inoculated at 1% into a larger culture containing 100 mg/mL ampicillin. Cultures were allowed to grow overnight with an induction using 0.5 mM IPTG at A_{280}=0.7-1.0. Cells were centrifuged at 10,000 x*g* for 30 minutes at 4ºC. The pellet was resuspended in lysis buffer (100 mM Tris, 5 mM $CaCl_2$, 0.5 mM ZnOAc, 0.05% Brij-35, pH 7.5, (EDTA-free) protease inhibitor) and cells were lysed using four cycles of freeze–thaw followed by tip sonication at 12W for 3x10s, alternating with ice to keep the suspension chilled. The solution was pelleted by centrifugation at 30,000 x*g* for 30 minutes at 4ºC. The supernatant was removed and the insoluble pellet was resuspended in pellet 20 mL of lysis buffer (with protease inhibitor) by vigorously pipetting to a homogeneous suspension then pelleted by centrifugation at 30,000 x*g* at 4ºC. The process was repeated once more to wash the pellet with 20 mL MilliQ water containing protease inhibitor. The washed pellet containing the bacterial inclusion bodies was resuspended at 4ºC using extraction buffer (20 mM Tris–HCl, 500 mM NaCl, 10 % glycerol, 8 M urea, pH 8.0) and allowed to solubilize for 1-2 hours at room temperature on an orbital shaker. The extraction mixture was centrifuged at 30,000 x*g* for 30 minutes and the supernatant was filtered through a 0.45 µm filter in preparation of N^{i2+} affinity chromatography.

4.5.6 Column refolding

MMPs were purified using a modified column refolding protein.[112] Four joined 5 mL HisTrap FF columns charged with Ni^{2+} were equilibrated with extraction buffer containing 20mM imidazole. The clarified supernatant was loaded equally onto each column then joined and washed with extraction buffer for 10 column volumes (CV). Samples were taken through a stepwise titration with 10 CV at 8 M, 6 M, 4 M, 2 M,1 M, and 0 M Urea by combining extraction buffer with refolding buffer (20 mM Tris–HCl pH 8.0, 500 mM NaCl, 10 % glycerol, 0.5 mM oxidized glutathione, 5 mM reduced glutathione) at desired ratios. For example, 8M Urea = 100% extraction buffer and 6 M = 75% extraction buffer, 25% refolding buffer. Bound protein was eluted with refolding buffer containing 400 mM imidazole. Fractions were analyzed by SDS-page, pooled, then dialyzed against 20 mM Tris–HCl, 50 mM NaCl, 0.1 mM DTT before purification by size-exclusion chromatography.

4.5.7 Size-exclusion chromatography

Dialyzed samples were concentrated using Amicon 10 kDa MWCO spin filters before purification by size exclusion chromatography. Briefly, pure enzyme was isolated on a Dionex FPLC equipped with a Superdex 75 column (GE Healthcare) operated at a flow rate of 0.5 mL/min in 20 mM Tris–HCl, 50 mM NaCl, 0.1 mM DTT. The eluate was monitored at 280 nm. Samples were analyzed by SDS-Page with like fractions combined.

4.5.8 Matrix-assisted laser desorption and ionization (MALDI)- time of flight (TOF)

Mass spectrometry of truncated MMP-8 was determined by MALDI-TOF. Purified proteins were desalted using Amicon 10K microcentrifuge spin filters (Millipore) by

washing 5X with water. The desalted protein was collected and diluted into 75% acetonitrile, 0.1% TFA in water. Desalted proteins were spotted on top of a pre-formed layer of saturated sinapinic acid matrix. Mass spectra were obtained on a Microflex LT mass spectrometer (Bruker Daltonics) operated in linear, positive mode. Mass spectra were analyzed with the FLEX Analysis software (Bruker Daltonics).

4.5.9 Enzyme activity

Activity of purified MMPs was determined using the EnzChek™ Gelatinase/Collagenase Assay Kit (Life Technologies). Activity was measured following manufacturer recommendations with activity calibrated using a known amount of clostridium collagenase supplied with the kit. One unit is defined as the amount of enzyme required to liberate 1 µmole of L-leucine equivalents from collagen in 5 hours at 37ºC.

4.5.10 Western blot

The Western blot was performed on truncated MMP-8 in free form and attached to a DSPE-PEG2K-maleimide lipid using standard techniques. Proteins were loaded on a 4-20% SDS-PAGE Gel (BioRad) and transferred onto a blotting membrane (BioRad). The blotting membrane was incubated with blocking buffer (20 mM Tris, 140 mM NaCl, 5% Milk, 0.1%Tween, 1% PMSF, pH 7.5), washed then mixed overnight with 1:5000 Rabbit Anti-MMP-8 (Thermo Fisher) at 4°C. The next day, the membrane was thoroughly washed before addition of the secondary antibody (1:10000 anti-rabbit HRP (Jackson)). Following a 1 h incubation, the membrane was washed before addition of Pierce ECL Western Blotting Substrate (Thermo). The membrane was then imaged using a film

development cassette (GE) and visualized using a Kodak Image Station (Kodak; Rochester, NY).

4.5.11 Zymography

Truncated MMP-8 gelatin zymography was performed following BioRad protocols. Protein samples were mixed 1:1 with zymogram loading buffer (BioRad), then loaded onto a zymography gel (BioRad) and run in 1X Tris-Glycine containing 0.1% SDS (BioRad). After 90 min at 100V the gel was extracted and washed thoroughly with water before being placed in renaturation solution (BioRad) for 30 minutes. Gels were transferred into Development Solution (BioRad) at 37ºC overnight and subsequently stained with Coomassie Brilliant-Blue R-250 (BioRad) for 1 hour at room temperature. Loss of gelatin was visualized by development with destaining solution (BioRad) for 1 hour until clear bands appear against background.

4.5.12 Protein homology modeling

A homology model of MMP-8 was produced in PyMol. Using a known structure of MMP-13 (1SU3) and the sequence of MMP-8 (P22894) a model of the protein structure was generated in PyMol following standard program functions.

4.5.13 Liposome attachment

Truncated MMP-8-His_6-Cys harboring a terminal cysteine was attached to liposomes both covalently and non-covalently. Liposomes were made using a thin- film method. Dry lipid films were rehydrated in 20 mM MES, 140 mM NaCl, pH 6 or 20 mM HEPES, 140 mM NaCl, pH 7.5. Each sample was heated at 60ºC for 1 hour and

subsequently sonicated at 60ºC for 10 min. Liposomes were then extruded 11-13 times through a 100 nm polycarbonate membrane then processed for protein attachment.

4.5.13.1 Non-covalent attachment

MMP-8-His_6-Cys was attached to liposomes by exploiting the affinity between His_6 and NiNTA as done previously.[186] Liposomes were produced in 20 mM HEPES, 140 mM NaCl, pH 7.4 containing 1,2-distearoyl-*sn*-glycero-3-phosphocholine (DSPC), Cholesterol,1,2-dioleoyl-*sn*-glycero-3-[(N-(5-amino-1-carboxypentyl)iminodiacetic acid)succinyl] (nickel salt) (DGS-NTA) at 59:40:01. Liposomes at 1:1 molar ratio of NTA lipid to His_6-tagged MMP-8 were mixed with MMP-8 for 1 hour at room temperature. Bound versus unbound protein was separated on a Sepharose CL-4B column under gravity flow. Liposomes with associated protein eluted in the void volume ahead of free protein and percent bound was determined by measuring protein concentration with reducing agent compatible microBCA kit (Thermo Fisher).

4.5.13.2 Covalent attachment

MMP-8-His_6-Cys was attached to liposomes by exploiting the reactivity of the terminal cysteine. Liposomes were produced in 20 mM MES, 140 mM NaCl, pH 6 then added to a dry film of 1,2-distearoyl-*sn*-glycero-3-phosphoethanolamine-N-[maleimide (polyethyleneglycol)-2000] (DSPE-PEG2K-maleimide) by mixing for 30 minutes at 60ºC to yield liposomes containing DSPC, Cholesterol, 1,2-distearoyl-*sn*-glycero-3-phosphoethanolamine-N-(polyethyleneglycol)-2000 (DSPE-PEG2K), and DSPE-PEG2K-maleimide at 55:40:02:03. With the DSPE-PEG2K-maleimide incorporated into the outer membrane liposomes were mixed with MMP-8-His_6-Cys at a 1:4 molar ratio of protein to

maleimide in 20 mM MES, 140 mM NaCl, pH 6. The reaction proceeded for 5 hours at room temperature and unreacted maleimides were quenched with excess addition of cysteine to a final concentration of 0.5 mM for an additional hour. Unreacted protein was separated from liposomes on a Sepharose CL-4B size exclusion column in 20 mM HEPES, 140 mM NaCl, pH 7.4 and percent bound was determine by measuring protein concentration with a reducing agent compatible microBCA kit (Thermo Fisher).

5 Chapter 5: MMP-8 treatment of human CEP enhances solute uptake

5.1 Introduction

Low back pain is the most common and costly musculoskeletal condition,[187] and is significantly associated with intervertebral disc degeneration.[188] The only medical interventions currently available for disc degeneration are surgical measures aimed at removing possible sources of pain and restoring biomechanical function. Hence, development of noninvasive treatments is an important goal. Non-surgical treatments to regenerate the disc and alleviate pain have focused on transplanting new cells to produce matrix lost during degeneration,[189–191] or by injecting growth factors,[192] genes,[193] or other macromolecules[194,195] to stimulate matrix synthesis or reduce catabolism and inflammation. These therapies require a rich nutrient supply to support the higher metabolic demands and to ensure cell survival and proliferation. However, poor nutrient supply to the avascular and degenerated disc[196] may limit the utility of these treatments.[197–199] Development of treatment approaches to enhance nutrient supply may therefore expand the application and utility of these cell and growth-factor therapies.

Nutrients entering the disc and exiting metabolites must diffuse across the cartilage endplate (CEP). Solute diffusion could be hindered by age- or degeneration-related changes to the CEP matrix, including loss of hydration [200,201] and increased calcification,[202,203] and alterations in extracellular matrix composition.[200,201] Specifically, loss of hydration prevents solutes from diffusing freely within the CEP;[204] and increased calcification, proteoglycan or collagen limit the amount of pore space available to solutes.[177,205] For example, aggrecan, the most abundant proteoglycan, is tightly packed with only a few nanometers of space between subunits.[206] In addition, the type II collagen

network limits the opening of pore space by restricting swelling of the matrix when hydrated.[207]

Strategies for enhancing CEP permeability are underexplored. Since greater matrix content associates with reduced solute uptake,[177] matrix depletion should facilitate an improved solute uptake. Clostridium collagenases have been used previously to remove disc matrix,[50,208] making them potentially attractive candidates for improving CEP permeability. Therapeutically, however, they may be imprecise because of their broad substrate specificity[52] in addition to the immunogenicity of the bacterial enzyme.[70] Human matrix metalloproteinases (MMPs), on the other hand, have selectivity for the collagen in the CEP matrix (mainly type II collagen) and aggrecan. MMP-8 (Collagenase-2) may be particularly fitting since it was previously used to enhance tissue permeability.[110,111] Here, we sought to enhance CEP permeability by characterizing enzymatic removal of matrix components using human MMP-8. We hypothesized that reduction of the CEP matrix will remove barriers to solute transport and improve solute uptake.

5.2 Results

5.2.1 MMP-8 Purification & Activity

Active truncated (M100-G262) MMP-8 was recombinantly expressed and purified from *E. coli.* as described in Chapter 4. This active 19 kDa enzyme was used in subsequent experiments.

5.2.2 MMP-8 activity in CEP tissue

MMP-8 liberated matrix from intact human CEP tissues following overnight incubation. MMP-8 displayed a dose-dependent reduction in sGAG from CEP tissue

(Figure 5-1A). Upward of 20% of sGAG was released in the highest dose investigated. The reduction in sGAG mirrored a decrease in computed fixed-charge density based on sGAG content (Figure 5-2). Fourier transform resonance (FTIR) spectroscopy of CEP sections showed that MMP-8 treated samples had lower aggrecan, which corroborated the reduction in sGAG (Figure 5-1B, Table 5-1). Representative sections of treated and control CEP samples showed a decrease in the aggrecan sugar peak area at the wavenumber range of 960-1185 cm^{-1} (Figure 5-1B, Table 5-1). The decrease in aggrecan with MMP-8 was significant at all depth-wise positions measured from the nucleus pulposus-CEP interface to the CEP-bone interface (Table 5-1).

Although MMP-8 treatment greatly released sGAG from CEP samples, it caused only minimal changes to tissue collagen (Figure 5-1C, D). Quantification of released hydroxyproline, as a proxy for collagen, showed no difference compared to control (Figure 5-1C). However, FTIR analysis of the collagen, showed that the Amide I peak from tissue sections demonstrated changes to CEP collagen with treatment across the entire tissue albeit to a lesser degree than the effects of MMP-8 on sGAG content (Table 5-1). The discrepancy between the FTIR and hydroxyproline data may be the result of microscopic changes to collagen, which are not reflected by changes in hydroxyproline content.[53] To determine if enzymatic treatment had any broader effects on the CEP matrix, FTIR analysis of the 1338 cm^{-1} : amide II ratio was performed. A decrease in this ratio is reflective of collagenase activity,[209] which was observed in treated samples (Figure 5-1E, Table 5-1).

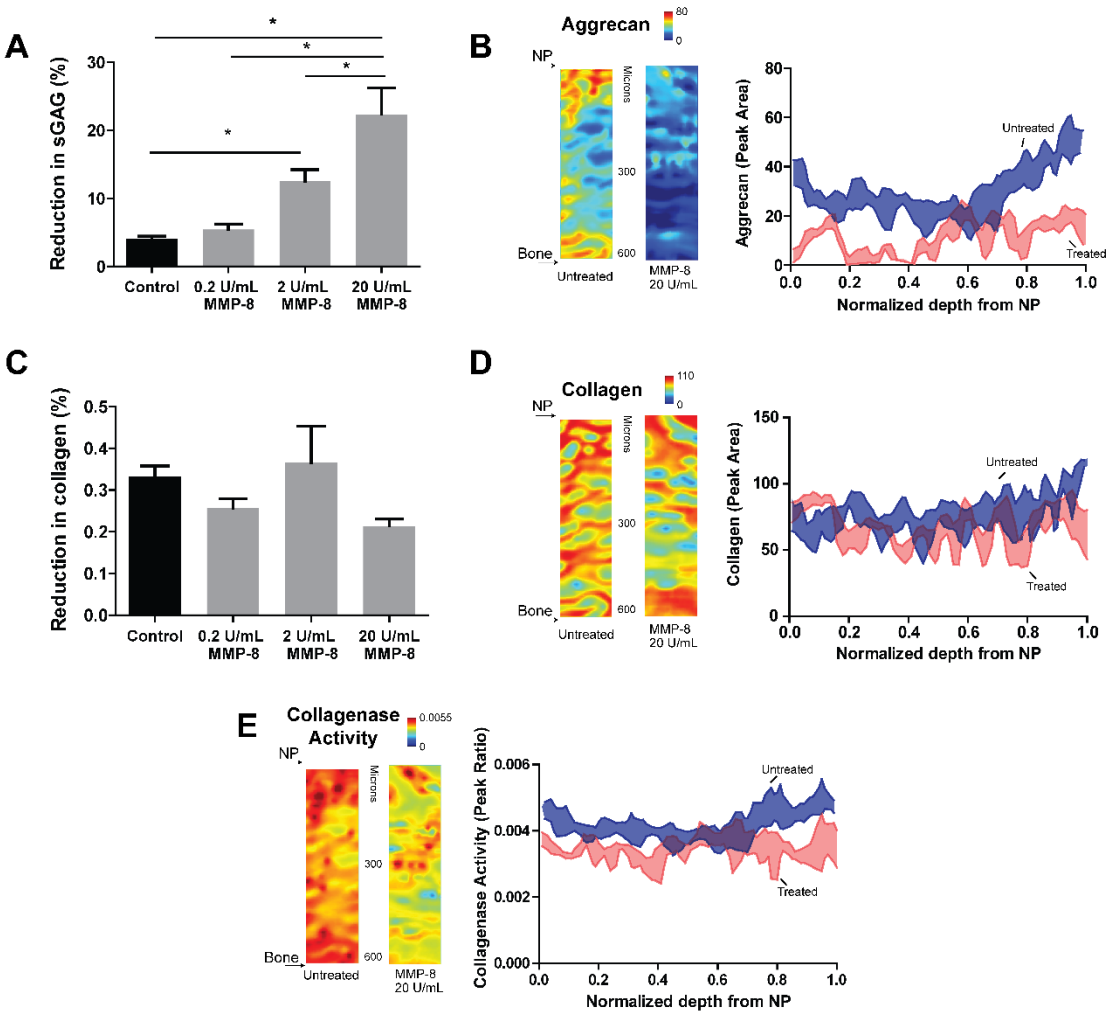

Figure-5-1: MMP-8 treatment reduces the CEP matrix. CEP samples were treated for 18 hours with MMP-8. A) Treatment increased the removal of sGAG, evaluated by DMMB quantification. B) Representative FTIR images (left) and spatial plots (right) of the normalized proteoglycan content (sugar, 960-1185 cm^{-1}). C) MMP-8 caused limited changes to tissue collagen by hydroxyproline measurements. D) Representative FTIR images (left) and spatial plots (right) of the collagen content (Amide I, 1595-1710 cm^{-1}) illustrating changes to CEP collagen. (E) Representative FTIR images (left) and spatial plots (right) demonstrating collagenase digestion, indicated by decreases in 1338:amide II peak area ratio.[209] Bars represent SEM. * One-way ANOVA, $p<0.0001$ with Tukey's post-hoc test, $p<0.05$.

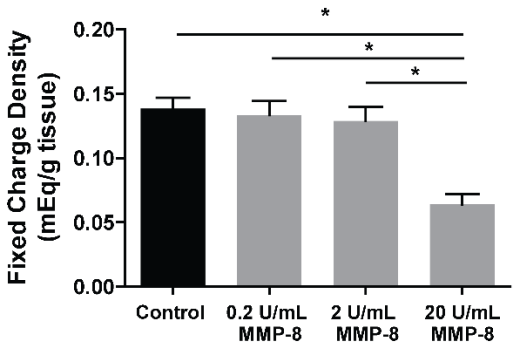

Figure 5-2: MMP-8 treatment on CEP fixed charge density. MMP-8 treatment causes a dose-dependent decrease in calculated fixed charge density. *One-way ANOVA, $p<0.0001$ with Tukey's post-hoc test, $p<0.05$.

Table 5-1: Comparison of spectral characteristics between MMP-8 treated and untreated CEPs

	Untreated	Treated	*p*-value
0.25 normalized depth from NP			
Amide I peak area	88.0 ± 23.2	64.1 ± 10.5	< 0.05
Collagenase activity ratio	0.0051 ± 0.0006	0.0037 ± 0.0011	< 0.05
Aggrecan	46.6 ± 26.3	17.51 ± 17.2	< 0.02
0.50 normalized depth from NP			
Amide I peak area	72.8 ± 13.0	58.1 ± 4.0	< 0.05
Collagenase activity ratio	0.0050 ± 0.0008	0.0034 ± 0.0008	< 0.005
Aggrecan	0.58 ± 0.22	8.28 ± 12.2	< 0.01
0.75 normalized depth from NP			
Amide I peak area	78.5 ± 11.41	65.3 ± 6.3	< 0.05
Collagenase activity ratio	0.0050 ± 0.0007	0.0034 ± 0.0003	< 0.001
Aggrecan	43.2 ± 18.6	18.6 ± 14.9	< 0.02

Data are given as mean ± SD for 3 regions per section and n= 3 sections/group

5.2.3 MMP-8 activity on CEP Uptake

To resolve if the matrix reduction caused by MMP-8 treatment enhanced CEP permeability, we measured uptake of a 376 Da-sized fluorescent solute. MMP-8 treatment increased uptake in CEP tissue at all doses investigated (Figure 5-3A). Site-matched samples showed a 16, 19, and 24% increase in uptake with 0.2 U/mL, 2 U/mL, and 20

U/mL MMP-8, respectively. Treatment also increased uptake of considerably larger 100 nm liposomal nanoparticles into CEP tissues (Figure 5-4). Surprisingly, there was no significant difference in fold change in uptake with increasing the amount of MMP-8 (Figure 5-3B) despite substantial differences in the amount of liberated sGAG (Figure 5-1A).

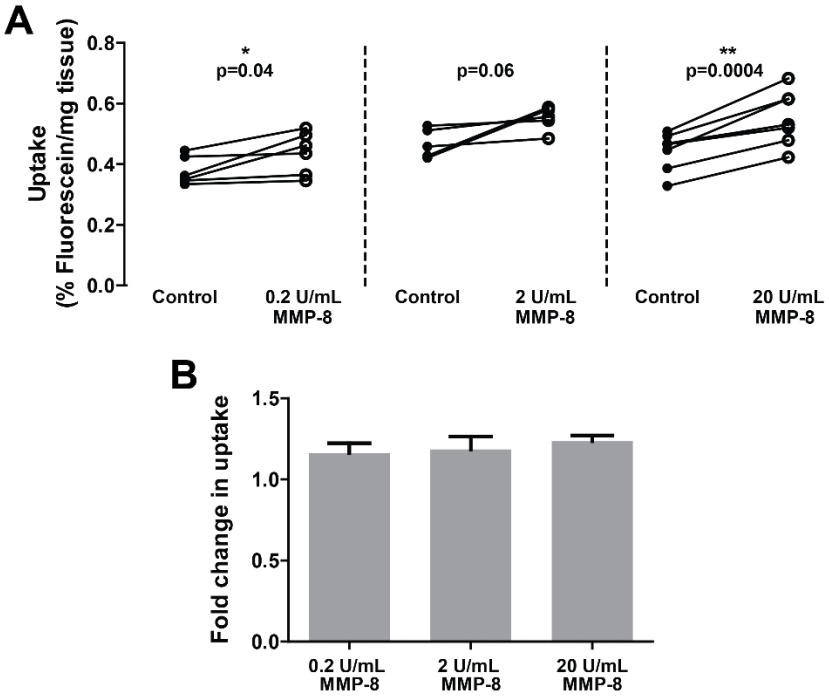

Figure-5-3: MMP-8 improves sodium fluorescein uptake in CEP tissues. A) CEP samples treated for 18 hours with 0.2 (left), 2 (middle) or 20 (right) U/mL of MMP-8 show increased percent uptake of sodium fluorescein. B) Fold change in uptake shows no change with increasing MMP-8 dose. Each pair represents site-matched matched biopsy halves taken from 1 of 4 cadaver spines. Bars represent SEM. *p< 0.05, paired *t*-test, **p < 0.001 paired *t*-test.

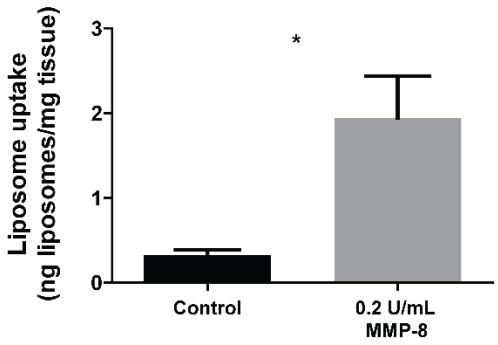

Figure 5-4: MMP-8 treatment increases CEP nanoparticle uptake. CEP tissues treated with MMP-8 enhance uptake of fluorescently labeled, 100 nm lipid nanoparticles. **t*-test, $p<0.05$. n=6 CEP/group.

5.2.4 Determinants of CEP Uptake with MMP-8 treatment

Considering variation in sGAG could not account for differences in uptake, we looked into the other major matrix component, collagen, to determine if collagen quantity or quality played a role in limiting the effects of MMP-8 treatment on CEP uptake. Uptake was more strongly related to the degree of non-enzymatic glycation than to the amount of collagen in tissue samples (Figure 5-5). Separating MMP-8-treated samples into low and high collagen content (>700 µg/mg dry weight) hinted that samples with higher collagen content had lower solute uptake (Figure 5-5A). The difference however, was not significant. We next explored collagen quality to determine if excessive cross-linking may be involved in limiting tissue permeability. Advanced glycation end-products (AGEs) are formed through non-enzymatic glycation of the free amino groups of proteins and lipids by reducing sugars. AGE accumulation occurs in low-turnover proteins of the disc, such as collagen,[210] and AGE accumulation is increased with aging and with type 2 diabetes.[211]

Solute uptake was significantly lower in the treated CEP samples with high AGE concentration (>.75 ng quinine fluorescence/µg collagen; Figure 5-5B).

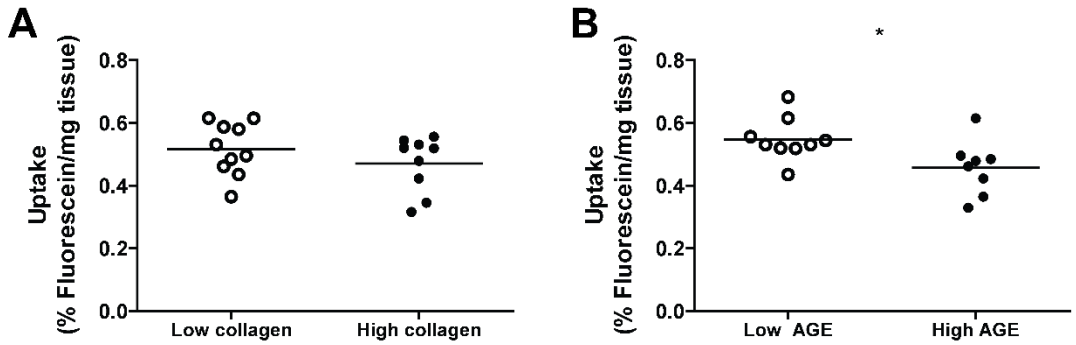

Figure-5-5: Collagen restricts sodium fluorescein uptake in CEP tissues. CEP samples were treated for 18 hours with MMP-8. A) Samples with higher collagen (>700 µg/mg dry weight) exhibited lower uptake. B) Normalized high AGE concentration (>0.75 ng/µg collagen) significantly restricts sodium fluorescein uptake. *n*=8-10 CEP samples per group taken from 4 cadaver spines. **t*-test, $p < 0.03$.

5.2.5 Role of AGE concentration on CEP permeability

After discovering that high AGE content restricted permeability enhancement following MMP-8 treatment, we explored the potential implications of this limitation. CEP samples were grouped by donor to determine if matrix depletion and permeability enhancement are donor-specific. Donors with greater AGE content had poorer solute uptake (Figure 5-6). Donor 4 and to a lesser extent, donor 1, had higher AGE contents than other donors studied (Figure 5-6A), and the elevated AGE levels coincided with lower uptake (Figure 5-6B). This was true despite donor 4 having no differences in total sGAG (Figure 5-6C) and less total collagen – which one might expect to increase tissue permeability (Figure 5-6D).[177]

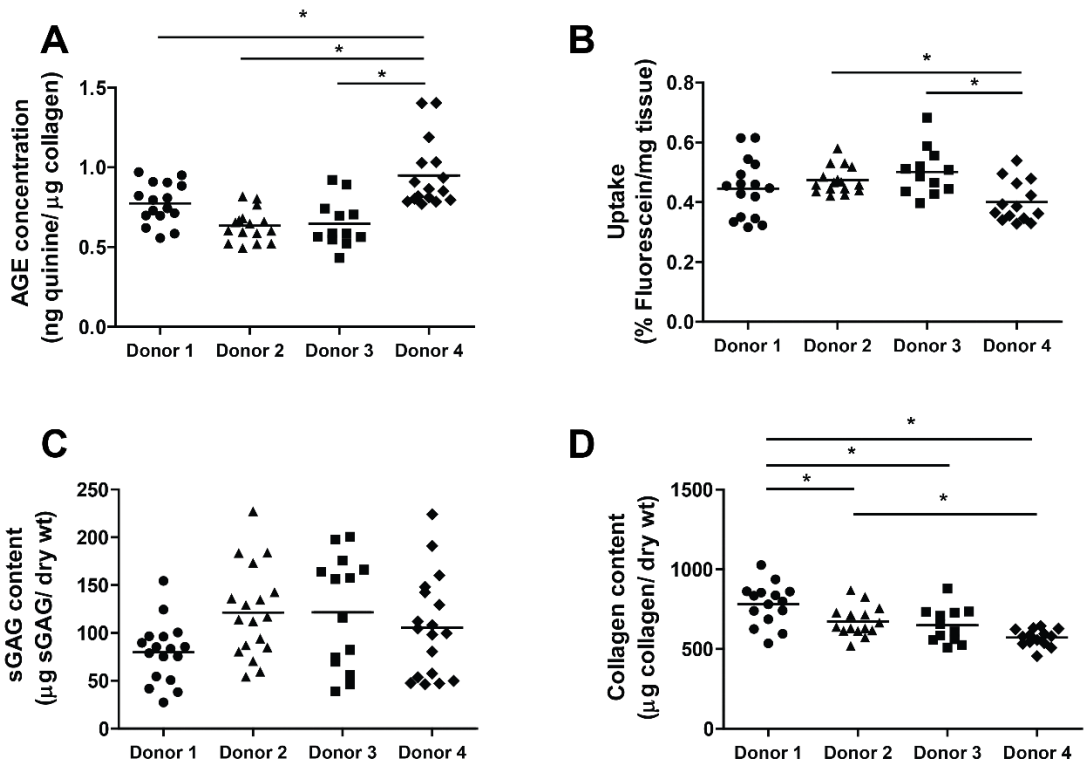

Figure-5-6: CEP donors exhibit varying levels of ECM components and permeability. A) Comparison of AGE content between donors. Donor 1 and donor 4 had CEP tissues with elevated AGE concentration. B) Fluorescein uptake was lower in CEP tissues from donor 4, which had the highest AGE content. (C) sGAG content was lowest in CEP tissues from donor 1. D) Collagen content was lowest in donor 4. *n*=12-16 samples per group taken from 4 cadaver spines. *One-way ANOVA, $p<0.05$ with Tukey's post-hoc test *$p<0.05$.

5.3 Discussion

This study shows that removal of CEP matrix components with MMP-8 improves tissue uptake of lower molecular weight solutes and 100 nm liposomes. Sodium fluorescein uptake increased 16-24% with increasing MMP-8 dose (Figure 5-3). Treated samples showed a reduction in sGAG and spectral decreases in collagen (Figure 5-1). This result affirms what was found by others in that increased matrix deposition hinders CEP solute transport.[177,200–203] However, the fold change in uptake did not vary between doses despite differences in the amount of liberated matrix.

The reduction in sGAG ranged from 5-30% with MMP-8 treatment without changes to the fold change in uptake. sGAG is hydrophilic and promotes tissue swelling through interactions with water. The loss of sGAG and the associated loss in fixed charge density likely limited the ability for the tissue to hydrate and take in solute.[201] This could explain why uptake did not scale with increasing sGAG clearance. There is likely a narrow therapeutic window where removal of a portion of sGAG is beneficial, but removal of too much, while creating space for the transport of solutes, is counterproductive since it negatively impacts the hydration of the CEP. Notably, even with the greatest losses in sGAG there were no visible signs of tissue damage.

Changes to collagen were not as pronounced as changes to sGAG. Measurements of hydroxyproline showed no significant changes to liberated collagen. This finding is consistent with other studies looking to improve tissue penetration which showed limited changes to collagen with collagenase treatment (Tables 1-1-1-6). FTIR analysis however, did show a reduction in the Amide I band and in the 1338/Amide II ratio which are sensitive to collagenase activity.[209] The change in spectral intensity may reflect slight changes to the collagen structure. Nevertheless, the spectral data supports that reduction in the CEP matrix promotes tissue penetration.

An unexpected finding was the role of AGEs on CEP permeability. AGEs were found to limit solute uptake in treated samples since samples with higher AGEs displayed lower uptake (Figure 5-5). AGEs accumulate with age and can reduce permeability by increasing tissue stiffness[210] and decreasing water content.[212] In observing the data by donor, donor 4 with the highest level of AGEs (and similar sGAG but lower collagen content) had the lowest uptake (Figure 5-6). This result suggests that on top of the amount

of matrix being important for CEP permeability, the condition of the matrix is also important. AGEs also impair the ability of MMPs to digest collagen[213] further highlighting their ability to restrict the effects of collagenase treatment. Altogether, these results may inform which patients are not good candidates for matrix reduction, stem-cell or growth factor therapies since AGE accumulation can occur with diseases such as chronic inflammation or type 2 diabetes.[214]

5.4 Conclusion

In conclusion, removal of CEP matrix constituents with MMP-8 increases tissue uptake. This effect does not scale with a reduction in sGAG and is sensitive to the level of AGEs. The improvement in uptake was observed under static conditions and further studies to evaluate the magnitude of the effect under load to better reflect the natural environment of the CEP in the spine will be needed. In addition, to translate this approach, special precaution will be needed to safely deliver enzymes to the CEP with limited off-target digestion. This delivery could be achieved by attaching the enzyme to a liposome to limit off-target migration. In summary, we demonstrate that matrix reduction offers a novel approach to improve solute uptake in the CEP. This approach can potentially be used to treat or prevent disc degeneration as well as improve the utility of stem cell and growth factor therapies.

5.5 Materials and methods

5.5.1 Instrumentation

Fluorescence or absorbance measurements were performed on a FluoroLog-3 spectrofluorimeter (Horiba Jobin Yvon) with data collection using FluorEssence software

or on a SpectraMax M5 microplate reader with data collection using SoftMaxPro. High-performance liquid chromatography (HPLC) was performed on an Agilent 1100 HPLC. Fourier transform infrared spectroscopy (FTIR) imaging was performed on a Spotlight 400 FTIR Imaging System from Perkin Elmer. Cryo-sectioning was done using a Microm HM550 cryostat. Particle size measurements were carried out using a Malvern Nano-ZS Dynamic Light Scattering Instrument (Westborough, MA).

5.5.2 Materials

Terrific Broth (TB), and isopropyl β-D-1-thiogalactopyranoside (IPTG) were purchased from VWR (Radnor, PA). Nickel Sepharose high performance resin prepacked in 5 mL HiTrap columns (HisTrap FF) and a Superdex 75 size exclusion chromatography (SEC) column were purchased from GEHealthcare (Piscataway, NJ). EDTA-free protease inhibitor solution was purchased from BiMake (Houston, TX). Amicon spin filters were purchased from Millipore (Billerica, MA). MMP-8 antibody (PA5-28246) and Pierce ECL Western Blotting Substrate were purchased from Thermo Fisher (Waltham, MA). SDS and zymogram materials and buffers were purchased from BioRad (Hercules, CA). Enzymatic activity was assayed using an EnzChek™ Gelatinase/Collagenase Assay Kit purchased from Life Technologies (Carlsbad, CA). BL1(DE3) competent cells, Gibson Assembly Mastermix, and T4 DNA ligase were purchased from New England Biolabs (Ipswich, MA). All lipids were purchased from Avanti Polar Lipids (Alabaster, AL). MMP-8 (30915305) cDNA was purchased from GE Dharmacon (Lafayette, CO). AccQ-Tag derivatization kit was purchased from Waters (Milford, MA). Barium fluoride (BaF_2) windows for FTIR imaging were purchased from Edmund Optics (Barrington, NJ). Cartilage endplates were acquired from four fresh cadaveric spines with no history of

musculoskeletal disorders. All other reagents were purchased from Sigma–Aldrich (St. Louis, MO).

5.5.3 MMP-8 expression and purification

MMP-8 was cloned, purified and characterized as described in Chapter 4.

5.5.4 Liposome formation

Liposomes were made using a thin- film method. Dry lipid films containing 1,2-distearoyl-*sn*-glycero-3-phosphocholine (DSPC),1,2-distearoyl-glycero-3phosphoethanolamine-N-(polyethyleneglycol)-2000 (DSPE-PEG2K), DiD at 55:40:05:.02 were rehydrated in 20 mM HEPES, 140 mM NaCl, pH 7.4. Each sample was heated at 60ºC for 1 hour and subsequently sonicated at 60ºC for 10 min. Liposomes were then extruded 11-13 times through a 100 nm polycarbonate membrane with subsequent verification of the particle size.

5.5.5 Cartilage Endplate Treatment

Intact human cartilage endplates were harvested from four fresh cadaveric lumbar spines (age range: 38–66 years old; mean age: 56 ± 10 years) with no history of musculoskeletal disorders. From each L4 and L5 disc, full-thickness CEP samples including any calcified cartilage, were removed from the subchondral bone with a razor blade. A 5 mm-diameter circular biopsy was prepared and bisected to create two halves: one half for treatment and the other for site-matched control. CEP samples were placed in 100 µL of collagenase reaction buffer (50 mM Tris-HCl, 150 mM NaCl, 5 mM $CaCl_2$, 0.2 mM sodium azide, pH 7.6) with or without 0.2-20 U/mL recombinant MMP-8 (n = 6 site-matched half biopsies per group). Samples were placed on an orbital shaker and

mixed overnight for 18 hours at 37°C. The digest supernatant was removed and stored for subsequent biochemical analysis. Samples were washed 3X with PBS, blotted dry, and transferred to a new tube containing 200 µL of 0.1 mg/mL sodium fluorescein (376 Da). After mixing overnight at 4°C, samples were extracted, blotted dry, weighed, and dehydrated by lyophilization at 80°C for 2 hours. The dehydrated samples were re-weighed and dissolved in 200 µL of 1 mg/mL papain at 60°C overnight. Papain digests were centrifuged at 2,000 x*g* for 20 minutes, and the supernatant was extracted for subsequent analysis of protein and fluorescein contents.

5.5.6 Sodium Fluorescein Uptake

Papain digests were diluted in PBS and fluorescein concertation was determined by fluorescence emission (Ex. 450, Em. 516) compared to a standard curve of known fluorescein concentration. Percent uptake was computed by dividing the mass of fluorescein in the tissue by the total fluorescein added. Results were analyzed using a paired t-test between control and treated halves.

5.5.7 Proteoglycan Content

Sulfated glycosaminoglycan (sGAG) content was measured using a dimethylmethylene blue assay.[215] Percent sGAG released from the CEP was computed by dividing the sGAG in the reaction digests by the total sGAG from both the reaction and papain digests. Fixed charge density was estimated assuming two moles of charge per mole of sGAG in the tissue and a molecular weight of 502.5 g/mole sGAG:

$$\text{Fixed Charge Density (mEq/g wet tissue)} = \left(\frac{\text{2 mol charges}}{\text{502.5g GAG}}\right)\left(\frac{\text{Weight GAG (g)}}{\text{Weight Tissue (g)}}\right)$$

Samples were analyzed using a one-way ANOVA with a Tukey's post-test.

5.5.8 Collagen Content

Collagen content was determined by quantifying hydroxyproline from acid-neutralized hydrolysates. A 20 µL aliquot of reaction and papain digests were hydrolyzed in 230 µL of 6 N HCL for 18 hours at 110°C. Samples were neutralized with sodium hydroxide and derivatized using Waters AccQ-Tag Derivatization kit following manufacturer directions. Samples were analyzed by HPLC on a C8 column with a gradient of 0-15% of MeOH with 0.1% TFA in H_2O with 0.1% TFA. Hydroxyproline concentration was determined by calculating the peak area compared to a standard curve. Total collagen was calculated from hydroxyproline assuming that it accounts for 13.5% of the collagen mass. Low-high collagen boundary was defined using the mean collagen content across all CEP samples. Samples were analyzed using a one-way ANOVA with a Tukey's post-hoc test.

5.5.9 Advanced Glycation End Product Content

The total concentration of advanced glycation end products (AGEs) was determined by fluorimetric assay. Fluorescence readings of the neutralized lysates (Ex. 370nm, Em. 440nm) were referenced to a quinine sulfate standard[216] and then normalized to collagen content. Low-high AGE boundary was defined using the mean AGE concentration across all CEP samples. A t-test was used to compare treatment

effects between samples with high and low AGE concentrations, and one-way ANOVA with a Tukey's post-hoc test was used to test for differences between donors.

5.5.10 FTIR Imaging

Following overnight treatment, CEP samples were flash-frozen in Optimal Cutting Temperature (OCT) compound. Next, 7 µm-thick sections were placed on BaF_2 windows and imaged using a Spotlight 400 FTIR Imaging System (Perkin Elmer). Images were acquired in transmittance mode with a 4 cm^{-1} spectral resolution and a 6.25 µm pixel size. Spatial maps of collagen (1595-1710 cm^{-1} amide I peak area), the aggrecan (960-1185 cm^{-1} sugar peak area), and the collagenase activity ratio (ratio of collagen's 1338 cm^{-1} CH_2 side chain vibration peak area to collagen's 1480-1590 cm^{-1} amide II peak area) were acquired in 0.8 mm x 0.2 mm regions of interest. Images analysis was performed using a custom code (IDL 8.6). Depth-wise distributions of FTIR indices were averaged for three regions-of-interest per section (n = 3 sections/sample) and compared using a t-test.

6 Summary and Future Work

6.1 Summary

In this dissertation, we describe several approaches to improve nanoparticle drug delivery through modification of the drug carrier or the target tissue. Chapter 1 provides an overview of the various strategies employed to enhance nanoparticle delivery with a focus on the use of collagenases. We highlight pivotal work on modifications to drug carriers and the use of collagenases to improve drug penetration. Both of these areas guided the studies in subsequent chapters.

Chapter 2 details the synthesis and characterization of a novel class of inverse sulfolipids with the potential for the release of drug cargo by sulfatases at the target tissue. These sulfolipids feature a cationic amine with a terminal anionic sulfate. They displayed some of the highest phase transition temperatures for a gel to crystalline conversion reported compared to lipids of similar chain length. In addition, they formed amorphous aggregates instead of the spherical vesicles observed with similar lipids. Promoting vesicle formation by inclusion of a bulky spacer between the sulfate and quaternary amine to limit intermolecular interactions, or additives such as tocopherol to induce bilayer curvature were unsuccessful. Furthermore, assays with extracellular sulfatases showed that, contrary to our hypothesis, these lipids were not sulfatase substrates. Although the biophysical properties were unique, we elected to pursue other avenues since these lipids were unable to form vesicles or serve as sulfatase substrates.

In chapter 3, we continued to use synthetic approaches to interrogate lipid biophysics. We synthesized two sterol anchored polyethylene glycol (PEG) lipids,

DiCHEMS-PEG and DiCHOL-PEG to improve the stability of PEG in the liposomal bilayer. The primary difference between these two novel lipids is the presence of an ester group (DiCHEMS-PEG) instead of ether group (DiCHOL-PEG) extending from the hydroxyl of cholesterol. These sterol-anchored PEGs displayed a series of canonical liposome properties when mixed with DSPC lipids. Fluorescence anisotropy showed a loss in the lipid phase transition with increasing amounts of DiCHEMS-PEG or DiCHOL-PEG. They were able to form vesicles which could encapsulate carboxy fluorescein (CF) and only released approximately 12% of CF over 7 days in serum. In addition, they limited nonspecific adhesion of serum proteins to the surface of liposomes. Interestingly, liposomes with DiCHEMS-PEG exhibited increased cellular uptake in the presence of ApoE3 than liposomes containing a more conventional DSPE-PEG. The DiCHEMS-PEG had almost four-times more uptake than the other lipids while the DiCHOL-PEG displayed only minor increases in cellular uptake compared to DSPE-PEG lipids. The *in vivo* pharmacokinetics mirrored the cellular uptake results. Liposomes with DiCHEMS-PEG or DiCHOL-PEG lipids were cleared more rapidly than liposomes containing DSPE-PEG. This surprising result suggests that the sterol anchor may promote increased interactions with lipoproteins *in vivo*. Although the lipids did not enhance liposome circulation, they likely altered the tissue distribution of the liposomes while preserving liposome integrity which could be useful for liposome drug delivery purposes.

We next shifted our focus to the other key method to improve liposomal delivery by modifying the target tissue. Chapter 4 focuses on the recombinant expression and purification of MMP-8 from bacteria for removal of inhibitory tissue components which limit drug delivery. Initially, we looked to express both full-length and truncated MMP-8

from the periplasm space of bacteria. Despite success in smaller preparative cultures, scaling up to 1 L cultures failed to produce any active protein. We switched to purification from bacterial inclusion bodies with mixed results. The truncated MMP-8 required ample space to refold while bound to a NiNTA column and could be purified at yields up to 900 µg/L. The full-length protein, however, would undergo post-production processing upon purification. This breakdown with full-length MMP-8 also occurred when purifying MMP-1, MMP-9, and MMP-13. Several additives including polymers, sugars, and chelators (Table 4-1) were added to help improve enzyme stability and increase protein refolding with little success. Next, to provide a chaperone to aid in refolding and a fluorescent tag for tracking, we created a fusion protein between MMP-8 and mKate. Fusions occurred at both the N and C-terminus of MMP-8. In smaller cultures, truncated MMP-8 fusion proteins with mKate were purified while retaining enzymatic activity. The C-terminal fusion protein displayed lower activity likely due to the proximity of mKate to the active site of the enzyme. When increasing the production scale, the truncated MMP-8 fusion proteins underwent the same post-production processing as all full-length fusion proteins.

Moving forward, we modified truncated MMP-8 for potential use in drug delivery. When expressed with a terminal His_6-Cys tag, truncated MMP-8 was attached to liposomes while retaining its activity. Attachment to liposomes was achieved non-covalently through the His_6 of the protein with a NiNTA lipid, and covalently through a reaction between the terminal cysteine of the protein and a reactive maleimide on a DSPE-PEG lipid. The covalent attachment had higher activity likely due to a PEG 2 kDa spacer between the enzyme and liposome surface. While the yield from recombinant

expression of truncated MMP-8 was not as high as desired, we produced enough enzyme to assess its ability to increase tissue uptake in cartilage endplates (CEP).

Chapter 5 presents a good test-case for the use of matrix reduction strategies to improve tissue uptake. Here, we showed that truncated MMP-8 treatment of CEP tissue improved solute uptake. MMP-8 treatment removed upwards of 30% of sulfated glycosaminoglycans (sGAG) in CEP tissues. Measurements of hydroxyproline as a proxy for collagen showed no significant difference in treated samples. This lack of change in collagen is consistent with other collagenase studies (Tables 1-1 - 1-6) and may be due to improper clearance of digested fragments. FTIR imaging of sections from CEP tissues mirrored the loss in proteoglycan by a reduction in the sugar peak area at 960-1185 cm^{-1}. Contrary to the biochemical results, FTIR also showed a reduction in the collagen Amide I peak and the 1338 to Amide II (1480-1590 cm^{-1} ratio), which are sensitive to collagenase digestion. These changes to the CEP matrix facilitated an increase in uptake of both sodium fluorescein and 100 nm liposomes. Increasing the enzyme dose did not increase sodium fluorescein uptake, likely because of a loss in tissue hydration caused by a large decrease in sGAG. In addition, elevated levels of advanced glycation endproducts (AGE), which are responsible for cross-linking macromolecules, limited the effect of MMP-8 treatment. These AGEs appear to be donor-dependent, where samples with higher crosslinks showed lower uptake of sodium fluorescein. This is the first experiment to demonstrate an approach to improve CEP uptake and the role of AGEs on CEP permeability.

6.2 Future Work

The work from this dissertation describes strategies with the potential to improve the delivery of nanomaterials and opens several avenues for future studies. Chapter 2 and 3 describe the unique biophysical properties of sulfolipids and sterol-anchored PEGs, respectively. Although these molecules are well-characterized, further work is needed to solidify their best application. Newer sulfolipids designed to reduce the headgroup interactions or mimic sulfatase substrates may provide sulfolipids which are able to form vesicles suitable for triggered drug release (Figure 6-1). Additionally, testing if the newer sulfolipids are substrates for both extracellular or lysosomal sulfatases may help identify an appropriate niche to use these lipids in drug or gene delivery. The formation of a cationic particle by sulfate removal in the extracellular space would increase membrane delivery while sulfate removal in the lysosome would facilitate lysosomal escape for cytoplasmic delivery.[148] Depending on the drug or target, one location would be preferred.

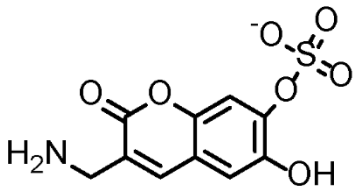

Figure 6-1: Potential sulfolipid headgroup. The headgroup mimics known SULF substrates and separates the cationic amine and anionic sulfate

A more complete understanding of the biodistribution of the DiCHOL-PEG and DiCHEMS-PEG lipids is worth pursuing. These lipids are cleared more rapidly than lipids containing DSPE-PEG, but the mechanism of this clearance is not fully understood. Efforts to understand the organ accumulation of these lipids would be informative towards

this goal. Particularly, understanding the roles of hepatocytes or Kupffer cells in hepatic clearance is important since they have demonstrated ApoE-dependent accumulation liposomes.[165] Simultaneously, it would be advantageous to determine if these lipids could be used to target the delivery of drugs to liver hepatocytes. Additionally, utilizing a similar synthetic scheme to anchor other polymers known to extend plasma circulation, such as HPMA, PMOX, or PDMA[217] may open additional opportunities for this sterol-anchor approach.

In regards to purifying MMPs, the largest opportunity for future success would entail purification from the periplasmic space. A recent publication has detailed expression of MMP-2, MMP-9, and MMP-14 from the periplasmic space,[218] using a pMopac16 vector with Jude-I cells. This expression system may enable purification of other MMPs, including MMP-8, from the periplasmic space. It would also be fruitful to produce MMPs in long-circulating forms to enable their use for matrix removal. This attribute could be achieved through expression of MMPs with a FcRN binding peptide[182] to reduce clearance from endothelial cells or to attach PEG to the enzyme surface in order to limit nonspecific protein adhesion. Alternatively, MMPs could be produced from locally delivered MMP mRNA constructs. This would presumably overcome the refolding problem since the enzymes would be produced in recipient mammalian cells and could provide a sustained amount of the MMP for a longer duration of action.

Lastly, cartilage endplate experiments present the complexities of matrix removal. We broadly show that removal of matrix improves uptake; however, it remains unclear which matrix constituents should be removed to maximize changes in uptake. The use of hyaluronidases and aggrecanases would aid in revealing the balance between GAG

removal and tissue hydration without confounding such effects by changes in collagen. Bacterial collagenases could be used to isolate the role of collagen in restraining uptake but the translational potential of these enzymes is limited. After distinguishing the key matrix components responsible for limited tissue uptake, combinations of MMPs which target these components should be tested. Based on our work, the role of cross-links on CEP uptake should also be further explored. Cross-links can be induced non-enzymatically through ribose glycation,[219] which can be used to interrogate their effects on CEP permeability. Studies should also be repeated under load to better reflect compressive forces in the spinal cord. Findings from CEP studies can be further applied to other diseases that feature excess collagen including cancer and fibrosis.

6.3 Conclusions

Liposomes are the most successful class of nanoparticle therapeutics. Advances to improve tissue penetration, particle stability, and the release of drug cargo will be imperative to the continued translation of these therapies into the clinic. Here, we detail several of these approaches as well as future work to enhance the use of nanoparticle therapies. The work described has broad potential implications in the multitude of diseases utilizing liposomal approaches including pain, infection, and cancer.[130] We are optimistic that the growth in knowledge in the field will promote the continued clinical adoption of liposomal therapeutics particularly from matching a suitable liposome with the appropriate therapeutic area.

7 References

1. Siegel, R. L., Miller, K. D. & Jemal, A. Cancer statistics, 2018. *CA. Cancer J. Clin.* **68,** 7–30 (2018).
2. Brigger, I., Dubernet, C. & Couvreur, P. Nanoparticles in cancer therapy and diagnosis. *Adv. Drug Deliv. Rev.* **64,** 24–36 (2012).
3. Scott, A. M., Allison, J. P., Wolchok, J. D. & Hughes, H. Monoclonal antibodies in cancer therapy. **12,** 1–8 (2012).
4. Zylberberg, C. & Matosevic, S. Pharmaceutical liposomal drug delivery: a review of new delivery systems and a look at the regulatory landscape. *Drug Deliv.* **23,** 3319–3329 (2016).
5. Weiner, G. J. Building better monoclonal antibody-based therapeutics. *Nat. Publ. Gr.* **15,** 361–370 (2015).
6. Tran, S., DeGiovanni, P.-J., Piel, B. & Rai, P. Cancer nanomedicine: a review of recent success in drug delivery. *Clin. Transl. Med.* **6,** 44 (2017).
7. Park, K. Controlled drug delivery systems: Past forward and future back. *J. Control. Release* **190,** 3–8 (2014).
8. Lee, B. K., Yun, Y. H. & Park, K. Smart nanoparticles for drug delivery: Boundaries and opportunities. *Chem. Eng. Sci.* **125,** 158–164 (2015).
9. Fang, M., Yuan, J., Peng, C. & Li, Y. Collagen as a double-edged sword in tumor progression. *Tumor Biol.* **35,** 2871–2882 (2014).
10. Karousou, E. *et al.* Collagen VI and Hyaluronan: The Common Role in Breast Cancer. *Biomed Res. Int.* **2014,** 1–10 (2014).
11. Xiao, W. *et al.* Normalizing Tumor Vessels to Increase the Enzyme-Induced Retention and Targeting of Gold Nanoparticle for Breast Cancer Imaging and Treatment. *Mol. Pharm.* **14,** 3489–3498 (2017).
12. Venning, F. A., Wullkopf, L. & Erler, J. T. Targeting ECM Disrupts Cancer Progression. *Front. Oncol.* **5,** 1–15 (2015).
13. Bonnans, C., Chou, J. & Werb, Z. Remodelling the extracellular matrix in development and disease. *Nat. Rev. Mol. Cell Biol.* **15,** 786–801 (2014).
14. Gkretsi, V., Stylianou, A., Papageorgis, P., Polydorou, C. & Stylianopoulos, T. Remodeling Components of the Tumor Microenvironment to Enhance Cancer Therapy. *Front. Oncol.* **5,** (2015).
15. Jain, R. K. Normalizing tumor microenvironment to treat cancer: bench to bedside to biomarkers. *J. Clin. Oncol.* **31,** 2205–2218 (2013).
16. Jain, R. & Stylianopoulos, T. Delivering nanomedicine to solid tumors. *Nat. Rev. Clin. Oncol.* **7,** 653–664 (2010).

17. Stylianopoulos, T., Munn, L. L. & Jain, R. K. Reengineering the Physical Microenvironment of Tumors to Improve Drug Delivery and Efficacy: From Mathematical Modeling to Bench to Bedside. *Trends in Cancer* **4,** 292–319 (2018).

18. Whatcott, C. J., Han, H., Posner, R. G., Hostetter, G. & Von Hoff, D. D. Targeting the Tumor Microenvironment in Cancer: Why Hyaluronidase Deserves a Second Look. *Cancer Discov.* **1,** 291–296 (2011).

19. Shepard, H. M. Breaching the Castle Walls: Hyaluronan Depletion as a Therapeutic Approach to Cancer Therapy. *Front. Oncol.* **5,** 192 (2015).

20. Goins, B., Phillips, W. T. & Bao, A. Strategies for improving the intratumoral distribution of liposomal drugs in cancer therapy. *Expert Opin. Drug Deliv.* **13,** 1–17 (2016).

21. Manthe, R. L., Foy, S. P., Krishnamurthy, N., Sharma, B. & Labhasetwar, V. Tumor Ablation and Nanotechnology. *Mol. Pharm.* **7,** 1880–1898 (2010).

22. Lai, C., Fite, B. Z. & Ferrara, K. W. Ultrasonic Enhancement of Drug Penetration in Solid Tumors. *Front. Oncol.* **3,** 1–7 (2013).

23. Pattni, B. S., Chupin, V. V & Torchilin, V. P. New Developments in Liposomal Drug Delivery. *Chem. Rev.* **115,** 10938–10966 (2015).

24. Beckenlehner, K. *et al.* Hyaluronidase enhances the activity of Adriamycin in breast cancer models in vitro and in vivo. *J. Cancer Res. Clin. Oncol.* **118,** 591–596 (1992).

25. Lokeshwar, V. B., Mirza, S. & Jordan, A. Targeting hyaluronic acid family for cancer chemoprevention and therapy. *Adv. Cancer Res.* **123,** 35–65 (2014).

26. Nagy, N. *et al.* 4-Methylumbelliferone Treatment and Hyaluronan Inhibition as a Therapeutic Strategy in Inflammation, Autoimmunity, and Cancer. *Front. Immunol.* **6,** 1–11 (2015).

27. Morohashi, H. *et al.* Study of hyaluronan synthase inhibitor, 4-methylumbelliferone derivatives on human pancreatic cancer cell (KP1-NL). *Biochem. Biophys. Res. Commun.* **345,** 1454–1459 (2006).

28. Saito, T. *et al.* 4-Methylumbelliferone leads to growth arrest and apoptosis in canine mammary tumor cells. *Oncol. Rep.* **29,** 335–342 (2013).

29. Nakazawa, H. *et al.* 4-methylumbelliferone, a hyaluronan synthase suppressor, enhances the anticancer activity of gemcitabine in human pancreatic cancer cells. *Cancer Chemother. Pharmacol.* **57,** 165–170 (2006).

30. Kohli, A. G., Kivimäe, S., Tiffany, M. R. & Szoka, F. C. Improving the distribution of Doxil® in the tumor matrix by depletion of tumor hyaluronan. *J. Control. Release* **191,** 105–14 (2014).

31. Plattt, V. M. & Szoka, F. C. Anticancer therapeutics: Targeting macromolecules and nanocarriers to hyaluronan or CD44, a hyaluronan receptor. *Mol. Pharm.* **5,** 474–486 (2008).

32. Sugahara, K. *et al.* Identification of the reaction products of the purified hyaluronidase from stonefish (Synanceja horrida) venom. *Biochem. J.* **283 (Pt 1,** 99–104 (1992).

33. Baumgartner, G., Gomar-Höss, C., Sakr, L., Ulsperger, E. & Wogritsch, C. The impact of extracellular matrix on the chemoresistance of solid tumors – experimental and clinical results of hyaluronidase as additive to cytostatic chemotherapy. *Cancer Lett.* **131,** 85–99 (1998).

34. Bookbinder, L. H. *et al.* A recombinant human enzyme for enhanced interstitial transport of therapeutics. *J. Control. Release* **114,** 230–241 (2006).

35. Buhren, B. A. *et al.* Hyaluronidase: from clinical applications to molecular and cellular mechanisms. *Eur. J. Med. Res.* **21,** 5 (2016).

36. McAtee, C. O., Barycki, J. J. & Simpson, M. A. Emerging roles for hyaluronidase in cancer metastasis and therapy. *Adv. Cancer Res.* **123,** 1–34 (2014).

37. Scodeller, P. Hyaluronidase and other Extracellular Matrix Degrading Enzymes for Cancer Therapy: New Uses and Nano-Formulations. *J. Carcinog. Mutagen.* **05,** 2–6 (2014).

38. Hingorani, S. *et al.* PEGPH20 improves pfs in patients with metastatic pancreatic ductal adenocarcinoma: A randomized phase 2 study in combination with nab-paclitaxel/gemcitabine. *Ann. Oncol.* **28,** mdx262.002-mdx262.002 (2017).

39. Halozyme. Halozyme Initiates Clinical Trial Of PEGPH20 With Anti-PDL1 Immunotherapy In Cholangiocarcinoma And Gallbladder Cancer Patients. *Press Release* (2018).

40. Diop-Frimpong, B., Chauhan, V. P., Krane, S., Boucher, Y. & Jain, R. K. Losartan inhibits collagen I synthesis and improves the distribution and efficacy of nanotherapeutics in tumors. *Proc. Natl. Acad. Sci. U. S. A.* **108,** 2909–14 (2011).

41. Chauhan, V. P. *et al.* Angiotensin inhibition enhances drug delivery and potentiates chemotherapy by decompressing tumour blood vessels. *Nat. Commun.* **4,** 2516 (2013).

42. Liu, J. *et al.* TGF- blockade improves the distribution and efficacy of therapeutics in breast carcinoma by normalizing the tumor stroma. *Proc. Natl. Acad. Sci.* **109,** 16618–16623 (2012).

43. Murphy, J. E. *et al.* TGF-B1 inhibition with losartan in combination with FOLFIRINOX (F-NOX) in locally advanced pancreatic cancer (LAPC): Preliminary feasibility and R0 resection rates from a prospective phase II study. *J. Clin. Oncol.* **35,** 386–386 (2017).

44. Barry-hamilton, V. *et al.* Allosteric inhibition of lysyl oxidase – like-2 impedes the development of a pathologic microenvironment. *Nat. Med.* **16,** 1005–1013 (2010).

45. Benson, A. B. *et al.* A Phase II Randomized, Double-Blind, Placebo-Controlled Study of Simtuzumab or Placebo in Combination with Gemcitabine for the First-

Line Treatment of Pancreatic Adenocarcinoma. *Oncologist* **22,** 241-e15 (2017).

46. Papageorgis, P. *et al.* Tranilast-induced stress alleviation in solid tumors improves the efficacy of chemo- and nanotherapeutics in a size-independent manner. *Sci. Rep.* **7,** 1–12 (2017).

47. Polydorou, C., Mpekris, F., Papageorgis, P., Voutouri, C. & Stylianopoulos, T. Pirfenidone normalizes the tumor microenvironment to improve chemotherapy. *Oncotarget* **8,** 24506–24517 (2017).

48. Vennin, C. *et al.* Transient tissue priming via ROCK inhibition uncouples pancreatic cancer progression, sensitivity to chemotherapy, and metastasis. *Sci. Transl. Med.* **9,** (2017).

49. Incio, J. *et al.* Metformin reduces desmoplasia in pancreatic cancer by reprogramming stellate cells and tumor-associated macrophages. *PLoS One* **10,** 1–23 (2015).

50. Sussman, B. J., Bromley, J. W. & Gomez, J. C. Injection of Collagenase in the Treatment of Herniated Lumbar Disk: Initial Clinical Report. *JAMA J. Am. Med. Assoc.* **245,** 730–732 (1981).

51. Kafienah, W., Buttle, D. J., Burnett, D. & Hollander, A. P. Cleavage of native type I collagen by human neutrophil elastase. *Biochem. J.* **330 (Pt 2,** 897–902 (1998).

52. French, M. F., Bhown, A. & Van Wart, H. E. Identification of Clostridium histolyticum collagenase hyperreactive sites in type I, II, and III collagens: Lack of correlation with local triple helical stability. *J. Protein Chem.* **11,** 83–97 (1992).

53. Erikson, A., Tufto, I., Bjønnum, A. B., Bruland, Ø. S. & Davies, C. D. L. The impact of enzymatic degradation on the uptake of differently sized therapeutic molecules. *Anticancer Res.* **28,** 3557–3566 (2008).

54. Baronzio, G., Parmar, G. & Baronzio, M. Overview of Methods for Overcoming Hindrance to Drug Delivery to Tumors, with Special Attention to Tumor Interstitial Fluid. *Front. Oncol.* **5,** 165 (2015).

55. Venditto, V. J. & Szoka, F. C. Cancer nanomedicines: So many papers and so few drugs! *Adv. Drug Deliv. Rev.* **65,** 80–88 (2013).

56. Alexandrakis, G. *et al.* Two-photon fluorescence correlation microscopy reveals the two-phase nature of transport in tumors. *Nat. Med.* **10,** 203–207 (2004).

57. Netti, P. A., Berk, D. A., Swartz, M. A., Grodzinsky, A. J. & Jain, R. K. Role of extracellular matrix assembly in interstitial transport in solid tumors. *Cancer Res.* **60,** 2497–503 (2000).

58. Eikenes, L., Tufto, I., Schnell, E. a., Bjørkøy, A. & Davies, C. D. L. Effect of collagenase and hyaluronidase on free and anomalous diffusion in multicellular spheroids and xenografts. *Anticancer Res.* **30,** 359–368 (2010).

59. Magzoub, M., Jin, S. & Verkman, A. S. Enhanced macromolecule diffusion deep in

tumors after enzymatic digestion of extracellular matrix collagen and its associated proteoglycan decorin. *FASEB J.* **22,** 276–284 (2007).

60. Choi, J. *et al.* Intraperitoneal immunotherapy for metastatic ovarian carcinoma: Resistance of intratumoral collagen to antibody penetration. *Clin. Cancer Res.* **12,** 1906–1912 (2006).

61. Eikenes, L., Bruland, Ø. S., Brekken, C. & De Lange Davies, C. Collagenase increases the transcapillary pressure gradient and improves the uptake and distribution of monoclonal antibodies in human osteosarcoma xenografts. *Cancer Res.* **64,** 4768–4773 (2004).

62. Hassid, Y., Eyal, E., Margalit, R., Furman-Haran, E. & Degani, H. Non-invasive imaging of barriers to drug delivery in tumors. *Microvasc. Res.* **76,** 94–103 (2008).

63. Kohli, A. G., Kierstead, P. H., Venditto, V. J., Walsh, C. L. & Szoka, F. C. Designer lipids for drug delivery: From heads to tails. *J. Control. Release* **190,** 274–287 (2014).

64. Allen, T. M. & Cullis, P. R. Liposomal drug delivery systems: from concept to clinical applications. *Adv. Drug Deliv. Rev.* **65,** 36–48 (2013).

65. Yan, Z. *et al.* Tumor-penetrating peptide mediation: An effective strategy for improving the transport of liposomes in tumor tissue. *Mol. Pharm.* **11,** 218–225 (2014).

66. Barua, S. & Mitragotri, S. Challenges associated with Penetration of Nanoparticles across Cell and Tissue Barriers: A Review of Current Status and Future Prospects. *Nano Today* **9,** 223–243 (2014).

67. Appelbe, O. K., Zhang, Q., Pelizzari, C. A., Weichselbaum, R. R. & Kron, S. J. Image-Guided Radiotherapy Targets Macromolecules through Altering the Tumor Microenvironment. *Mol. Pharm.* **13,** 3457–3467 (2016).

68. Yu, F. T. H., Chen, X., Wang, J., Qin, B. & Villanueva, F. S. Low Intensity Ultrasound Mediated Liposomal Doxorubicin Delivery Using Polymer Microbubbles. *Mol. Pharm.* **13,** 55–64 (2016).

69. Zheng, X. *et al.* Ultrasound-guided intratumoral administration of collagenase-2 improved liposome drug accumulation in solid tumor xenografts. *Cancer Chemother. Pharmacol.* **67,** 173–182 (2011).

70. Wharf, C., Kingdom, U. & European Medicines Agency. Assessment report Xiapex. *Report* (2011).

71. Lee, S. *et al.* Extracellular matrix remodeling in vivo for enhancing tumor-targeting efficiency of nanoparticle drug carriers using the pulsed high intensity focused ultrasound. *J. Control. Release* **263,** 68–78 (2017).

72. Kato, M., Hattori, Y., Kubo, M. & Maitani, Y. Collagenase-1 injection improved tumor distribution and gene expression of cationic lipoplex. *Int. J. Pharm.* **423,** 428–434 (2012).

73. Uyechi, L. S., Gagné, L., Thurston, G. & Szoka, F. C. Mechanism of lipoplex gene delivery in mouse lung: Binding and internalization of fluorescent lipid and DNA components. *Gene Ther.* **8,** 828–836 (2001).

74. Villegas, M. R., Baeza, A. & Vallet-Regí, M. Hybrid Collagenase Nanocapsules for Enhanced Nanocarrier Penetration in Tumoral Tissues. *ACS Appl. Mater. Interfaces* **7,** 24075–24081 (2015).

75. Murty, S. *et al.* Nanoparticles Functionalized with Collagenase Exhibit Improved Tumor Accumulation in a Murine Xenograft Model. *Part. Part. Syst. Charact.* **31,** 1307–1312 (2014).

76. Dachs, G. U., Dougherty, G. J., Stratford, I. J. & Chaplin, D. J. Targeting gene therapy to cancer: a review. *Oncol. Res.* **9,** 313–25 (1997).

77. Lo, H. W., Day, C. P. & Hung, M. C. Cancer-Specific Gene Therapy. *Adv. Genet.* **54,** 233–255 (2005).

78. Cemazar, M. *et al.* Hyaluronidase and Collagenase Increase the Transfection Efficiency of Gene Electrotransfer in Various Murine Tumors. *Hum. Gene Ther.* **23,** 128–137 (2012).

79. Kuriyama, N., Kuriyama, H., Julin, C. M., Lamborn, K. R. & Israel, M. A. Protease pretreatment increases the efficacy of adenovirus-mediated gene therapy for the treatment of an experimental glioblastoma model. *Cancer Res.* **61,** 1805–9 (2001).

80. Stenn, K. S., Link, R., Moellmann, G., Madri, J. & Kuklinska, E. Dispase, a neutral protease from Bacillus polymyxa, is a powerful fibronectinase and type IV collagenase. *J. Invest. Dermatol.* **93,** 287–90 (1989).

81. McKee, T. D. *et al.* Degradation of fibrillar collagen in a human melanoma xenograft improves the efficacy of an oncolytic herpes simplex virus vector. *Cancer Res.* **66,** 2509–2513 (2006).

82. Maeda, A. & DaCosta, R. S. Optimization of the dorsal skinfold window chamber model and multi-parametric characterization of tumor-associated vasculature. *IntraVital* **3,** e27935 (2014).

83. Jeannine Schreiter, Sophia Meyer, Christian Schmidt, Ronny M. Schulz, S. L. Dorsal skinfold chamber models in mice. *GMS Interdiscip. Plast. Reconstr. Surg.* **6,** 1–8 (2017).

84. Seo, B. R., DelNero, P. & Fischbach, C. In vitro models of tumor vessels and matrix: Engineering approaches to investigate transport limitations and drug delivery in cancer. *Adv. Drug Deliv. Rev.* **69–70,** 205–216 (2014).

85. Huang, K., Boerhan, R., Liu, C. & Jiang, G. Nanoparticles Penetrate into the Multicellular Spheroid-on-Chip: Effect of Surface Charge, Protein Corona, and Exterior Flow. *Mol. Pharm.* **14,** 4618–4627 (2017).

86. Fracasso, G. & Colombatti, M. Effect of therapeutic macromolecules in spheroids. *Crit. Rev. Oncol. Hematol.* **36,** 159–78 (2000).

87. Zanoni, M. *et al.* 3D tumor spheroid models for in vitro therapeutic screening: a systematic approach to enhance the biological relevance of data obtained. *Sci. Rep.* **6,** 19103 (2016).

88. Takechi-Haraya, Y., Goda, Y. & Sakai-Kato, K. Control of Liposomal Penetration into Three-Dimensional Multicellular Tumor Spheroids by Modulating Liposomal Membrane Rigidity. *Mol. Pharm.* **14,** 2158–2165 (2017).

89. Goodman, T. T., Olive, P. L. & Pun, S. H. Increased nanoparticle penetration in collagenase-treated multicellular spheroids. *Int. J. Nanomedicine* **2,** 265–74 (2007).

90. Cui, M. *et al.* Multifunctional Albumin Nanoparticles As Combination Drug Carriers for Intra-Tumoral Chemotherapy. *Adv. Healthc. Mater.* **2,** 1236–1245 (2013).

91. Yata, T. *et al.* Modulation of extracellular matrix in cancer is associated with enhanced tumor cell targeting by bacteriophage vectors. *Mol. Cancer* **14,** 110 (2015).

92. Amar, S. & Fields, G. B. Potential clinical implications of recent matrix metalloproteinase inhibitor design strategies. *Expert Rev. Proteomics* **12,** 445–447 (2015).

93. Cao, J., Chiarelli, C., Kozarekar, P. & Adler, H. L. Membrane type 1-matrix metalloproteinase promotes human prostate cancer invasion and metastasis. *Thromb. Haemost.* **94,** 770–778 (2005).

94. Foley, C. J. *et al.* Matrix metalloprotease-1a promotes tumorigenesis and metastasis. *J. Biol. Chem.* **287,** 24330–24338 (2012).

95. Kudo, Y. *et al.* Matrix metalloproteinase-13 (MMP-13) directly and indirectly promotes tumor angiogenesis. *J. Biol. Chem.* **287,** 38716–38728 (2012).

96. Pulukuri, SMK and Rao, J. S. Matrix Metalloproteinase-1 Promotes Prostate Tumor Growth and Metastasis. *Int. J. Oncol.* **32,** 757–765 (2008).

97. Sarkar, S. K., Marmer, B., Goldberg, G. & Neuman, K. C. Single-Molecule Tracking of Collagenase on Native Type I Collagen Fibrils Reveals Degradation Mechanism. *Curr. Biol.* **22,** 1047–1056 (2012).

98. Tester, A. M. *et al.* Pro-Matrix Metalloproteinase-2 Transfection Increases Orthotopic Primary Growth and Experimental Metastasis of MDA-MB-231 Human Breast Cancer Cells in Nude Mice. *Cancer Res.* **64,** 652–658 (2004).

99. Yonemura, Y. *et al.* Membrane-type 1 matrix metalloproteinase enhances lymph node metastasis of gastric cancer. *Clin. Exp. Metastasis* **18,** 321–327 (2000).

100. Zucker, S. *et al.* Tumorigenic potential of extracellular matrix metalloproteinase inducer. *Am. J. Pathol.* **158,** 1921–1928 (2001).

101. Diener, B., Carrick, L. & Berk, R. S. In vivo studies with collagenase from Pseudomonas aeruginosa. *Infect. Immun.* **7,** 212–217 (1973).

102. López, B., González, A. & Díez, J. Circulating biomarkers of collagen metabolism

in cardiac diseases. *Circulation* **121,** 1645–54 (2010).

103. Choi, I.-K., Strauss, R., Richter, M., Yun, C.-O. & Lieber, A. Strategies to increase drug penetration in solid tumors. *Front. Oncol.* **3,** 193 (2013).

104. Hingorani, S. R. *et al.* Randomized phase II study of PEGPH20 plus nab-paclitaxel/gemcitabine (PAG) vs AG in patients (Pts) with untreated, metastatic pancreatic ductal adenocarcinoma (mPDA). *J. Clin. Oncol.* **35,** 4008 (2017).

105. Chalikias, G. K. & Tziakas, D. N. Biomarkers of the extracellular matrix and of collagen fragments. *Clin. Chim. Acta* **443,** 39–47 (2015).

106. Brown, E. *et al.* Dynamic imaging of collagen and its modulation in tumors in vivo using second-harmonic generation. *Nat. Med.* **9,** 796–800 (2003).

107. Breite, A. G., McCarthy, R. C. & Dwulet, F. E. Characterization and Functional Assessment of Clostridium Histolyticum Class I (C1) Collagenases and the Synergistic Degradation of Native Collagen in Enzyme Mixtures Containing Class II (C2) Collagenase. *Transplant. Proc.* **43,** 3171–3175 (2011).

108. Watanabe, K. Collagenolytic proteases from bacteria. *Appl. Microbiol. Biotechnol.* **63,** 520–526 (2004).

109. Lu, P., Takai, K., Weaver, V. M. & Werb, Z. Extracellular matrix degradation and remodeling in development and disease. *Cold Spring Harb Perspect Biol* **3,** 1–24 (2011).

110. Mok, W., Boucher, Y. & Jain, R. K. Matrix metalloproteinases-1 and -8 improve the distribution and efficacy of an oncolytic virus. *Cancer Res.* **67,** 10664–10668 (2007).

111. Cheng, J. *et al.* Human matrix metalloproteinase-8 gene delivery increases the oncolytic activity of a replicating adenovirus. *Mol. Ther.* **15,** 1982–1990 (2007).

112. Singh, K. K., Jain, R., Ramanan, H. & Saini, D. K. Matrix-Assisted Refolding, Purification and Activity Assessment Using a 'Form Invariant' Assay for Matrix Metalloproteinase 2 (MMP2). *Mol. Biotechnol.* **56,** 1121–1132 (2014).

113. Nam, D. H. & Ge, X. Direct production of functional matrix metalloproteinase--14 without refolding or activation and its application for in vitro inhibition assays. *Biotechnol. Bioeng.* **113,** 717–23 (2016).

114. Parkar, A. a. *et al.* Large-Scale Expression, Refolding, and Purification of the Catalytic Domain of Human Macrophage Metalloelastase (MMP-12) in Escherichia coli. *Protein Expr. Purif.* **20,** 152–161 (2000).

115. Pathak, N., Hu, S. I. & Koehn, J. a. The expression, refolding, and purification of the catalytic domain of human collagenase-3 (MMP-13). *Protein Expr. Purif.* **14,** 283–288 (1998).

116. Ho, T. F. *et al.* Gene expression, purification and characterization of recombinant human neutrophil collagenase. *Gene* **146,** 297–301 (1994).

117. Rasch, M. G., Lund, I. K., Illemann, M., Høyer-Hansen, G. & Gårdsvoll, H. Purification and characterization of recombinant full-length and protease domain of murine MMP-9 expressed in Drosophila S2 cells. *Protein Expr. Purif.* **72,** 87–94 (2010).

118. Hadler-Olsen, E., Fadnes, B., Sylte, I., Uhlin-Hansen, L. & Winberg, J.-O. Regulation of matrix metalloproteinase activity in health and disease. *FEBS J.* **278,** 28–45 (2011).

119. Gutiérrez-Fernández, A. *et al.* Matrix metalloproteinase-8 functions as a metastasis suppressor through modulation of tumor cell adhesion and invasion. *Cancer Res.* **68,** 2755–2763 (2008).

120. Eckhard, U. *et al.* Active site specificity profiling of the matrix metalloproteinase family: Proteomic identification of 4300 cleavage sites by nine MMPs explored with structural and synthetic peptide cleavage analyses. *Matrix Biol.* **49,** 37–60 (2016).

121. Hong, C. S. *et al.* Ectopic Matrix Metalloproteinase 9 Expression in Human Brain Tumor Cells Enhances Oncolytic HSV Vector Infection. *Gene Ther* **17,** 1200–1205 (2010).

122. Warwick, D., Arandes-Renú, J. M., Pajardi, G., Witthaut, J. & Hurst, L. C. Collagenase Clostridium histolyticum : emerging practice patterns and treatment advances. *J. Plast. Surg. Hand Surg.* **50,** 251–261 (2016).

123. Alipour, H., Raz, A., Zakeri, S. & Dinparast Djadid, N. Therapeutic applications of collagenase (metalloproteases): A review. *Asian Pac. J. Trop. Biomed.* **6,** 975–981 (2016).

124. Gilpin, D. *et al.* Injectable Collagenase Clostridium Histolyticum: A New Nonsurgical Treatment for Dupuytren's Disease. *J. Hand Surg. Am.* **35,** 2027–2038.e1 (2010).

125. Yang, K. K. & Bennett, N. Peyronie's Disease and Injectable Collagenase Clostridium histolyticum: Safety, Efficacy, and Improvements in Subjective Symptoms. *Urology* **94,** 143–147 (2016).

126. McCallon, S. K., Weir, D. & Lantis, J. C. Optimizing wound bed preparation with collagenase enzymatic debridement. *J. Am. Coll. Clin. Wound Spec.* **6,** 14–23 (2014).

127. Özcan, C., Ergün, O., Çelik, A., Çördük, N. & Özok, G. Enzymatic debridement of burn wound with collagenase in children with partial-thickness burns. *Burns* **28,** 791–794 (2002).

128. Abe, H. *et al.* Effective Prevention of Liver Fibrosis by Liver-targeted Hydrodynamic Gene Delivery of Matrix Metalloproteinase-13 in a Rat Liver Fibrosis Model. *Mol. Ther. - Nucleic Acids* **5,** e276 (2016).

129. Liu, J. *et al.* Truncated active human matrix metalloproteinase-8 delivered by a chimeric adenovirus-hepatitis B virus vector ameliorates rat liver cirrhosis. *PLoS One* **8,** e53392 (2013).

130. Bobo, D., Robinson, K. J., Islam, J., Thurecht, K. J. & Corrie, S. R. Nanoparticle-Based Medicines: A Review of FDA-Approved Materials and Clinical Trials to Date. *Pharm. Res.* **33,** 2373–2387 (2016).

131. Sarkar, N. R. *et al.* "Uncorking" of liposomes by matrix metalloproteinase-9. *Chem. Commun.* 999–1001 (2005). doi:10.1039/B416827E

132. Zhu, G., Mock, J. N., Aljuffali, I., Cummings, B. S. & Arnold, R. D. Secretory phospholipase A 2 responsive liposomes. *J. Pharm. Sci.* **100,** 3146–3159 (2011).

133. Bhattacharjee, a *et al.* Classification of human lung carcinomas by mRNA expression profiling reveals distinct adenocarcinoma subclasses. *Proc. Natl. Acad. Sci. U. S. A.* **98,** 13790–5 (2001).

134. Lai, J. *et al.* hSulf1 sulfatase promotes apoptosis of hepatocellular cancer cells by decreasing heparin-binding growth factor signaling. *Gastroenterology* **126,** 231–248 (2004).

135. Lai, J.-P. *et al.* Sulfatase 2 up-regulates glypican 3, promotes fibroblast growth factor signaling, and decreases survival in hepatocellular carcinoma. *Hepatology* **47,** 1211–22 (2008).

136. Lemjabbar-Alaoui, H. *et al.* Sulf-2, a heparan sulfate endosulfatase, promotes human lung carcinogenesis. *Oncogene* **29,** 635–46 (2010).

137. Pasca di Magliano, M. *et al.* Common activation of canonical Wnt signaling in pancreatic adenocarcinoma. *PLoS One* **2,** e1155 (2007).

138. Rosen, S. D. & Lemjabbar-Alaoui, H. Sulf-2: an extracellular modulator of cell signaling and a cancer target candidate. *Expert Opin. Ther. Targets* **14,** 935–949 (2010).

139. Diez-Roux, G. & Ballabio, A. Sulfatases and human disease. *Annu. Rev. Genomics Hum. Genet.* **6,** 355–79 (2005).

140. Vivès, R. R., Seffouh, A. & Lortat-Jacob, H. Post-Synthetic Regulation of HS Structure: The Yin and Yang of the Sulfs in Cancer. *Front. Oncol.* **3,** 331 (2014).

141. Kreuger, J. *et al.* Fibroblast growth factors share binding sites in heparan sulphate. *Biochem. J.* **389,** 145–150 (2005).

142. Rueda, P. *et al.* Homeostatic and tissue reparation defaults in mice carrying selective genetic invalidation of CXCL12/proteoglycan interactions. *Circulation* **126,** 1882–95 (2012).

143. Ono, K., Hattori, H., Takeshita, S., Kurita, A. & Ishihara, M. Structural features in heparin that interact with VEGF165 and modulate its biological activity. *Glycobiology* **9,** 705–11 (1999).

144. Perttu, E. K., Kohli, A. G. & Szoka, F. C. Inverse-phosphocholine lipids: a remix of a common phospholipid. *J. Am. Chem. Soc.* **134,** 4485–8 (2012).

145. Kohli, A. G., Walsh, C. L. & Szoka, F. C. Synthesis and characterization of betaine-

like diacyl lipids: zwitterionic lipids with the cationic amine at the bilayer interface. *Chem. Phys. Lipids* **165,** 252–9 (2012).

146. Perttu, E. K. & Szoka, F. C. Zwitterionic sulfobetaine lipids that form vesicles with salt-dependent thermotropic properties. *Chem. Commun. (Camb).* **47,** 12613–5 (2011).

147. Singer, M. S. *et al.* SULF2, a heparan sulfate endosulfatase, is present in the blood of healthy individuals and increases in cirrhosis. *Clin. Chim. Acta* **440,** 72–78 (2015).

148. Nguyen, J. & Szoka, F. C. Nucleic acid delivery: the missing pieces of the puzzle? *Acc. Chem. Res.* **45,** 1153–62 (2012).

149. Tiffany, M. & Szoka, F. C. Co-localization of fluorescent labeled lipid nanoparticles with specifically tagged subcellular compartments by single particle tracking at low nanoparticle to cell ratios. *J. Drug Target.* **24,** 857–864 (2016).

150. Millán, J. L. Alkaline phosphatases. *Purinergic Signal.* **2,** 335–341 (2006).

151. Hanson, S. R., Best, M. D. & Wong, C.-H. Sulfatases: structure, mechanism, biological activity, inhibition, and synthetic utility. *Angew. Chem. Int. Ed. Engl.* **43,** 5736–63 (2004).

152. Aikawa, T., Yokota, K., Kondo, T. & Yuasa, M. Intermolecular Interaction between Phosphatidylcholine and Sulfobetaine Lipid: A Combination of Lipids with Antiparallel Arranged Headgroup Charge. *Langmuir* **32,** 10483–10490 (2016).

153. Aikawa, T., Okura, H., Kondo, T. & Yuasa, M. Comparison of Carboxybetaine with Sulfobetaine as Lipid Headgroup Involved in Intermolecular Interaction between Lipids in the Membrane. *ACS Omega* **2,** 5803–5812 (2017).

154. Huang, Z. & Szoka, F. C. Sterol-Modified Phospholipids : Cholesterol and Phospholipid Chimeras with Improved Biomembrane Properties. *J. Am. Chem. Soc.* **130,** 15702–15712 (2008).

155. Gabizon, A. *et al.* Prolonged circulation time and enhanced accumulation in malignant exudates of doxorubicin encapsulated in polyethylene-glycol coated liposomes. *Cancer Res.* **54,** 987–92 (1994).

156. Drummond, D. C., Meyer, O., Hong, K., Kirpotin, D. B. & Papahadjopoulos, D. Optimizing liposomes for delivery of chemotherapeutic agents to solid tumors. *Pharmacol. Rev.* **51,** 691–743 (1999).

157. Immordino, M. L., Dosio, F. & Cattel, L. Stealth liposomes: Review of the basic science, rationale, and clinical applications, existing and potential. *International Journal of Nanomedicine* **1,** 297–315 (2006).

158. Borden, M. A. *et al.* Lateral phase separation in lipid-coated microbubbles. *Langmuir* **22,** 4291–4297 (2006).

159. Lozano, M. M. & Longo, M. L. Complex formation and other phase transformations

mapped in saturated phosphatidylcholine/DSPE-PEG2000 monolayers. *Soft Matter* **5,** 1822 (2009).

160. Chou, T. & Chu, I. Thermodynamic characteristics of DSPC / DSPE-PEG 2000 mixed monolayers on the water subphase at different temperatures. *Colloids Surfaces B Biointerfaces* **27,** 333–344 (2003).

161. Dos Santos, N. *et al.* Improved retention of idarubicin after intravenous injection obtained for cholesterol-free liposomes. *Biochim. Biophys. Acta - Biomembr.* **1561,** 188–201 (2002).

162. Miyoshi, T. & Kato, S. Detailed Analysis of the Surface Area and Elasticity in the Saturated 1,2-Diacylphosphatidylcholine/Cholesterol Binary Monolayer System. *Langmuir* **31,** 9086–9096 (2015).

163. Kohli, A. G., Kieler-Ferguson, H. M., Chan, D. & Szoka, F. C. A robust and quantitative method for tracking liposome contents after intravenous administration. *J. Control. Release* **176,** 86–93 (2014).

164. Sou, K., Endo, T., Takeoka, S. & Tsuchida, E. Poly(ethylene glycol)-modification of the phospholipid vesicles by using the spontaneous incorporation of poly(ethylene glycol)-lipid into the vesicles. *Bioconjug. Chem.* **11,** 372–379 (2000).

165. Yan, X. *et al.* The role of apolipoprotein E in the elimination of liposomes from blood by hepatocytes in the mouse. *Biochem. Biophys. Res. Commun.* **328,** 57–62 (2005).

166. Venditto, V. J., Watson, D. S., Motion, M., Montefiori, D. & Szoka, F. C. Rational design of membrane proximal external region lipopeptides containing chemical modifications for HIV-1 vaccination. *Clin. Vaccine Immunol.* **20,** 39–45 (2013).

167. Watson, D. S., Endsley, A. N. & Huang, L. Design considerations for liposomal vaccines: influence of formulation parameters on antibody and cell-mediated immune responses to liposome associated antigens. *Vaccine* **30,** 2256–72 (2012).

168. Shaghaghi, M., Keyvanloo, A., Huang, Z., Szoka, F. C. & Thewalt, J. L. Constrained Versus Free Cholesterol in DPPC Membranes: A Comparison of Chain Ordering Ability Using Deuterium NMR. *Langmuir* **33,** 14405–14413 (2017).

169. Akinc, A. *et al.* Targeted delivery of RNAi therapeutics with endogenous and exogenous ligand-based mechanisms. *Mol. Ther.* **18,** 1357–1364 (2010).

170. Cooper, A. D. Hepatic uptake of chylomicron remnants. *J. Lipid Res.* **38,** 2173–2192 (1997).

171. Venditto, V. J. *et al.* Sulfated quaternary amine lipids: a new class of inverse charge zwitterlipids. *Chem. Commun. (Camb).* **50,** 9109–11 (2014).

172. Musumeci, D. & Montesarchio, D. Synthesis of a cholesteryl-HEG phosphoramidite derivative and its application to lipid-conjugates of the anti-HIV 5'TGGGAG$^{3'}$ Hotoda's sequence. *Molecules* **17,** 12378–92 (2012).

173. Page-McCaw, A., Ewald, A. J. & Werb, Z. Matrix metalloproteinases and the regulation of tissue remodelling. *Nat. Rev. Mol. Cell Biol.* **8,** 221–233 (2007).

174. Cathcart, J., Pulkoski-Gross, A. & Cao, J. Targeting matrix metalloproteinases in cancer: Bringing new life to old ideas. *Genes Dis.* **2,** 26–34 (2015).

175. Fingleton, B. MMPs as therapeutic targets - still a viable option? *Semin. cell Dev. Biol. cell Dev. Biol.* **19,** 61–68 (2009).

176. Steplewski, A. & Fertala, A. Inhibition of collagen fibril formation. *Fibrogenesis Tissue Repair* **5,** S29 (2012).

177. Roberts, S., Urban, J. P. G., Vans, H. & Eisenstein, S. M. Transport properties of the human cartilage endplate in relation to its composition and calcilification. *Spine* **21,** 415–420 (1996).

178. Windsor, L. J. & Steele, D. L. Matrix Metalloproteinase Protocols. **622,** 67–81 (2010).

179. Lichte, a, Kolkenbrock, H. & Tschesche, H. The recombinant catalytic domain of membrane-type matrix metalloproteinase-1 (MT1-MMP) induces activation of progelatinase A and progelatinase A complexed with TIMP-2. *FEBS Lett.* **397,** 277–82 (1996).

180. Knäuper, V., Docherty, A. J. P., Smith, B., Tschesche, H. & Murphy, G. Analysis of the contribution of the hinge region of human neutrophil collagenase (HNC, MMP-8) to stability and collagenolytic activity by alanine scanning mutagenesis. *FEBS Lett.* **405,** 60–64 (1997).

181. Li, S. *et al.* A highly functional mini-dystrophin/GFP fusion gene for cell and gene therapy studies of Duchenne muscular dystrophy. *Hum. Mol. Genet.* **15,** 1610–22 (2006).

182. Sockolosky, J. T., Tiffany, M. R. & Szoka, F. C. Engineering neonatal Fc receptor-mediated recycling and transcytosis in recombinant proteins by short terminal peptide extensions. *Proc. Natl. Acad. Sci.* **109,** 16095–16100 (2012).

183. Gräslund, S. *et al.* Protein production and purification. *Nat. Methods* **5,** 135–146 (2008).

184. Imai, K. & Okada, Y. Purification of matrix metalloproteinases by column chromatography. *Nat. Protoc.* **3,** 1111–1124 (2008).

185. Sockolosky, J. T. & Szoka, F. C. Periplasmic production via the pET expression system of soluble, bioactive human growth hormone. *Protein Expr. Purif.* **87,** 129–135 (2013).

186. Platt, V. *et al.* Influence of multivalent nitrilotriacetic acid lipid-ligand affinity on the circulation half-life in mice of a liposome-attached His6-protein. *Bioconjug. Chem.* **21,** 892–902 (2010).

187. Haralson, R. H. & Zuckerman, J. D. Prevalence, health care expenditures, and

orthopedic surgery workforce for musculoskeletal conditions. *JAMA* **302,** 1586–7 (2009).

188. Chou, D. *et al.* Degenerative magnetic resonance imaging changes in patients with chronic low back pain: A systematic review. *Spine (Phila. Pa. 1976).* **36,** 43–53 (2011).

189. Vedicherla, S. & Buckley, C. T. Cell-based therapies for intervertebral disc and cartilage regeneration— Current concepts, parallels, and perspectives. *J. Orthop. Res.* **35,** 8–22 (2017).

190. Sakai, D. & Schol, J. Cell therapy for intervertebral disc repair: Clinical perspective. *J. Orthop. Transl.* **9,** 8–18 (2017).

191. Vadalà, G., Russo, F., Ambrosio, L., Loppini, M. & Denaro, V. Stem cells sources for intervertebral disc regeneration. *World J. Stem Cells* **8,** 185 (2016).

192. Bae, W. C. & Masuda, K. Emerging Technologies for Molecular Therapy for Intervertebral Disk Degeneration. *Orthop. Clin. North Am.* **42,** 585–601 (2011).

193. Woods, B. I., Vo, N., Sowa, G. & Kang, J. D. Gene Therapy for Intervertebral Disk Degeneration. *Orthop. Clin. North Am.* **42,** 563–574 (2011).

194. Gawri, R. *et al.* Best paper NASS 2013: Link-N can stimulate proteoglycan synthesis in the degenerated human intervertebral discs. *Eur. Cells Mater.* **26,** 107–119 (2013).

195. Wang, H. *et al.* Inflammatory Cytokines Induce NOTCH Signaling in Nucleus Pulposus Cells. *J. Biol. Chem.* **288,** 16761–16774 (2013).

196. Urban, J. P. G., Smith, S. & Fairbank, J. C. T. Nutrition of the intervertebral disc. *Spine (Phila. Pa. 1976).* **29,** 2700–9 (2004).

197. Huang, Y. C., Urban, J. P. G. & Luk, K. D. K. Intervertebral disc regeneration: Do nutrients lead the way? *Nat. Rev. Rheumatol.* **10,** 561–566 (2014).

198. Gu, W. Y., Zhu, Q., Gao, X. & Brown, M. D. Simulation of the Progression of Intervertebral Disc Degeneration due to Decreased Nutrient Supply. *Spine (Phila. Pa. 1976).* **39,** E1411–E1417 (2014).

199. Shirazi-Adl, A., Taheri, M. & Urban, J. P. G. Analysis of cell viability in intervertebral disc: Effect of endplate permeability on cell population. *J. Biomech.* **43,** 1330–1336 (2010).

200. Antoniou, J. *et al.* The human lumbar intervertebral disc: Evidence for changes in the biosynthesis and denaturation of the extracellular matrix with growth, maturation, ageing, and degeneration. *J. Clin. Invest.* **98,** 996–1003 (1996).

201. Bishop, P. B. & Pearce, R. H. The proteoglycans of the cartilaginous end-plate of the human intervertebral disc change after maturity. *J. Orthop. Res.* **11,** 324–331 (1993).

202. Aoki, J. *et al.* End plate of the discovertebral joint: degenerative change in the

elderly adult. *Radiology* **164,** 411–4 (1987).

203. Benneker, L. M., Heini, P. F., Alini, M., Anderson, S. E. & Ito, K. 2004 Young investigator award winner: Vertebral endplate marrow contact channel occlusions and intervertebral disc degeneration. *Spine (Phila. Pa. 1976).* **30,** 167–173 (2005).

204. Maroudas, A. & Venn, M. Chemical composition and swelling of normal and osteoarthrotic femoral head cartilage. *Ann. Rheum. Dis.* **36,** 399–406 (1977).

205. Wu, Y. *et al.* Region and strain-dependent diffusivities of glucose and lactate in healthy human cartilage endplate. *J. Biomech.* **49,** 2756–2762 (2016).

206. Urban, J. P. G. & Maroudas, A. The measurement of fixed charge density in the intervertebral disc. *Biochim. Biophys. Acta* **586,** 166–78 (1979).

207. Maroudas, A. Proteoglycan Osmotic-Pressure and the Collagen Tension in Normal, Osteoarthritic Human Cartilage. *Semin. Arthritis Rheum.* **11,** 36–39 (1981).

208. Wittenberg, R. H., Oppel, S., Rubenthaler, F. A. & Steffen, R. Five-year results from chemonucleolysis with chymopapain or collagenase: A prospective randomized study. *Spine (Phila. Pa. 1976).* **26,** 1835–1841 (2001).

209. West, P. A., Torzilli, P. A., Chen, C., Lin, P. & Camacho, N. P. Fourier transform infrared imaging spectroscopy analysis of collagenase-induced cartilage degradation. *J. Biomed. Opt.* **10,** 014015 (2005).

210. Sivan, S. S. *et al.* Age-related accumulation of pentosidine in aggrecan and collagen from normal and degenerate human intervertebral discs. *Biochem. J.* **399,** 29–35 (2006).

211. Fields, A. J. *et al.* Alterations in intervertebral disc composition, matrix homeostasis and biomechanical behavior in the UCD-T2DM rat model of type 2 diabetes. *J. Orthop. Res.* **33,** 738–746 (2015).

212. Jazini, E. *et al.* Alterations in T2 Relaxation Magnetic Resonance Imaging of the Ovine Intervertebral Disc Due to Nonenzymatic Glycation. *Spine (Phila. Pa. 1976).* **37,** E209–E215 (2012).

213. DeGroot, J. *et al.* Age-related decrease in susceptibility of human articular cartilage to matrix metalloproteinase-mediated degradation: the role of advanced glycation end products. *Arthritis Rheum.* **44,** 2562–2571 (2001).

214. Vlassara, H. & Uribarri, J. Advanced glycation end products (AGE) and diabetes: Cause, effect, or both? *Curr. Diab. Rep.* **14,** 1–17 (2014).

215. Farndale, R. W., Buttle, D. J. & Barrett, A. J. Improved quantitation and discrimination of sulphated glycosaminoglycans by use of dimethylmethylene blue. *BBA - Gen. Subj.* **883,** 173–177 (1986).

216. Vashishth, D. Advanced glycation end-products and bone fractures. *IBMS Bonekey* **6,** 268–278 (2009).

217. Kierstead, P. H. *et al.* The effect of polymer backbone chemistry on the induction

of the accelerated blood clearance in polymer modified liposomes. *J. Control. Release* **213,** 1–9 (2015).

218. Cal, S. *Proteases and Cancer*. **1731,** (Springer New York, 2018).

219. Krishnakumar, G. S. *et al.* Ribose mediated crosslinking of collagen-hydroxyapatite hybrid scaffolds for bone tissue regeneration using biomimetic strategies. *Mater. Sci. Eng. C* **77,** 594–605 (2017).

Publishing Agreement

It is the policy of the University to encourage the distribution of all theses, dissertations, and manuscripts. Copies of all UCSF theses, dissertations, and manuscripts will be routed to the library via the Graduate Division. The library will make all theses, dissertations, and manuscripts accessible to the public and will preserve these to the best of their abilities, in perpetuity.

I hereby grant permission to the Graduate Division of the University of California, San Francisco to release copies of my thesis, dissertation, or manuscript to the Campus Library to provide access and preservation, in whole or in part, in perpetuity.

Author Signature 

Date: Jun 14, 2018